THERMOLUMINESCENT MECHANISMS IN MgO EXPOSED TO ULTRAVIOLET RADIATION

by

WANDA CECILIA LAS

A dissertation sumitted in partial fulfillment of

the requirements for the degree of

Doctor of Philosophy

University of Washington
1980

THERMOLUMINESCENT MECHANISMS IN MgO EXPOSED TO ULTRAVIOLET RADIATION

by

Wanda Cecilia Las

A dissertation submitted in partial fulfillment
of the requirements for the degree of

Doctor of Philosophy

University of Washington

1980

Approved by Thomas D. Stoebe
(Chairperson of Supervisory Committee)

Program Authorized
to Offer Degree Metallurgical Engineering

Date May 23, 1980

Doctoral Dissertation

In presenting this dissertation in partial fulfillment of the requirements for the Doctoral degree at the University of Washington, I agree that the Library shall make its copies freely available for inspection. I further agree that extensive copying of this dissertation is allowable only for scholarly purposes. Requests for copying or reproduction of this dissertation may be referred to University Microfilms, 300 North Zeeb Road, Ann Arbor, Michigan 48106, to whom the author has granted "the right to reproduce and sell (a) copies of the manuscript in microform and/or (b) printed copies of the manuscript made from microform."

Signature Wanda Cecilia Lee

Date May 23, 1980

University of Washington

Abstract

THERMOLUMINESCENT MECHANISMS IN MgO EXPOSED TO ULTRAVIOLET RADIATION

By Wanda Cecilia Las

Chairperson of the Supervisory Committee: Professor Thomas G. Stoebe
Division of Metallurgical
Engineering

Recent studies in MgO have shown that charge transfer mechanisms occur involving transition metal ions such as Fe, Cr, Mn and V. These impurities are thought to be related to the property of "direct thermoluminescence" (TL) observed when MgO is exposed to ultraviolet (UV) radiation. In this research, charge transfer mechanisms in MgO are investigated as caused by UV radiation, the sensitization phenomenon and the TL sensitivity to UV radiation are studied and their dependence on the impurity content determined. The observations of TL sensitivity are then correlated, enabling the construction of a model for charge transfer in UV-irradiated MgO.

MgO crystals, obtained from Spicer Co. and Norton Co., were studied in the "as received" condition, and after heat treatments in the reducing and oxidizing atmospheres of CO/CO_2 and air, respectively. It was observed that the reducing treatment decreased the TL response to UV, which is related to the reduction of Fe^{3+} impurity ions to Fe^{2+}. Oxidizing treatments, on the other hand, sensitized both crystals.

The ESR technique was employed to measure the concentrations of Fe^{3+}, Cr^{3+}, Mn^{2+} and V^{2+} before and after the UV exposure and

after the TL reading. The Norton crystals were grouped into one set of relatively pure crystals and two groups of less pure samples. The proposed TL mechanism is one of direct charge transfer between Fe^{3+} and Cr^{2+}, and between Fe^{3+} and Mn^{2+}, respectively, for the two groups of less pure samples where no V-type centers are believed to be involved. In the relatively pure MgO-Norton crystals, the TL mechanism involves charge transfer from the impurities to vacancies, forming V-type centers, mainly V_{Al}; these centers are identified by their low stability, which corresponds to the rapid fading of TL peak 1 in that material. Other trapping centers, such as V_{Fe} are possibly related to the sensitization effect in these samples.

In the Spicer crystals, the proposed TL mechanism is charge transfer between the Fe^{3+}, Mn^{3+} and V^{3+} ions and V-type centers mostly the intrinsic V^{-} centers, the stability of which corresponds to the slow fading observed in that material.

The sensitization of TL peak 3 in Norton samples is possibly associated with the conversion of Mn^{2+} to Mn^{3+} where Mn^{2+} ions act as hole traps for that peak. In Spicer crystals, the TL mechanism for Mn is reversed, and Mn^{2+} is identified as a recombination center

The Cr^{3+} R-emission lines are effective only when the high energy UV radiation of 249 nm is employed; this behavior is related to the supralinearity of TL peak 1. While V^{3+} is an activator center, V^{2+} is not a recombination center, but the TL response is a power function of $[V^{2+}]$.

The major activator centers are Fe^{3+} in Norton crystals, and Fe^{3+}, Mn^{3+} and V^{3+} in Spicer samples. The recombination center

common to both samples and to all TL peaks, as revealed by partial TL readings, is the Fe^{2+} ion. The "direct TL" is interpreted as the result of charge transfer mechanisms between impurities in different valence states and V-type centers. This behavior is expected to be generally valid for samples with low total impurity content, while a direct charge transfer between impurities is probably the mechanism in samples with high total impurity content, where the additional effect of concentration quenching of TL is present.

TABLE OF CONTENTS

LIST OF FIGURES

LIST OF TABLES

LIST OF DEFINITIONS AND SYMBOLS

TL_i	Thermoluminescence output in A/g where i indicates the peak number.
T_i	Temperature of peak i in °C.
T_m	Maximum temperature of TL reading, in °C.
I_t	Total irradiance defined as the radiant flux density at a given distance from the center of a source, integrated in time, whose units are Watt-sec/cm^2 (Ws/cm^2).
Δt_{UV-TL}	Time interval between a UV exposure and a TL reading.
β	Heating rate in °C/s.
OA	Optical Absorption.
ESR	Electron Spin Resonance.
IR	Infrared
R_1	Ratio between the impurity concentration before the UV exposure and the impurity concentration after the UV exposure.
R_2	Ratio between the impurity concentration after the UV exposure and after the TL reading.
R_2-T_m	Same as above, but TL reading carried out up to temperature T_m.
R_3-T_m-T_m'	Ratio between the impurity concentration after TL reading carried out up to T_m, and the impurity concentration after TL reading carried out up to T_m', where $T_m' > T_m$.
r_{12}	Ratio between TL peak 1 and TL peak 2 outputs.
r_{13}	Ratio between TL peak 1 and TL peak 3 outputs.
r_{14}	Ratio between TL peak 1 and TL peak 4 outputs.
$\alpha(\lambda)$	Optical absorption coefficient in cm^{-1} at a given wavelength λ in nm.

$\alpha_{ieff}(\lambda)$	Effective absorption coefficient in cm^{-1} for TL peak i at a given wavelength λ in nm.
h	Holes.
$\underline{h}$	Planck's constant.
e^-	Electrons.
Treatment a)	Non-monochromatic exposure to UV light type ii).
Treatment b)	UV exposure to 249 nm, I_t = 0.2 Ws/cm^2.
Treatment c)	UV exposure to 289 nm, I_t = 0.2 Ws/cm^2.
Treatment d)	Non-monochromatic exposure to UV light type i), I_t = 27.6 Ws/cm^2.

ACKNOWLEDGMENTS

The author wishes to express her sincere appreciation to her advisor, Professor Thomas Stoebe, for his constant encouragement and support in the accomplishment of this work. She also wishes to thank Professors Y. K. Rao and O. J. Whittemore for valuable discussions and permission to use some of their equipment. In addition, special thanks are due to Misses Vera Lima and Elisa Lima for their assistance with some of the TL measurements.

The author thanks the Instituto de Pesquisas Energéticas e Nucleares and the Fundaçaõ de Amparo à Pesquisa de Saõ Paulo, Brasil, for their financial support. The support of the U.S. Bureau of Radiological Health, U.S. Department of Health, Education and Welfare, for program support through grant FD00639-09, and for the loan of the EG & G radiometer is also acknowledged with thanks.

Finally, the author wishes to express her gratitude to her family and friends for their understanding and moral support.

Chapter 1

INTRODUCTION

1.1 Thermoluminescence in Solids

The thermoluminescence (TL) of a material is characterized by the emission of light occurring when an irradiated solid is heated. A more correct term would be thermostimulated luminescence, to imply that the emitted light is not created by heat, but is the result of the energy stored by radiation which is released by thermal excitation.

Emission of light is also observed when a material is subjected to an electron beam or to mechanical stresses, to mention only a few of the modes of excitation. In the first case, the process is called cathodoluminescence (CL) and in the second, triboluminescence.

TL materials, called phosphors, are in general ionic crystals, in which the valence band is completely occupied and the conduction band is empty. These bands are separated by a gap of forbidden energy levels, which is about 8.7eV in MgO (1). On the other hand, impurities and lattice defects always present in the crystal introduce metastable energy levels in the energy gap, which are called traps. These may be associated with color centers defined as a special electronic configuration responsible for absorption bands in the otherwise transparent region of the crystal (2).

When the crystal is exposed to ionizing radiation such as X- or γ-rays, band to band transitions occur. This is illustrated in fig. 1a where the electrons from the valence band go to the conduction band leaving holes behind. Both charges are free to wander until they become trapped in the metastable energy levels, which are supposed to be empty before irradiation. Traps labeled S are shallow traps and those labeled D are deep traps. During the heating process, the probability of either charge being released increases with temperature. In fig. 1b the electron goes to the conduction band and recombines with a trapped hole, for example, emitting light in the process. If the holes are thermally more unstable than the electrons, the emission occurs as shown in fig. 1c. The recombination process may involve other centers in addition to holes, and these entities are generally called emission centers. There are cases, though, where the recombination can occur by radiationless transitions, where the energy is released as phonons to the lattice, thus decreasing the efficiency of luminescence (3). The recombination sites that cause this type of transitions are called "quenchers."

When the crystal is exposed to UV light, band to band transitions cannot occur, since the UV energy, usually between 3eV and 6eV, is lower than the energy gap. In this case, a description of the mechanism must assume that there are already filled traps below the conduction band which can be activated by UV light. There are two ways that this can be achieved. One possible situation,

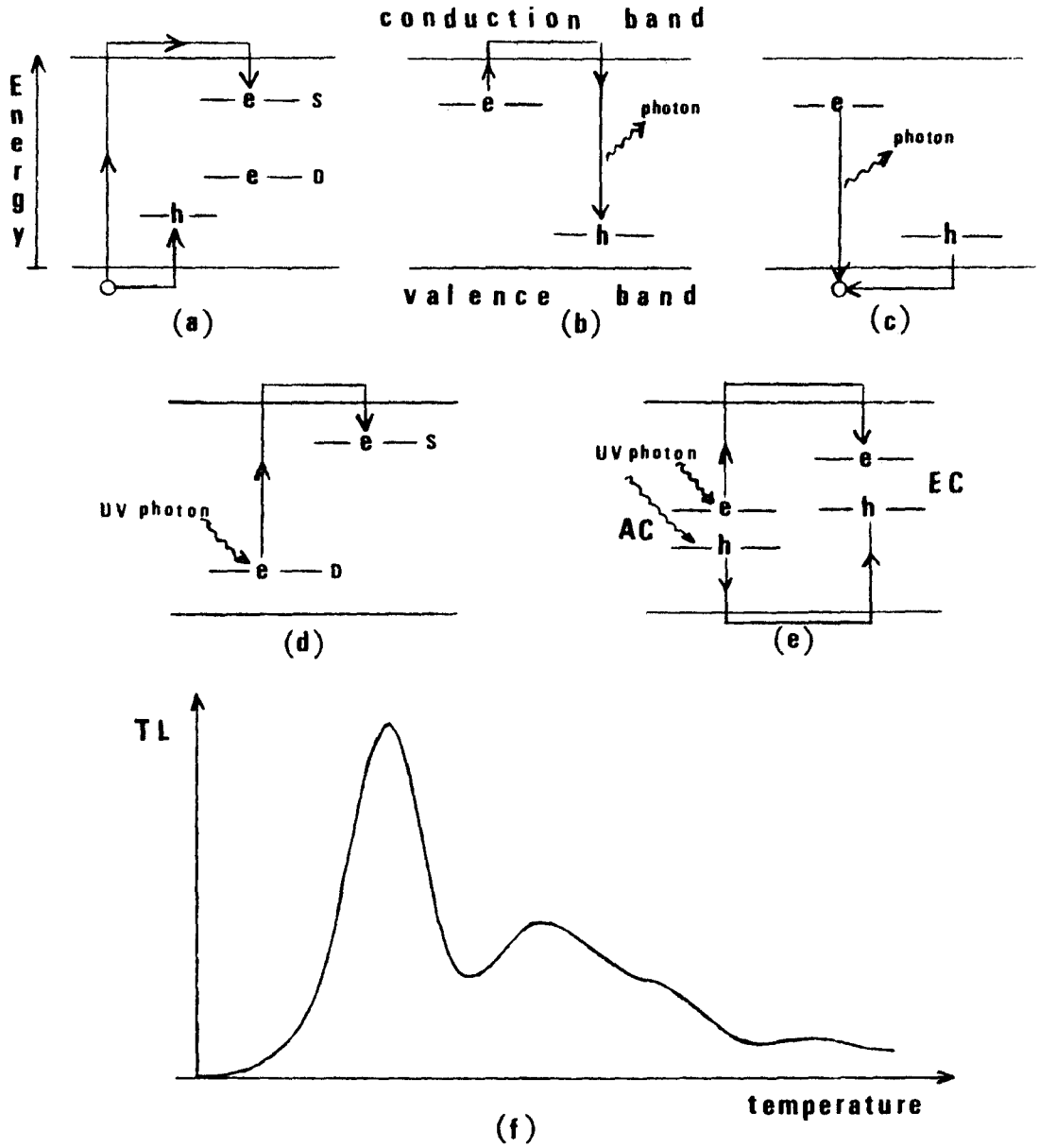

Fig. 1. Schematic representations of the TL process. (a) Irradiation traps charges in metastable states; S and D are shallow and deep traps, respectively; e are electrons and h are holes. (b) and (c) Recombination of charges during heating causing photon emission. (d) UV excitation transfers charges from deep to shallow traps. (e) UV excitation transfers charges from activator centers, AC, to emission centers, EC. (f) TL glow curve: TL output vs. temperature.

shown in fig. 1d, is to have filled deep traps as a consequence of high-energy radiation, where the charges can be transferred by UV light to shallow traps via the conduction band (4). A second possibility shown in fig. 1e, is to have activation centers, called activators, already present in the energy gap as a characteristic of the material. These include, in general, impurities that can change their valence state, such as the rare-earths in CaF_2 (5). When the UV light excites these activation centers (AC), the charges, either electrons or holes, are captured in trap centers. Subsequent heating produces luminescence, as already explained in figs. 1b and 1c. There is also a possibility for recapture to occur, where the recombination or emission center (EC) would be the activator itself. In all processes shown, the centers were considered to become ionized, but it is also possible to have tunneling processes where the charges are trapped without passing through the conduction band.

The emitted light measured as a function of temperature constitutes the TL glow curve. It has been said that the TL glow curve is the parameter that best characterizes the material. The TL emission spectrum, however, is a better characterization since it permits an analysis of the emitted wavelengths as a function of temperature.

A typical glow curve is shown in fig. 1f. The emitted light intensity is low in the beginning, increases with temperature up to a maximum and decreases again, composing one of the TL peaks. The temperature of the TL peak is where the maximum amplitude occurs.

Each peak is associated with a different trap in the energy gap: the low temperature ones are associated with shallow traps and the high temperature ones, with deep traps. The build-up of the emission into a peak is a consequence of the escape probability of the charge from its trap. When the temperature is lower than the peak temperature, few charges are released, and the emitted light is weak. Heating the crystal further, the escape probability increases, more charges are released and the intensity increases, reaching a maximum. Beyond this point, the intensity decreases due to fewer charges remaining in the traps.

The shape of the glow curve depends on the host crystal, the impurities and defects incorporated, as well as the heating rate, thermal history and radiation treatments, as discussed in more detail in later chapters.

1.2 Objectives of This Research

Magnesium oxide, MgO, is a thermoluminescent (TL) material sensitive to X-rays (6,7), γ-rays (8,9) and ultraviolet light (UV) (7,10). As a UV detector, MgO is "direct reading" (11), meaning that following UV exposure, a signal is obtained without prior ionizing radiation. This differs from the UV sensitivity of materials such as CaF_2 (12,13), where the TL depends on prior irradiation and the mechanism is that of TL transfer, an indirect process. Both the "direct" TL response and the high sensitivity are major factors which make this solid a potential candidate for application in UV dosimetry.

It is likely that the direct TL property is related to the presence of one or more impurities, the identity and concentration of which are not yet known. Much has yet to be done to understand the basic TL mechanisms in MgO, especially concerning the identification of the emitted light during TL with specific impurities and defects in the lattice. These entities all play an important role in the TL sensitivity and so far there has been no explanation of the fact that the highest available purity of MgO is more sensitive to UV light than less pure MgO samples. There has been evidence for a mechanism of direct valence conversion between impurity ions in MgO (14) to explain the TL emission.

The specific objectives of this research are threefold: to investigate the charge transfer mechanisms in MgO as a result of the UV irradiation; to study the sensitization phenomenon and the TL sensitivity to UV radiation and their dependence on impurity content; and to correlate these observations on TL sensitivity with the charge transfer mechanisms.

The first objective, which is to determine the charge transfer mechanisms, is achieved by measuring the changes in concentration of impurities and related defects, due to UV irradiation and TL reading, using electron spin resonance (ESR), optical absorption (OA) in the UV and visible regions, and infrared (IR) techniques. Since the valence state of the impurities is believed to be important in the TL process, heat treatments in controlled atmosphere, which are known to change these valence states, are performed in

conjunction with TL, ESR, OA and IR to allow determination of the defect states responsible for the observed behavior.

The second objective is met by studying the sensitization phenomenon of samples heat treated in different ways, the reproducibility and stability of the TL response, the relationship between TL and the total UV irradiance, and the TL excitation spectrum. The TL sensitivity as a function of the impurity content is investigated using the techniques mentioned above.

Finally, to satisfy the third objective, a complete characterization of lattice defects in MgO is attempted in order to determine the TL mechanisms involved in the direct TL response. This is done using correlations between the variations observed in impurity concentrations and the TL response to UV light. This enables the proposition that reactions among impurities and defects are believed to be operative under UV light and subsequent TL readout. This characterization and the determination of mechanisms of TL in MgO comprise the objectives of this research.

Chapter 2

PROPOSED MODELS

The optical and magnetic properties of MgO have been studied extensively using ionizing radiations such as X-rays (6,7,15-17) and γ-rays (8,9,18-20), and UV light (7,10,11,14,16,21). Changes in impurity related properties using different heat treatments have been also investigated (22-26).

Charge transfer between different valence states of iron, chromium and vanadium ions, among other impurities, and V-type centers, is believed to play an important role in the TL mechanisms. These valence changes can be detected using ESR (16,23,24,27), magnetic circular dichroism (MCD) (24,27) and OA measurements (15,22,24,28). The current understanding of these effects and their role in TL in MgO are discussed below.

2.1 V-Type Centers

The most common defects encountered in MgO are the V-type centers. They all absorb near 540 nm (2.3eV) (29) and in some cases have identical ESR signals. They can be distinguished by their different production rates and thermal stabilities (29-31) or by ENDOR measurements (32). These V-type centers involve cation vacancies and can be intrinsic or associated with impurities. Possible configurations are represented in fig. 2. The V^- center (33) was originally identified and called H_1 or V_1 by Wertz et al. (34)

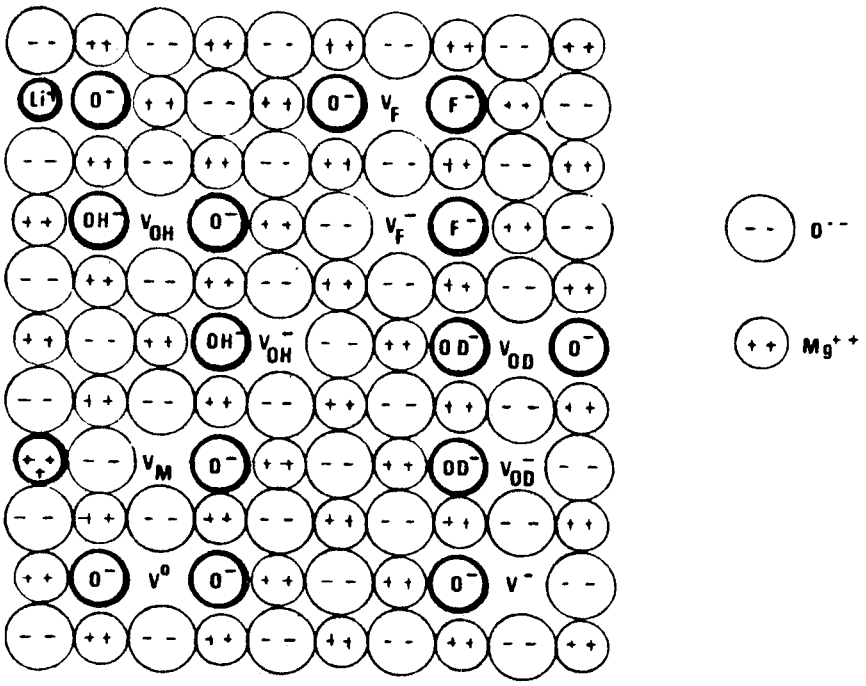

Fig. 2. Models for V-type centers in MgO. From the top left: Li° is a neutral center composed of Li^{+} and a hole trapped at an oxygen ion; V_F and $V_{\bar{F}}$ are cation vacancies associated with a fluorine ion F^{-}, the former having a hole trapped at the oxygen ion; V_{OH} and $V_{\bar{OH}}$ are analogous centers with the OH^{-} ion replacing the oxygen ion; V_{OD} and $V_{\bar{OD}}$ are analogous centers involving the deuterium ion; V_M is a vacancy associated to a trivalent impurity M, charge compensated by a hole trapped at the oxygen ion; V^{-} and V° are vacancies with one and two holes trapped at oxygen ions, respectively.

who considered it to be a hole trapped at a cation vacancy. Because of its axial symmetry, however, it has more recently been interpreted as a hole trapped at one of the O^{2-} ions surrounding the vacancy (23,25). The V° center (36) contains two trapped holes; related centers such as V_F^-, V_{OH}^- and V_{OD}^- have an F^-, OH^- or OD^- ion replacing the O^{2-} ion adjacent to the positive-ion vacancy and opposite to the O^- ion; they become V_F, V_{OH} and V_{OD}, respectively, when there is a trapped hole at the vacancy (29,32). The V_M center, where M is usually a substitutional trivalent ion, consists of a V^- center adjacent to the impurity ion. ENDOR has been used with success to identify the V_{Al} center and distinguish it from the V^- center (30,32), both of which have identical g-values in ESR.

The 540 nm absorption has been observed in MgO exposed to X-, γ- or UV radiation (37) and attributed to the V^- center. Abraham et al. (30), after studying the stability and formation of V^- and V_{Al} centers, point out that the V^- center, that had been previously reported as decaying at room temperature, was misinterpreted by researchers and is really the V_{Al} center. They also say that the V^- centers are produced by energetic particles, such as neutrons or electrons and are very stable at room temperature. They show that the mechanism of production is inconsistent with a knock-on production of Mg^{2+} vacancies and that the center can be produced by ionizing radiation of quite low energy. Nevertheless, Ziniker et al. (21) were unable to detect the V^- center under UV excitation, explaining that the energy is too low as compared to

X-rays, to produce a measurable amount of these centers. This seems to be reasonable, since they used samples in the "as received" condition, that is, without prior heat treatment. It has been observed, on the other hand, that the V^- center concentration is enhanced if the crystals are rapidly quenched from 1000° C (18), leading to an increased proportion of isolated vacancies (36).

The ESR spectrum of the V^- center is characterized by two absorptions, at $g_{\parallel} = 2.0032$ and at $g_{\perp} = 2.0385$. The amplitude of the latter is twice the amplitude of the former when the angle between the strong magnetic field and a principal axis is zero, due to the axial character of the center. Usually, this ESR signal is measured at 77K, since increasing the temperature up to 298K causes the linewidth to broaden by a factor of about 30 (34,36). Kappers et al. (36), who irradiated their samples with neutrons and subsequently with X-rays, say that the V_{Al} lines appear at the same position at 77K and 298K but that the intensity at 298K is 900 times smaller than at 77K. For the V^- center above 245K, only a single isotropic line appears for which $g_{iso} = 1/3\ (2g_{\perp} + g_{\parallel})$. By means of ESR and OA, Kappers et al. (36) studied the thermal stabilities of the V-type centers, concluding that V° centers decay by loss of one hole producing a stable V^- center, and that the V_M center presumably also decays by loss of a hole; both V° and V_M centers have decay constants of the same order of magnitude. A plot of $[V_M]$ against time shows two linear segments corresponding

to half-lives of 10.5 and 15.4 h. Luthra et al. (8) point out the striking similarity between the decay behavior of V_M centers and that of the 97° C glow peak. In an earlier work by Kappers et al. (31) the distinction between the V^- and V_{OH} centers is made, again because of their different thermal stabilities. V_{OH} is the less stable center of the two with a half-life of about 10 h.

The theory of a continuous energy distribution of traps once suggested by Soshea et al. (15) could be related to the different thermal stabilities of the V-type centers. Abraham et al. (30) report the presence of very stable V^- centers which vanish only after a 527° C annealing and in some cases, can be seen even after a 1227° C annealing followed by ionizing radiation. In subsequent work by the same group (29) they discuss the formation of these centers as being dependent on the presence of hydrogen ions, more specifically on the V_{OH}^- and V_{OD}^- initial concentrations. The mechanism would be the displacement of hydrogen at the V_{OH}^- site by intense ionizing radiation.

Infrared measurements have been helpful in identifying centers due to the OH-bond stretching vibration. Absorption lines at 3296 cm^{-1} and 3323 cm^{-1} have been interpreted as being due to V_{OH}^- and V_{OH} centers, respectively (29,38,39). A line at 3310 cm^{-1} was assumed to arise from V_{OH} centers associated with Fe^{3+} or Cr^{3+} impurities (38), but others reject these ions for Al^{3+} or Ca^{2+} (39). Henderson and Sibley (39) say that Fe-doped samples annealed at 1010° C in air followed by quenching show bands at 3296 cm^{-1},

3310 cm^{-1} and 3560 cm^{-1}, the latter being attributed to $Fe(OH)_2$ precipitates. Glass and Searle (38), on the other hand, report an intense line at 3550 cm^{-1} in MgO doped with Cr and V. A band at 3670 cm^{-1} was seen (39) in Co-doped samples, due probably to $Co(OH)_2$ precipitates. $Mg(OH)_2$ precipitates are responsible for a band at 3700 cm^{-1} and, as they dissolve with increasing temperature, the OH^- and OH^--M^{3+} associate centers increase in concentration as reflected by the increase in the 3296 cm^{-1} and 3310 cm^{-1} bands. A weak absorption at 1600 cm^{-1} superimposed on the increasing absorption near the MgO reststrahlen was observed in Ni^{2+} doped crystals.

The IR spectrum was not changed after UV irradiation according to Glass and Searle (38).

Analogous to the OH-centers, the OD-type centers involving the deuterium ion absorb in the region 2400-2800 cm^{-1} (29,39).

As opposed to V centers, other defects exist involving anion vacancies, and are called F-type centers. These are not normally seen under X, γ or UV radiation as V centers are, but can be produced by additive coloration (40), and electron or neutron irradiation (41). The F^+ center has one trapped electron at the oxygen-ion vacancy, while the F center has two trapped electrons. Both have a characteristic absorption band around 250 nm (41).

2.2 Control and Measurement of Transition-Metal Impurity Ions

It is well known that heating MgO in an atmosphere of CO (24,28), 94% N_2 and 6% H_2 (25), or vacuum (23), or the passage of electric current at high temperature (42), causes Fe^{3+} to reduce to the divalent state. This reduction is reported in the interval 1200°C-1500°C as being almost complete, about 99% (25), or reaching an equilibrium value (23) represented by the ratio Fe^{3+}/Fe^{2+}. At the early stages of reduction the spectra of V^{2+} and Cr^{3+} are respectively weakened and enhanced, indicating that V^{2+} and Cr^{2+} oxidize to V^{3+} and Cr^{3+} while Fe is being reduced. The over-all process can be summarized by the equation:

$$M^{2+} + Fe^{3+} \rightleftharpoons Fe^{2+} + M^{3+}$$

For prolonged treatments, however, the tendency is to have also Cr^{3+} and V^{3+} reduced to the divalent state. By heating in air or oxygen, the reverse process occurs, that is, Fe^{2+} converts to Fe^{3+}, but the conversion is not complete, as approximately 20% to 40% of Fe^{2+} remains (24,25).

Optical absorption and especially ESR, when supported by calculations in crystal field theory, are powerful techniques to study these impurities in different configurational symmetries. A review of optical properties related to the transition metal ion impurities in MgO is found in reference (43).

Henderson et al. (44), using ESR, report an axially symmetric spectrum of Fe^{3+} in MgO, arising from the presence of next

nearest neighbor vacancies along the [100] direction. The $g_{\parallel}$-value for this axial center is 2.0037 and, therefore, coincident with the g-value of the octahedral Fe^{3+} ion. The effective $g_{\perp}$-value is reported as 5.860. Wertz et al. (16) summarize the principal ESR lines of impurity ions, including those of Cr^{3+} in cubic, axial [100] and rhombic [110] sites where a positive vacancy near a Cr^{3+} ion causes the lowering in symmetry. Larkin et al. (45) identified Cr^{3+} in the three configurations above by measuring the optical absorption in MgO doped with Cr. Different field symmetries associated with ions such as Fe^{3+} and Cr^{3+} could play an important role in the charge transfer mechanisms.

The absorption bands at 210 nm and 285 nm have been assigned to Fe^{3+} through ESR and MCD by Cheng and Kemp (27). Thorp et al. (46) and Modine et al. (24) report a band at 970 nm due to Fe^{2+}; its ESR signal can be detected only at 4K, and that of Fe^{1+}, at 20K (16). Davidge (28), on the other hand, measured the OA of oxidized crystals and found a broad band at 1000 nm which he attributed to clusters of Fe^{3+} and vacancies. He also determined a linear relationship between the 285 nm band's absorption coefficient and the concentration of Fe^{3+}. This correlation can be expressed by $N = 1.0 \times 10^{17}\alpha$, where α is the absorption coefficient in cm^{-1} and N is the number of Fe^{3+} ions per cm^3. There is also evidence that for concentrations up to 300 ppm, 90% of the Fe^{3+} is present as single unassociated ions; the remainder occur as some form of cluster.

Wertz et al. (16), Krishnan (47) and Hansler and Segelken (22) report the decrease of Fe^{3+} concentration upon UV excitation, using ESR. An increase in Fe^{3+} concentration is observed, however, if the crystal is first subjected to a reducing treatment (15,16).

It is more difficult to reduce Cr^{3+}, which is the more stable state for Cr at room temperature. Haxby (48) and Wertz et al. (23) report, respectively, that Cr^{3+} can be reduced by X-irradiation and by treatment with lithium vapor. Weeks et al. (42) were able to reduce almost all Cr^{3+} by the passage of electric current (1000V/cm) in an atmosphere of air in the range 950° C-1250° C. Cr^{3+} (49) and V^{3+} (50) are reported to have absorption bands at 450 nm and 620 nm. The excitation spectrum of V-doped MgO shows that V^{2+} absorbs at 502 nm and around 714 nm (50). Wertz et al. (16) also report an absorption band at 310 nm due to V^{2+} and at 288 nm due to Cr^{3+}. Modine (51) studied V-doped crystals and assigned to V^{3+} the bands at 240 nm, 414 nm and 620 nm measured at room temperature. A possible explanation for the difference between Sturge's band at 450 nm and the 414 nm band is a perturbation due to charge-compensating vacancies. V^{3+} was undetected by ESR technique.

Although it has been observed that Fe^{3+}, Cr^{3+} and V^{2+} change valence depending on the treatment, it is generally accepted that the valence state and concentration of Mn^{2+} does not change upon heat treatment, X-irradiation or UV excitation (16,22,23,47). It does not change after passage of electric current at high

temperature either (42). On the other hand, other valence states have been reported in MgO, such as Mn^{4+}, which is known to be stable only in Li-doped samples (38,52). Challis et al. (53) concluded indirectly that 1 to 2% of Mn in Mn-doped MgO is found in the trivalent state, using thermal conductivity measurements and the dynamic Jahn-Teller theory. This work quotes Koidl and Blazey (54) who associate an absorption band at 520 nm to Mn^{3+} and which decreases with reducing heat treatment. This ion can also be detected in Al_2O_3 by its optical spectrum (55), for which a mechanism where UV light converts Mn^{4+} to Mn^{3+} by electron capture has been proposed. Sibley et al. (19) show in their fig. 3 that the concentration of Mn^{2+} changes with heat treatment at different temperatures in deformed and γ-irradiated MgO.

Other impurities, besides those mentioned above, are known to be present in nominally pure MgO. Although their concentration is much smaller, they could have an effect in the TL behavior. This will be dealt with later in this chapter.

2.3 Characterization of TL and Proposed Models

MgO has been investigated (10,11) as a possible candidate for UV dosimetry for its property of direct TL reading. This means that the low ionizing energy of the UV radiation is enough to induce TL without a pre-exposure to higher energy radiations such as X- or γ-rays. This indicates the importance of investigating charge transfer mechanisms in the TL process in MgO.

Much controversy exists as to a standard treatment in MgO, such as the 400° C, 1 hr. treatment used in LiF (56) to reset the sample to its original condition so that experimental reproducibility can be achieved. Ziniker et al. (21) mention that a prolonged heating at 423° C restores the MgO crystal to its former condition. Krishnan (47) says that this can be achieved by heating at 340° C for one hour. Luthra et al. (8) heated their samples at 147° C for 30 min. before using them for different experiments. Takeuchi et al. (10) obtained good reproducibility when their samples experienced an UV pre-irradiation followed by heating at 250° C. Dhar (11) states that such a heat treatment is not necessary, for reproducibility is within 5% in a test where repeated monochromatic excitation and TL measurement was carried out without intermediate sensitization or heat treatment. While this may be valid for low intensities of UV exposure, the TL sensitivity could decrease for higher intensities, as is the case for CaF_2 (4).

One important aspect in developing a UV dosimeter is the characterization of the TL excitation spectrum. Ziniker et al. (21) reported a general increase in efficiency of TL excitation with decreasing excitation wavelength, with maxima at about 290 nm and 250 nm, in an experiment where no corrections for absorbance were made. Kirsh et al. (9) measured the TL excitation spectrum between 110 nm and 300 nm for γ-irradiated and non-irradiated MgO, the former showing bands at 125 nm (10eV), 268 nm and 280 nm, and the latter, at 118 nm (10.5eV). They observed a structure in the 160-170 nm

range, which seems to correspond to the exciton spectrum. No special feature was seen at 143 nm (8.7eV), accepted as the value of the energy gap in MgO. Dhar (11) obtained a flat TL response in the range 280-320 nm, and in one case a maximum at 285 nm.

The temperatures of the TL peaks in MgO vary from sample to sample depending on the supplier, but are generally reported in the range that goes from room temperature to 200° C (10,21,47). The peak of lower temperature is called the dominant peak and has been observed by several workers at different temperatures ranging from 78° C to 145° C (6,15,21). In many cases this peak is actually composed of two overlapping peaks (21). In addition to the dominant peak, two other peaks of lower intensity appear, their temperature being also sample-dependent. In addition, several peaks have been reported at higher temperatures (21), especially after γ- and neutron irradiation (8). One particular peak at about 387° C was said to emit in the red above 700 nm (21) and to be non-reproducible. Luthra et al. (8) suggest that this peak could be due to the transfer of charges between the adsorbed oxygen ions and surface defect centers.

Deformation studies have been carried out in MgO which could lead to important consequences in the interpretation of the TL results. Sibley et al. (19) and Newton and Sibley (57) observed an optical absorption band at 215 nm, formed after deformation of the crystal, which is proportional to the percentage of deformation. A blue TL emission was observed (57) at about 430 nm in deformed

samples exposed to either 235 nm or γ-rays. The intensity of this peak increases with percentage deformation, and part of the emission is attributed to deformation induced by sample cleavage. No increase with deformation was seen for the red emission due to Cr^{3+}. Absorption and emission bands have a composite character, indicating different types of defects involved in deformation. Chen et al. (58) note that plastic deformation induces enhancement of trapped-hole defects in MgO which contains OH ions. Specifically, it produces defects which serve as effective electron traps during ionizing radiation such that more holes can be captured by V_{OH}^{-} sites to become V_{OH} centers, the same occurring for V_{Al} and V_F.

Datta et al. (59,60) used the cathodoluminescence (CL) technique to study the emission spectra of deformed and undeformed MgO crystals. They were very careful about correcting the spectrum, taking into account instrumental losses. The undeformed material shows two bands at 425 nm and 488 nm. After deformation, one band at 466 nm is seen. Panchromatic and monochromatic micrographs show that this band comes from the slipped planes of the crystal. Near the infrared, a broad band with unresolved peaks, the strongest at 726 nm, is detected, which is not affected by deformation and is thought to be due to iron impurities. Annealing treatments in air, CO or H_2 were carried out to change the valence state of iron. Oxidation produced changes in the blue emission but not in the red, and reduction had the opposite effect. The relative intensity of the red and blue bands increased with annealing time in the reducing

and oxidizing atmospheres, respectively. The origin of bands at 645 nm, after CO heat treatment, and at 490 nm, after air heat treatment, is still unknown.

One of the earliest works that attempted to establish qualitatively which TL mechanisms were operative in MgO was that by Hansler and Segelken (22). They proposed the following equations and found it convenient to assume the corresponding energy values for the red and blue emissions, based on the difference of the absorption and gap energies:

$$Fe^{3+} + e^{-} \rightarrow Fe^{2+} + 2.9eV \text{ (blue)}$$

$$Fe^{2+} + h \rightarrow Fe^{3+} + 2.0eV \text{ (red)}$$

$$Cr^{3+} + e^{-} \rightarrow Cr^{2+} + 2.7eV \text{ (blue)}$$

$$Cr^{2+} + h \rightarrow Cr^{3+} + 3.6eV \text{ (blue)}$$

They observed three TL peaks after UV irradiation, of which the low temperature one emitted red and blue and the high temperature one emitted blue. Wertz et al. (7) determined conclusively by fluorescence and TL measurements that the last of the Hansler and Segelken equations was actually responsible for the red emission of the R-lines. The TL would occur in stages, involving electrons or holes as follows:

$$Cr^{3+} + e^{-} \rightarrow Cr^{2+};\ Cr^{2+} + h \rightarrow Cr^{3+*} \rightarrow \text{R emission}$$

or

$$Cr^{3+} + h \rightarrow Cr^{4+};\ Cr^{4+} + e^{-} \rightarrow Cr^{3+*} \rightarrow R \text{ emission}$$

Later workers have considered only the first possibility. This process has been confirmed by Sibley et al. (19) and by Ziniker et al. (21).

In addition to the red emission, Wertz et al. (7) also observed a blue emission in X-irradiated samples and concluded that the following process occurs:

$$Fe^{1+} \rightarrow Fe^{2+} + e^{-}$$

$$Cr^{3+} + e^{-} \rightarrow Cr^{2+*} \rightarrow Cr^{2+} + \underline{h}\nu \text{ (blue)}$$

As to the increase in Fe^{3+} concentration seen by Hansler and Segelken between UV irradiation and heating through the dominant TL peak, Wertz et al. interpreted this as:

$$V^{-} \text{ centers} \rightarrow \text{cation vacancy} + h$$

$$Fe^{2+} + h \rightarrow Fe^{3+}$$

They did not assign any color to this reaction, preferring to have the blue component arising from Cr^{2+}, as already seen.

Sibley et al. (19) noticed an increase in Fe^{3+}, Cr^{3+} and V^{2+} concentrations as V^{-} centers annealed out and red and blue luminescence was given off. They proposed the following mechanism for the blue component:

$$Fe^{2+} + h \rightarrow Fe^{3+*} \rightarrow Fe^{3+} + \underline{h}\nu \text{ (blue)}$$

Ziniker et al. (21) were not able to see the blue emission, but they report instead an orange component and attribute it to Mn^{2+}. They say that the TL peaks at 75° C and 193° C emit mostly orange, while the 102° C TL peak emits red. Others (6,19,22) observed instead red and blue luminescence for the dominant TL peak (85° C-94° C).

Krishnan (47) concluded that, since the concentration of Mn^{2+} does not change during TL, the orange component is most likely due to the reactions:

$$V^- \text{ centers} \xrightarrow{TL} \text{cation vacancy} + h$$

$$Fe^{2+} + h \rightarrow Fe^{3+*} \rightarrow Fe^{3+} + \underline{h}\nu \text{ (orange)}$$

in samples with [Fe] > [Cr]. He also reported having seen red emission on 253 nm excitation in samples with high Fe content and, assuming this wavelength releases electrons (61), he proposed that:

$$Cr^{3+} + e^- \rightarrow Cr^{2+*} \rightarrow Cr^{2+} + \underline{h}\nu \text{ (red)}.$$

Using ESR, Krishnan (47) relates an observed increase in intensity in the 197° C TL peak with the increase in Fe^{3+} content and thus with the orange emission. The 92° C TL peak is also associated with this emission, where, besides the increase in Fe^{3+} concentration, he was able to detect a simultaneous decrease in the V^- center population. It is worth remembering that in this context the term V^- center employed up to this time by researchers could involve other less stable V-type centers as already explained.

At this point, it would be interesting to note that such processes as the oxidation-reduction of impurity ions by UV light are known to occur also in other systems, including CaF_2 doped with rare-earths (5).

Williams et al. (62) observed the luminescence of MgO excited by short pulses of 500-keV electrons at sample temperatures from 10K to 500K (227° C). The luminescence bands occurred at 253 nm, 376 nm and 730 nm. For the 253 nm band a theory of tunneling recombination between randomly distributed hole traps and electron traps, possibly OH^{2-} molecular ions, has been proposed. The 376 nm luminescence increased by release of holes from V-type centers and has been suggested to result from hole capture at Fe^{2+}. The 730 nm band is the well known Cr^{3+} R-line.

Takeuchi et al. (6) assumed the observed red and blue emissions as due to Cr and Fe, respectively, in X-irradiated MgO. They report that the blue TL is about 1/100 of the red TL. Also Chen and Sibley (18) saw both colors in the emission at room temperature (afterglow) after γ-irradiation, the red bands being 10 times higher than the blue bands. From the CL measurements of Datta et al. (59) a red/blue ratio of about 300 can be determined. The assumption that the 376 nm luminescence is due to hole recombination at Fe^{2+} ions does not agree with the observation that the luminescence decreases or is suppressed by doping with Fe (17,20, 38). Wertz et al. (7) report that by heating in oxygen, the Fe^{3+} concentration increased and the blue TL decreased.

Takeuchi et al. (14) report a direct valence conversion between iron and chromium impurity ions induced by UV at 150° C, where V^- centers are unstable. They consider the possible role of excitons for the mechanism of reaction. The exciton wave created by UV light would pass a Cr^{3+} ion, the exciton electron would tunnel through to its trapping level giving rise to a Cr^{2+} ion, and would leave a free hole, which, at 150° C could be trapped at an Fe^{2+} ion, resulting in the Fe^{3+} ion.

Luthra et al. (8) comment that although the TL emission varies in all doped samples, the glow curves have approximately the same character, indicating that the trapping centers responsible for TL belong to the host lattice.

As pointed out earlier, there are other impurities that could play an important role in the TL mechanisms besides Fe and Cr, referred to in the models as possible emission centers. As an example, V^{2+} is known to fluoresce at room temperature at 870 nm (R-line) when excited with UV light (50). A pair of lines occurring at 666 nm and 663 nm have been stated to be R-lines of Mn^{4+} (7). X-ray luminescence measurements at room temperature revealed bands in the region 800-935 nm interpreted as due to $Mg(OH)_2$ precipitates (39). Krishnan (47) measured the emission bands at 77K in MgO excited with broad band UV light, and attributed the observed lines at 654 nm and 659 nm to emission from Fe^{3+} in distorted octahedral site, and to Fe^{3+} with a nnn vacancy (FeV center), respectively. The 659 nm line was also suggested (38) as being due to Mn^{4+} vacancy

associates where the reaction taking place was possibly one involving the Mn^{3+} ion, a vacancy and a hole. Ni^{2+} presents sharp emission lines at 77K in the blue region (7) and also a luminescent band at 540 nm in Ni doped MgO (17). In other work (20) utilizing MgO doped with transition metal ions, it was observed that Cr^{3+}, Mn^{2+} and Ni^{2+} act as emission centers while Fe^{3+}, Co^{2+} and Cu^{2+} act as quenchers. The TL emission spectra of undoped MgO showed bands at 400 nm and 750 nm. MgO doped with Mn^{2+} and Ni^{2+} showed additional bands respectively at 600 nm and 490 nm. Only an emission band at 700 nm was seen in Cr^{3+}-doped MgO. The orange emission seen by Ziniker et al. (21) and reported as due to Mn^{2+}, is centered at 610 nm.

Chapter 3

EXPERIMENTAL METHODS

This chapter is divided in two sections. In the first part, a description of the material used and its preparation, and the equipment used for the various techniques will be given; in the second part, the methods of data analysis, and the associated experimental errors and limitations will be presented.

3.1 Materials and Experimental Techniques

3.1.1 Materials

The samples employed in this research were MgO single crystals supplied by the Spicer Co. (from Harwell) and by the Norton Co. Samples from these suppliers differ basically in the total amount of impurities, the Spicer crystals being purer than the Norton ones.

Table 1 relates the different samples used and the concentrations of the impurities, reported as oxides, as determined by spectrographic analysis. The transition metal ions Fe^{3+}, Cr^{3+}, Mn^{2+} and V^{2+} will be of main concern in this work, since they are important in the TL characteristics and can be detected via ESR even at very small amounts. Carbon has been reported (63) to be present in supposedly high-purity MgO in concentrations up to 1%, but so far, there is no evidence of carbon being related to thermoluminescence.

Table 1. Semiquantitative Spectrographic Analysis of MgO

Concentration (ppm)	Fe	Cr	Mn	Si	Al	Cu	Ag	Ca	Ti	Zn	Ni
Spicer											
S-C	<50	<10	<10	<30	150	10	<5	70	<50	na*	<20
S-D	<50	<10	<10	<30	50	<5	—	30	<50	na*	<20
Norton											
NP0	150	<10	<10	<30	150	5	—	150	<50	na*	<20
NP2	110	na*	3	20	60	na*	na*	30	8	20	50
NP3	110	na*	3	20	60	na*	na*	30	8	20	50
ND2	400	20	<10	<30	500	<5	—	70	<50	na*	<20
ND5	230	10	20	na*	2170	na*	na*	na*	na*	na*	na*
ND6	250	<10	<10	<30	250	5	—	70	<50	na*	<20
ND7	470	—	20	na*	330	na*	na*	na*	na*	na*	na*
ND9	170	20	20	na*	430	na*	na*	na*	na*	na*	na*
ND11	200	500	<10	<30	350	<5	—	200	<50	na*	<20

Note:

Each sample, except NP2 and NP3, also contains less than (ppm): 2000-Li, 20-Co, 50-Pb, 2000-Na, 20-Ba, 30-Mo, 100-B, 50-Sn, 100-Sr, 200-Zr.

*Not analyzed for.

The nomenclature utilized for the crystals is as follows: S-X, where S refers to Spicer and X is A, B, C, or D for decreasing sample sizes; all crystals were cleaved from the same block. NPn and ND-n, where N refers to Norton, P is pure, D is other than pure, and n is the number of each boule. Slabs of dimensions between (4.3 x 3.2 x 0.37) mm^3 and (7.8 x 6.4 x 1.60) mm^3 were cleaved from a larger block with chisel and hammer. All the Spicer crystals and one set of Norton samples, NP0, were polished with emery paper nos. 400 and 600 and subsequently with diamond paste of 3 μm and 0.25 μm particle size (64). The surface condition was controlled by examining the surface in a microscope at about 50x magnification. The polishing procedure improved considerably the surface optical condition of the Spicer crystals but not that of Norton. These were used in a series of heat treatments in controlled atmosphere described in the next topic. All samples were wiped in acetone and methanol, dried, wrapped in aluminum paper, put into black envelopes and stored in desicators.

3.1.2 Heat Treatments

Two kinds of heat treatments were performed in the present work. One type used a controlled atmosphere of CO and CO_2 at 1400° C; related experiments were also done in air at 1000° C and 1400° C. The second type of experiment used air at lower temperatures, ranging from 200° C to 400° C. The first type of experiment was carried out in a glowbar furnace, the temperature

being controlled by an ON/OFF proportioning controller. The samples were put in an alumina boat filled with MgO Spicer powder to avoid any possible contamination and thermal shock. The boat was inserted in a mullite tube initially containing N_2 gas, when the temperature had already reached 1400° C. Upon completion of the heat treatment, the furnace was flushed with N_2 gas, and the samples removed and cooled rapidly to room temperature onto a flat alumina block covered with MgO powder. The quenching process usually took from 3 to 5 minutes. The time for each heat treatment varied between 3 h. and 10 h., the longer times being necessary to meet equilibrium conditions. The equilibrium temperature was measured by a Pt-13% Rh thermocouple in contact with the boat and connected to a Hewlett-Packard digital voltmeter. A second thermocouple of the same type was used to control the temperature. The furnace was lined with fiber-frax in an attempt to avoid heat losses. The ends of the tube were closed with fiber and rubber stoppers, and cooled with a water-cooling system.

The atmosphere was a mixture of CO and CO_2. The flow rate, in moles/min., was controlled by two 1/8" flowmeters with tantalum and stainless steel balls for CO and CO_2, respectively. Each flowmeter was calibrated with its respective gas by the soap bubble method. The parameter varied here was the partial pressure ratio P_{CO}/P_{CO_2} which is proportional to the flow rate ratio. The mixing of the gases occurred before they entered the tube and a T-connector permitted either nitrogen or the mixture to flow into the furnace

compartment. The same set-up was utilized for the heat treatments in air, with the exception of the flowing gases.

The second type of heat treatment was carried out in a Marshall furnace with a Barber-Colman 520 solid state temperature controller. In this case, the samples were quenched on an aluminum block.

3.1.3 Optical System

The optical system consisted basically of Hg (200W) and Xe (75W) sources, each in a Schoeffel, LH-150, lamp-housing; a home-made power supply connected to an Electro Powerpacs igniter model 357, or a Shoeffel, LPS-251, power supply; a Jarrell-Ash, 82-410, .25 Meter Ebert monochromator; a Molectron pyroelectric radiometer model PR-100, or an EG & G radiometer consisting of the model 580-11A indicator unit and the model 580-20A detector head; and a dark chamber for the crystals. The schematic design is shown in fig. 3a. Two additional lenses of 4" and 5" focal lengths and 1 1/2" diameter were used, as indicated, to increase the light intensity at the sample position as well as on the radiometer detector head. The monochromator entrance and exit slits had widths of 2.5 mm and 1.0 mm, and in one case (see below, alignment type ii)), 1.0 mm and 0.15 mm, respectively. The linear dispersion was 1.65 nm/mm, yielding a resolution better than 5 nm for the largest slit. A Corning filter, type 7-54, transmitting about 86% at 320 nm and 5% at 240 nm and 410 nm, was used in all experiments

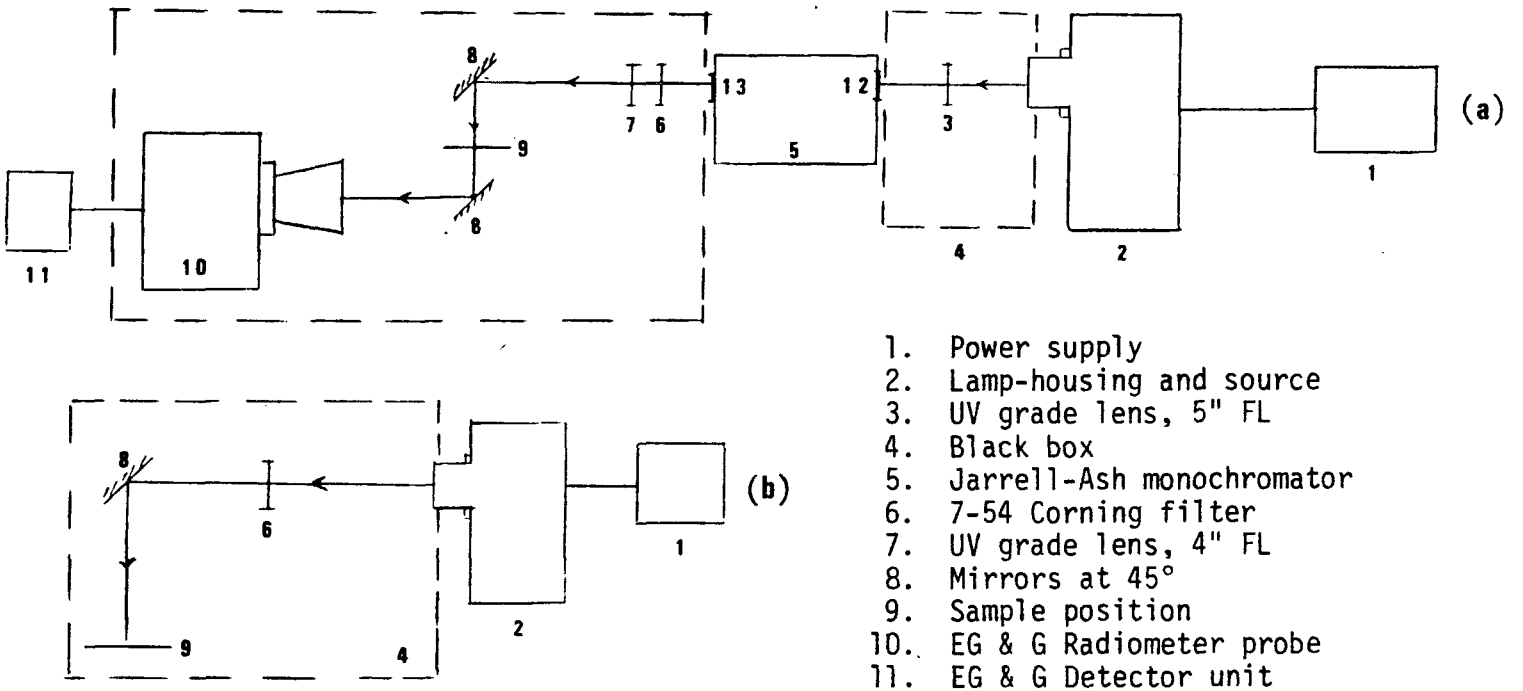

Fig. 3. Optical systems. (a) types ii) and iii), filtered non-monochromatic UV excitation and monochromatic UV excitation, respectively. (b) type i), filtered non-monochromatic UV excitation.

to assure that no visible light was present. Two mirrors, specially coated for better UV transmittance, were placed so to reflect the light on the sample and on the detector head, respectively.

UV irradiation is reported as the total irradiance, I_t, defined as the radiant flux density at a given distance from the center of a source, integrated in time. Its units are Ws/cm^2.

Three types of alignment were employed:

i) filtered non-monochromatic UV exposure: This consisted of the alignment shown in fig. 3b, where the effective UV spectrum is determined by the source spectral output and the filter transmittance;

ii) filtered non-monochromatic UV exposure: This consisted of the alignment in fig. 3a with the monochromator set at 0 nm. This arrangement, along with the smallest set of slits, was used when very low intensities were required. The TL yield at 27.6 Ws/cm^2 was roughly one-fourth that of case i) due to the different optics involved, including the use of lenses which cut off a higher percentage of the lower wavelengths.

iii) monochromatic excitation, using the alignment of fig. 3a.

The total irradiance, I_t, of the filtered UV radiation was monitored with the Molectron probe which had a constant spectral response in the region studied, and at a later stage with the EG & G radiometer. The former measures in W/cm^2, which, multiplied by the exposure time, gives I_t in Ws/cm^2. The monochromatic total irradiance was obtained by measuring the current in A with the EG & G

radiometer. Since the EG & G detector head had a variable spectral response, the conversion from A to W/cm^2 was made through a calibration curve in the range 200 nm-700 nm. The absolute value, in Ws/cm^2, was derived by using the Molectron probe which had a built-in calibration device. The total irradiance at the sample site was estimated as being equal to $I_R \times A_R/A_S$, where I_R is the total irradiance measured by the radiometer, and A_R and A_S are the illuminated areas on the detector head and on the sample position, respectively.

3.1.4 *Thermoluminescence (TL)*

All TL measurements were carried out in a Harshaw TL detector model 2000A coupled to an automatic picoammeter model 2000B. The light that is emitted, while the sample is being heated, is converted into current by a photomultiplier tube (PMT) sensitive in the region 300 nm-670 nm. There is also an infrared filter that transmits about 80% between 370 nm and 550 nm, and about 35% around 800 nm. The current and temperature were recorded in a Leeds & Northrup W/L two pen chart recorder. The TL readings were done in ambient atmosphere. No nitrogen was used since the triboluminescent peak occurred isolated from the TL peaks, at about 375° C. The maximum temperature, T_m, of a given TL run was chosen in the interval 250°C-350°C, no difference in the TL performance of the crystals being noticed. Lower values of T_m were utilized when studying crystals that needed to be partially read-out. The heating rate β was fairly

linear, approximately 1.0° C/s. A correction for the variations in heating rate is presented later in the discussion on experimental errors.

3.1.5 Optical Absorption (OA)

The optical absorption spectrum was measured in a spectrophotometer CARY-14, both in the visible (400 nm-700 nm) and UV (200 nm-400 nm) regions. The optical density, OD, is defined as

$$OD = \log_{10} \frac{I_o}{I}$$

where I_o is the incident light intensity and I is the transmitted light intensity. This formula is only an approximation, for it should include also the reflected light R, as in

$$OD = \log_{10} \frac{\exp(\alpha x_o)}{(1-R)^2}$$

In MgO, $(1-R)^2$ is of the order of 0.85.

The absorption coefficient α is defined in the expression

$$I = I_o \exp[-\alpha x_o],$$

where x_o is the crystal thickness in cm and α is in cm^{-1}. Therefore, α and OD are connected through the relation

$$\alpha x_o = \ln_{10} \times OD.$$

The instrument measures OD in a scale from 0 to 2 as a function of wavelength by comparing the light intensity transmitted by the crystal to that transmitted in air. The baseline, obtained by comparing air vs. air, was subtracted from each absorption curve.

3.1.6 Electron Spin Resonance (ESR)

The spectrometer used in this work, VARIAN model V-4502, operates at the microwave frequency of 9.5GHz, which requires a magnetic field of the order of 3400G to satisfy the resonance condition. The klystron oscillator generates the microwave radiation which is readily propagated in an X-band waveguide. The magnetic component of this radiation must be perpendicular to the static magnetic field Ho, in order for interaction with the magnetic dipoles to occur. To limit noise components while detecting the absorption signal, a field modulation device, operating at 100Kc, is employed, which superimposes an alternating component on the static field Ho, such that the magnetic field passes periodically through the resonant field Hr. To avoid distortion of the lines to be observed, the amplitude of the field modulation should be several times smaller than the width of the absorption line.

A typical spectrometer is represented schematically in fig. 4, according to the function of groups of components. There are four groups, namely:

—the source, which comprises the klystron and the components that control or measure the frequency and the intensity of the microwave beam;

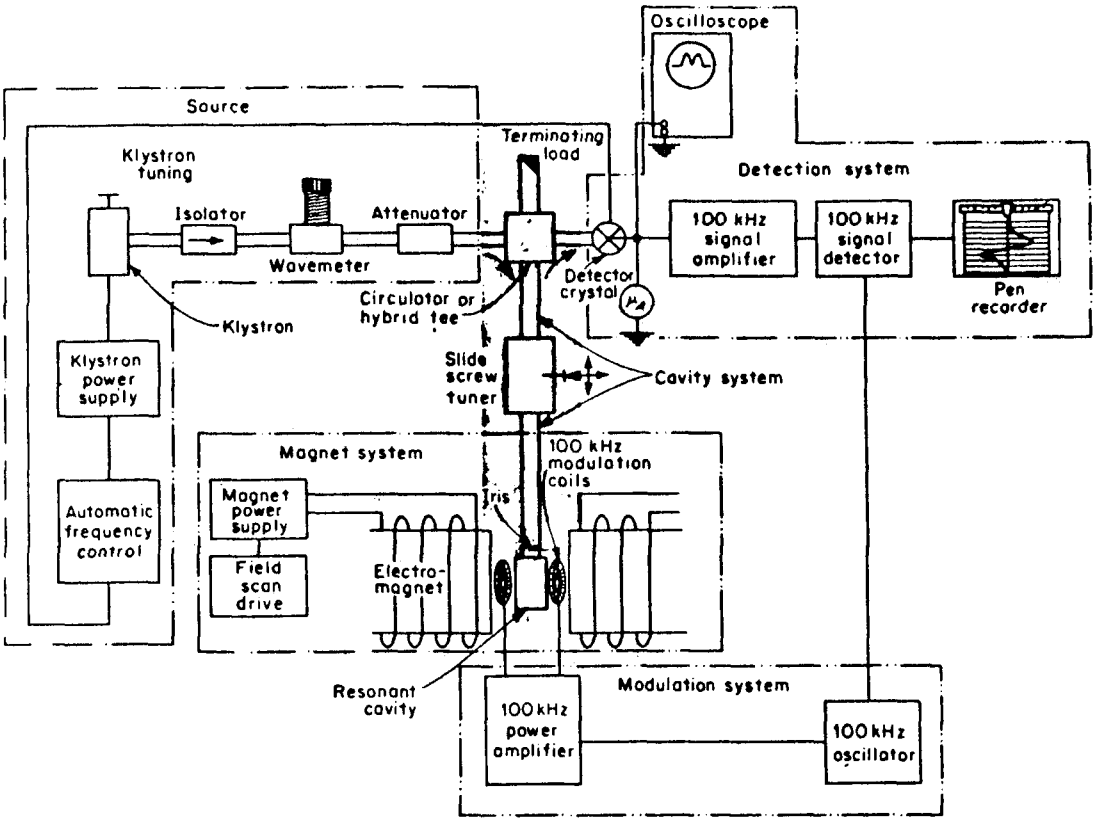

Fig. 4. Block diagram of a typical X-band ESR spectrometer employing 100 KHz phase sensitive detection, from reference 65.

—the cavity system, which includes the components which hold the sample and which direct and control the mocrowave beam to and from the sample;

—the detection and modulation systems which monitor, amplify and record the signal;

—the magnet system which provides a stable, linearly variable and homogeneous magnetic field of arbitrary magnitude.

The sample cavity is connected to the high power arm of the X-band microwave bridge and to the field modulation and control unit. Once the cavity is tuned for resonance, the ESR signal appears as the first derivative of the absorption curve and its amplitude is recorded as a function of the magnetic field Ho. Parameters such as modulation amplitude, field range, time constant, scanning time, were kept constant for each particular impurity being measured; only the signal amplitude was changed as needed. It was found appropriate to set the bridge attenuator at 15db and keep it constant throughout the experiments. References (65), (66) and (67) were extensively consulted, concerning the ESR theory of the transition metal ions in a crystalline field, as well as the experimental aspects of the ESR measurements.

3.1.7 Infrared transmittance (IR)

IR transmittance spectra were recorded in a Perkin-Elmer IR spectrometer in the region 4000 cm^{-1}-600 cm^{-1}. Only a few samples were examined, to verify qualitatively the existence of OH-related

centers. The crystals were measured before cleaving since a thickness of approximately 1 cm was necessary to be able to detect these centers. All spectra were recorded at room temperature.

3.2 Methods of Data Analysis

3.2.1 TL

Typical TL glow curves for Spicer and Norton crystals are shown in figs. 5 and 6, respectively, where the straight line represents the heating rate. The TL intensity was measured by taking the value of the current in A at the maximum of each glow peak, and dividing by the crystal weight, in grams, the units being then A/g. Other similar normalizations were made necessary, as explained below.

The temperature of each glow peak changes from sample to sample. Spicer shows three peaks: peak 1, or "dominant," at about 95° C, and peaks 2 and 3, or "shoulders," at 143° C and 180° C. These temperatures are not necessarily the same ones seen in the figures, but rather an average of all samples read out. Norton has four peaks numbered from 1 to 4, at about 74° C, 126° C, 162° C and 230° C, respectively. The peak temperature varies with heat treatment, as seen in fig. 6b, shifting to higher values when the crystal is heated in air. Chapter 4 will deal with this subject more specifically.

Since a large fluctuation in the TL output among crystals from the same block was observed, it was evident that other

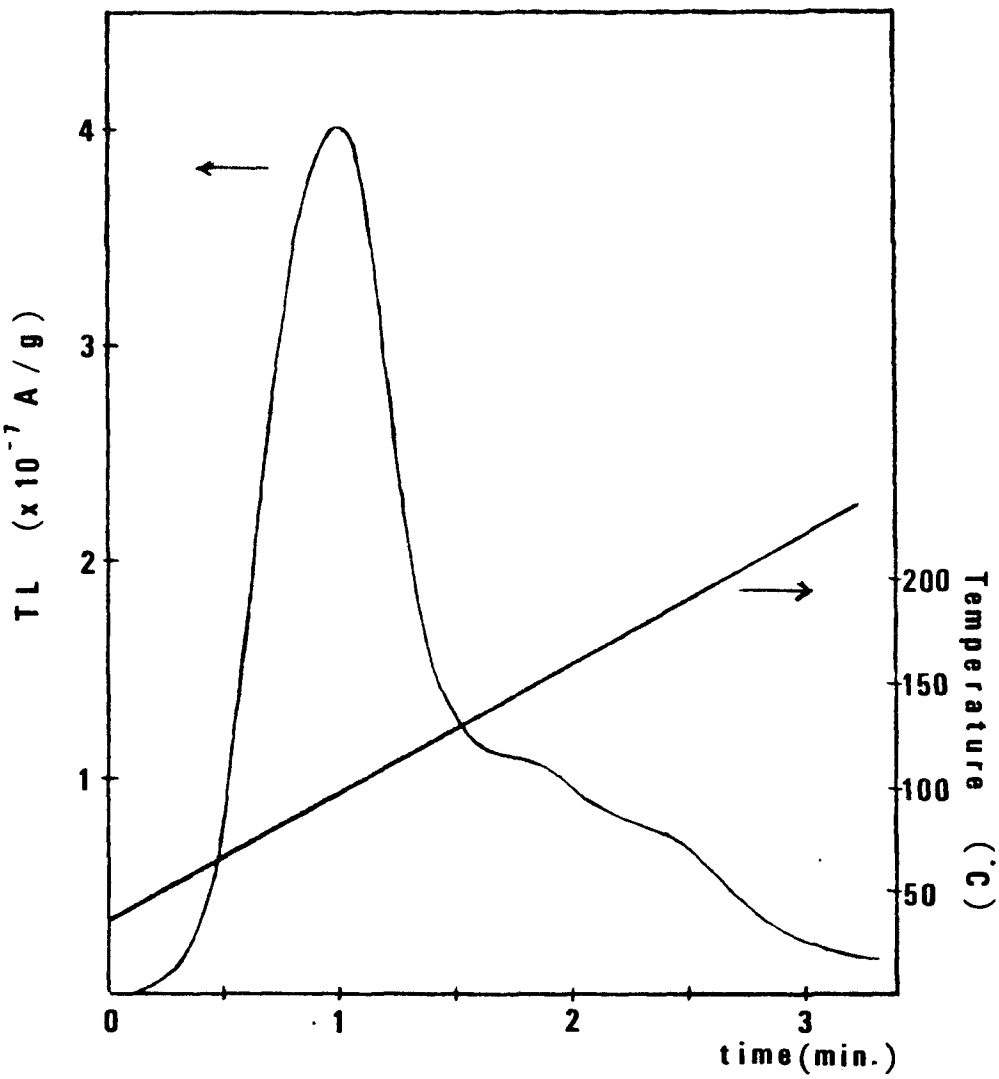

Fig. 5. TL glow curve of MgO, sample S-B6. Filtered non-monochromatic light, type i); I_t = 27.6 Ws/cm^2, β = 1° C/s. Time between UV exposure and TL reading: Δt_{UV-TL} = 24 h. Temperature shown as a function of time for reference.

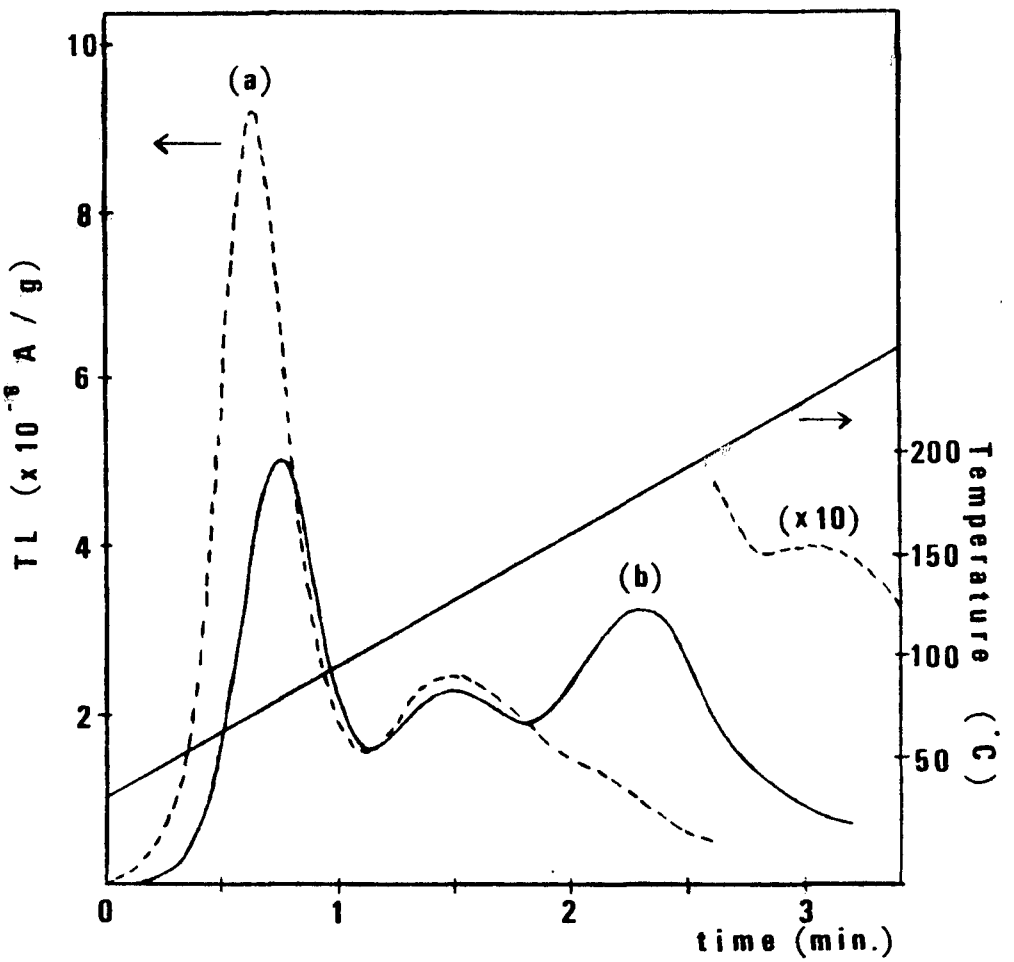

Fig. 6. TL glow curves for MgO, sample NP2-67. Filtered non-monochromatic light, type i); I_t = 27.6 Ws/cm^2, β = 1° C/s. (a) non-annealed; Δt_{UV-TL} = 0 h. (b) air annealed at 1400° C for 3 h.; Δt_{UV-TL} = 4.67 h.

parameters were affecting the results and should be taken into account. One of these is the crystal thickness. In fig. 7, the TL per weight for peaks 1 and 2 of Norton samples is plotted as a function of thickness on a semi-logarythmic scale. It is clear that the thicker the crystal, the lower the TL. The relationship is as follows:

$$TL_i = TL_{oi} \exp [-\alpha_{ieff} (\lambda) x_o]$$

where the subscript i refers to a specific peak, TL_{oi} is a constant in A/g, x_o is the crystal thickness in cm and $\alpha_{ieff}(\lambda)$ is the effective absorption coefficient for TL and, a priori, a function of the wavelength λ. $\alpha_{1,eff}$ was determined, for 289 nm, by the least squares fit as being equal to 8.63 cm^{-1} and $\alpha_{2,eff}$, to 8.91 cm^{-1}. This experiment was repeated, exposing the crystals to broad band filtered Xe light, type i), yielding $\alpha_{1,eff}$ = 12.47 cm^{-1} and $\alpha_{2,eff}$ = 13.29 cm^{-1}. Some TL results in this work have been normalized according to thickness, by dividing the TL per weight by $\exp [-\alpha_{ieff} (\lambda) x_o]$.

Another way of circumventing this problem of thickness dependence of TL was to choose three crystals of approximately the same thickness and use them repetitively in the same experiment, so that more reliable results were obtained. Corrections taking the surface area of each crystal into account showed that no correlation existed. It was observed that at least part of the inconsistency

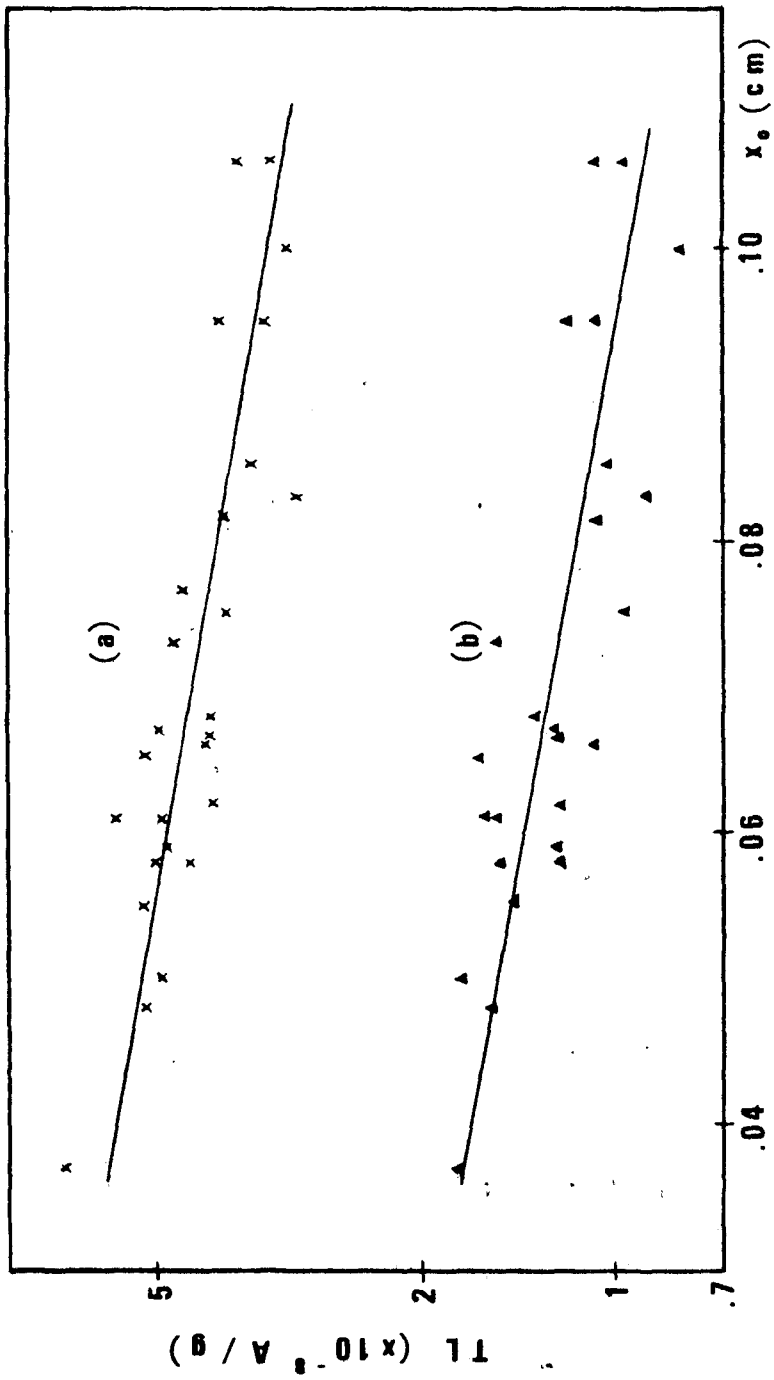

Fig. 7. TL output of a set of samples NP2 as a function of crystal thickness. I_t = 0.2 Ws/cm2; 289 nm. (a) peak 1, (b) peak 2.

in the TL sensitivity can be accounted for by the differences in impurity concentration as measured by ESR.

3.2.2 OA

Figure 8 shows typical absorption curves in the UV region for Spicer and Norton crystals. The bands at 210 nm and 285 nm are due to Fe^{3+} and the absorption coefficient of the 285 nm band was shown by Davidge to be proportional to the concentration of that impurity. In principle, this technique can be used to follow the changes in Fe^{3+} concentration. There are, however, some limitations, as related later.

In the visible region, no absorption bands were detected except for those of Cr^{3+} at 410 nm and 620 nm in samples which had a high concentration of this impurity. These samples were not interesting for our study, however, since no TL was observed under any irradiation condition.

The V-type center, which is known to absorb at 540 nm, could not be detected, probably due to its low concentration; UV light does not seem to be as efficient in populating the vacancies as X-rays (21).

3.2.3 ESR

A characteristic ESR spectrum is seen in fig. 9 for a Spicer crystal, showing the absorption lines for each paramagnetic impurity. Fe^{3+} is a ^6S ion with a six-fold spin degeneracy, producing five lines when subject to a strong magnetic field along a

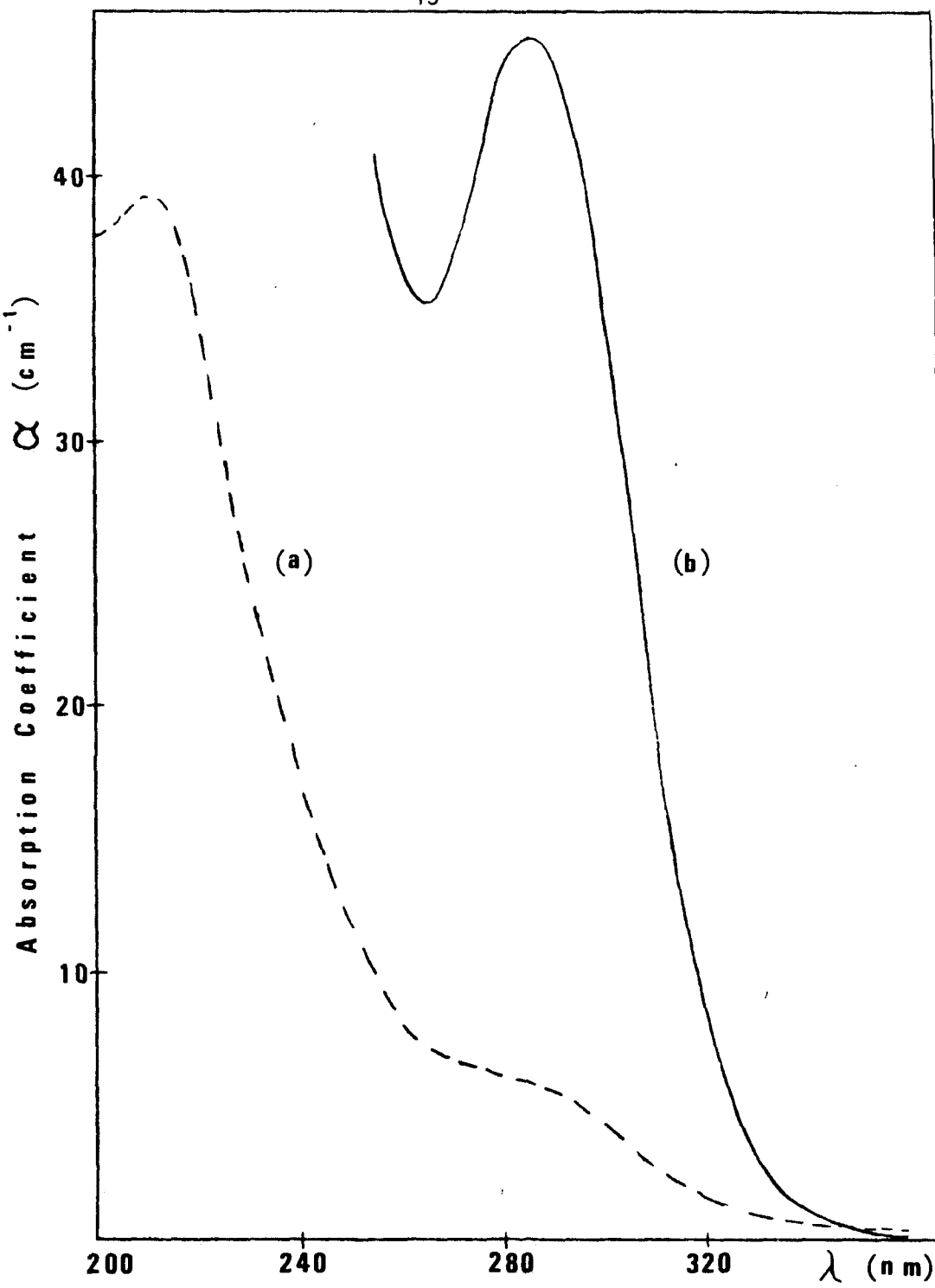

Fig. 8. Optical absorption bands of Fe^{3+} in "as-received" MgO, showing peaks at 210 nm and 285 nm. (a) sample S-A3, x_o = 0.115 cm; (b) sample NPO-40, x_o = 0.098 cm.

Fig. 9. ESR spectrum of sample S-B4 and a schematic representation of the Fe^{3+}, Cr^{3+}, Mn^{2+} and V^{2+} lines. For simplicity, only the first quintet of Mn^{2+} and the last triplet of V^{2+} are shown. $H \parallel [100]$.

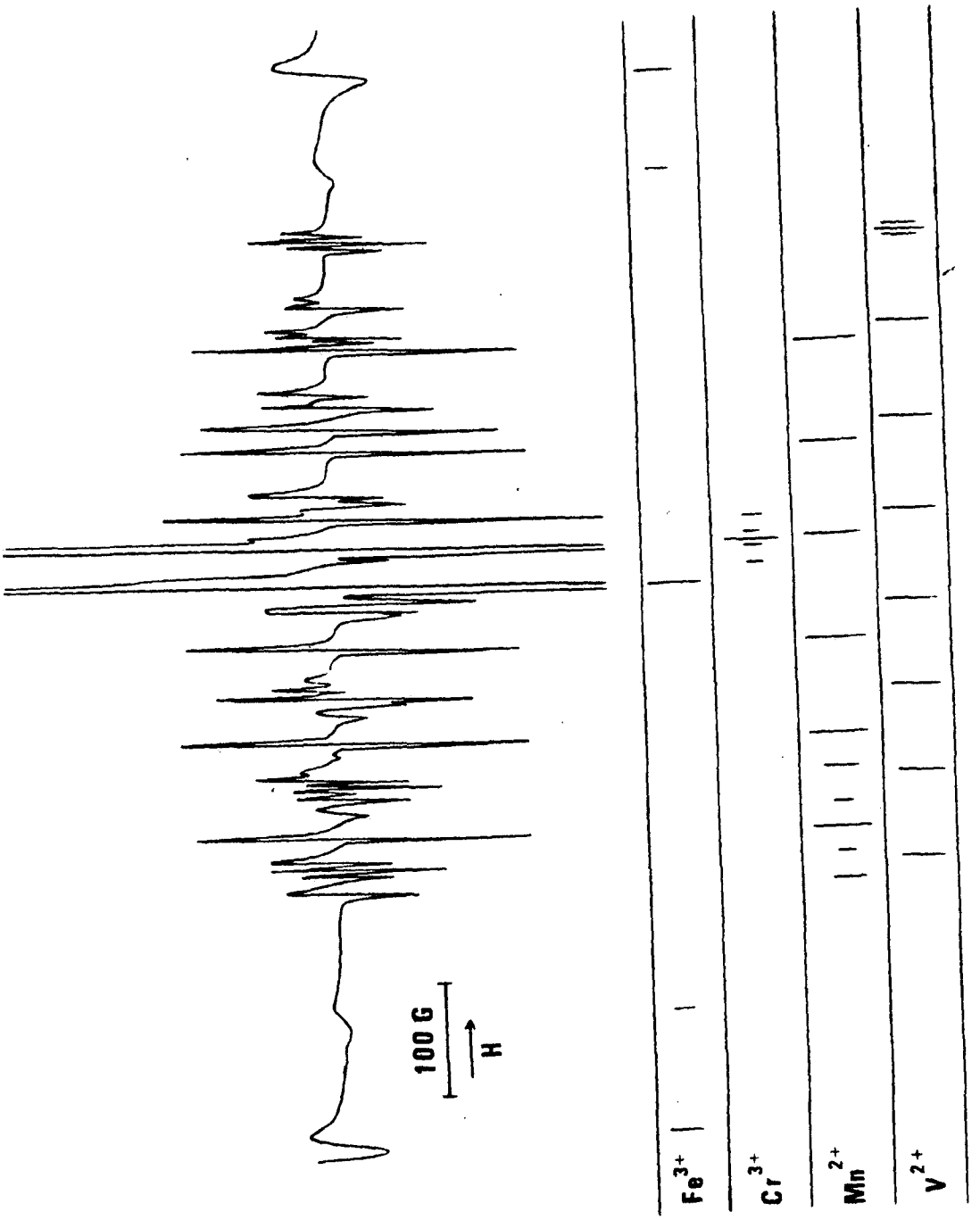
100 G
H
Fe^{3+}
Cr^{3+}
Mn^{2+}
V^{2+}

principal axis. This quintet, of which the central line is usually chosen as a convenient measure of Fe^{3+} concentration, corresponds to an orthogonal symmetry for this impurity. The ESR spectrum of substitutional Cr^{3+} ions in a purely cubic electric field consists of an isotropic line due to ^{50}Cr, ^{52}Cr and ^{54}Cr, upon which is centered a hyperfine quartet due to ^{53}Cr in 9.5% abundance. The shape of the principal line is reported to be Lorentzian and is taken as a measure of the Cr^{3+} concentration. Cr^{3+} can also be found in tetragonal symmetry if there exists a defect at one site located along the [100] direction. Some of our samples showed the lines from Cr^{3+} [100].

Being isoelectronic with Fe^{3+}, Mn^{2+} is expected to give a qualitatively similar spectrum, showing six quintets. The central lines of each group are due to the $+\frac{1}{2} \leftrightarrow -\frac{1}{2}$ transitions and the other four lines have a sufficiently large angular dependence so that there is overlapping of quintets at some orientations. The central line of the first quintet was used as a measure of the Mn^{2+} concentration. The four-fold spin degeneracy of V^{2+} is not lifted in a purely cubic electric field. Because of its nuclear spin of 7/2, there are eight hyperfine groups, each a triplet. The principal line of the first triplet served as a measure of the V^{2+} concentration.

Other paramagnetic impurities such as Fe^{2+}, Ni^{2+}, Co^{2+}, Cu^{2+} are also present in MgO, but cannot be detected either because their concentration is very small or because most of them show measureably

narrow lines only at very low temperatures (4K-77K). It is also known that the signal amplitude varies as 1/T (Curie's law). One example is the V-type center which shows a broad line at room temperature, and a sharp spectrum at 77K. This center is usually associated with different impurities (V_{Al}, V_{OH}, V_{OH}^-, V_{OD}, V_{OD}^-, etc.), but they all have the same g-value, being distinguishable only by ENDOR. Only some of the Spicer samples, when UV-irradiated, showed a faint indication of this broad absorption.

The g-value was determined by the relation $g_{ion} H_{ion} = g_{standard} H_{standard}$, where H is the magnetic field, and the standard used was DPPH, which has a known g-value of 2.0037.

The impurity concentration is proportional to the area under the absorption curve. This means that to get an accurate figure of its magnitude, a double integration of the first derivative signal should be carried out. Instead, a simple calculation can be employed, assuming a Gaussian or Lorentzian line shape. The calculation makes use of the linewidth ΔH_{pp}, the separation in Gauss between the minimum and maximum amplitudes, and of the amplitude, 2Y', itself:

$$\text{Area} = C \times \frac{2Y'}{2} \times \Delta H_{pp}^{\,2},$$

where C is a constant determined by the line shape. The line shape was determined to be Lorentzian for Fe^{3+}, Cr^{3+}, Mn^{2+} and V^{2+} and, in this case, C is equal to 3.63. The areas are reported in

chapters 4 and 5 in arbitrary units per gram (a.u./g). In order to compare concentrations, either with a known standard, in this case DPPH, or between the impurity ions, the Wertz and Bolton formula (65) was used. This formula gives the following ratios:

$$[Fe^{3+}]/[Mn^{2+}] = 0.52 \times A_{Fe}/A_{Mn} ,$$

$$[Cr^{3+}]/[Mn^{2+}] = 1.28 \times A_{Cr}/A_{Mn} \quad \text{and}$$

$$[V^{2+}]/[Mn^{2+}] = 1.02 \times A_{V}/A_{Mn} ,$$

where A_{Fe}, A_{Cr}, A_{Mn} and A_{V} are the areas in a.u./g of Fe^{3+}, Cr^{3+}, Mn^{2+} and V^{2+}, respectively. If the concentration of Mn^{2+}, for example, is known, the other impurity concentrations can be determined. Three samples, NP3, NPO and Spicer were compared with the standard DPPH, following the normal procedures, and $[Mn^{2+}]$ was determined, respectively, as 4.6 ppm, 4.8 ppm and 0.52 ppm. The deviation expected using this method is at least ±20%. These concentration values are of the same order of magnitude as those determined by spectrographic analysis in table 1.

To confirm these results, neutron activation analysis was carried out for the same samples, as above. These experiments gave the total Mn content as 9 ppm, 11 ppm and 0.7 ppm, respectively for NP3, NPO and Spicer. These values are proportional to those obtained from ESR, and indicate that possibly a small percentage of Mn could be present as Mn^{3+} and hence not detected using ESR. The relative accuracy of the neutron activation analysis is within ±5% for Mn.

This technique was also used to investigate [V]; the total concentration of this ion was determined as 0.8 ppm, 0.3 ppm and 0.6 ppm for NP3, NPO and Spicer, respectively. The accuracy of this method, when dealing with such small concentrations is very low, between 50% and 100%. These values are obtained when comparing the crystals with the standard, but the relative accuracy, that is, comparing one crystal to the other, is better, about ±25% for V^{2+}. In ESR, only the Spicer sample showed the presence of V^{2+}, with a concentration of 0.4 ppm. It could be speculated that since the analysis showed 0.6 ppm of total V, the remainder, 0.2 ppm, could be due to V^{3+}, but this is uncertain due to the poor accuracy of the methods utilized. The presence of Mn^{3+} and V^{3+} can be inferred by other measurements which will be discussed later in chapters 4 and 5

From the Mn^{2+} concentration, determined by ESR, and using the ratios above, Fe^{3+} and Cr^{3+} concentrations can be evaluated. Samples NP3, NPO and Spicer have, respectively, 18 ppm, 34 ppm and 1.7 ppm of Fe^{3+} and 7 ppm, 5.4 ppm and 0.6 ppm of Cr^{3+}. As it has been reported (24,25), between 60% and 80% of the Fe can be oxidized to Fe^{3+}, the remaining 20%-40% being mostly Fe^{2+}. Using the concentrations obtained for air heat treated samples in sections 4.2 and 5.2, the total Fe concentration is about 75 ppm plus 20%-40% for NP3 crystals, about 56 ppm plus 20%-40% for NPO crystals and about 8 ppm plus 20%-40% for Spicer samples. Comparing these results to the concentrations in table 1, it can be seen that after the air heat treatment about 70% of the total Fe is present as Fe^{3+} in NP3,

but these values are only 37% and >16% for NPO and Spicer crystals, respectively. This shows that annealing for 24 h. is more effective than annealing for only 3 h. for the oxidation of Fe^{2+} to Fe^{3+}.

The conversion factors between areas and concentrations for Fe^{3+}, Cr^{3+}, Mn^{2+} and V^{2+} are, respectively, 0.095, 0.24, 0.20 and 0.39, so that multiplying the areas in a.u./g by these values gives the concentrations in ppm. In order to compare the analysis results from table 1 with the results obtained from ESR, presented in the following chapters, these conversion factors are employed.

3.3 Experimental Errors and Limitations

3.3.1 Heat Treatments

The variation in temperature for the heat treatments done in the CO/CO_2 mixture was ±5° C and for those in air, ±10° C. The annealings in the Marshall furnace were done within 2° C of the reported temperature, as measured by an auxiliary chromel-alumel thermocouple. Calculated calibration curves for the flowmeters were available, giving lower flow rate values than the experimental ones; these were preferred.

3.3.2 TL

Figure 10a shows the TL output as a function of heating rate β, for one Spicer crystal successively UV-irradiated (type i)), I_t = 8.6 Ws/cm^2, and read out up to 250° C or 300° C. This gives a linear relationship expressed by

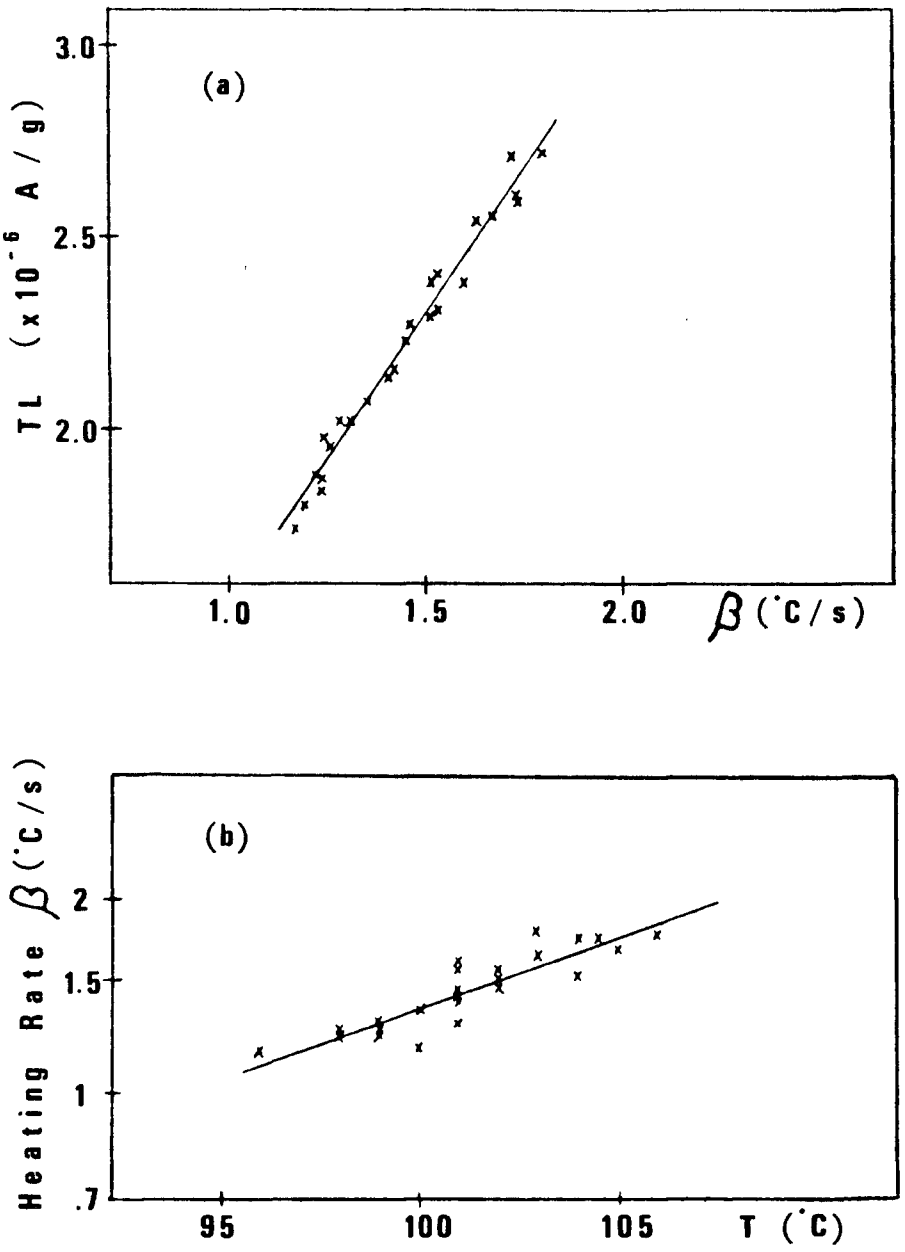

Fig. 10. TL output and heating rate relationships for sample S-B2. I_t = 8.6 Ws/cm^2, filtered non-monochromatic light, type i). (a) TL output as a function of heating rate. (b) Heating rate as a function of the temperature of peak 1.

$$TL_1 = (0.04 + 1.5\ \beta) \times 10^{-6} A/g$$

Where β is in °C/s. In this particular experiment β changed by almost a factor of 2. Under normal operating conditions, though, β varied about 25%. Since a variation in β affects the TL readings, these were normalized, fixing β at 1.0° C/s. Figure 10b shows the variation of β with the temperature of peak 1, fitted by $\beta = 0.0101 \exp [0.049\ T_1]$ (°C/s), where T_1 is the peak temperature in °C. This relation was used to correct for peak temperature shifts due to the experimental variation of β.

The TL reproducibility after correcting for weight, thickness and β is within 10% for peak 1 and 14% for peak 2 for the Norton samples of fig. 7. The errors in this work are reported as the standard deviation σ divided by the mean value. Besides the small differences in impurity concentration from one crystal to the other, the cleavage process itself may be responsible for the remaining non-reproducibility: Newton and Sibley (57) reported a blue (430 nm) TL emission due to deformation induced by sample cleavage, which increases in intensity with the percentage of deformation.

One limitation of the TL apparatus was the spectral range of the PMT, which did not extend beyond 670 nm; MgO is known to emit lines due to Cr^{3+} (R lines) and also lines due to other impurities in this wavelength region.

3.3.3 OA

A variation of about 35% in the determination of Fe^{3+} concentration, using ESR, was observed in adjacent crystals cleaved from the same block. In order to eliminate this influence when determining the error in the OA measurements, the absorption coefficient was divided by the Fe^{3+} concentration. This ratio,

$$\alpha(285\ nm)/[Fe^{3+}],$$

was calculated for each crystal in a series of ten, from which the standard deviation of 9% was derived. Possibly, the surface condition of the polished crystals contributed to this value of 9%, for non-polished crystals had only 4% deviation.

The intensity of the 210 nm band in polished Spicer crystals was difficult to determine, 200 nm being the limit of detection. In addition, the OA baseline presented a maximum at the same position as the band. The 285 nm band was only a perceptible shoulder as compared to a much better resolved band in Norton samples, indicating that these contain much more Fe^{3+} than the Spicer ones. The error in determining $\alpha(210\ nm)/[Fe^{3+}]$ in this case was about 33%. It is worth noting that Newton and Sibley (57) observed the formation of a 215 nm absorption band in Spicer crystals deformed by cleavage.

The crystal thickness presented a limitation in measuring α. This is because even a thin Norton sample (x_o = 0.4 mm) was too thick to determine the 210 nm band within the detection range, while

a thick Spicer crystal (x_o = 1.7 mm) was too thin to obtain a resolved 285 nm band.

3.3.4 ESR

The standard deviations in measuring the amplitude 2Y' and the linewidth, ΔH_{pp}, were determined as ranging from 1.9% to 5.4% for the former, and from 0.8% to 3.5% for the latter, for the four ions studied. The deviations in area were: 7.8%, 3.8%, 5.1% and 8.4% for Fe^{3+}, Cr^{3+}, Mn^{2+} and V^{2+}, respectively, in one Spicer crystal; and 4.3%, 1.6% and 4.3% for Fe^{3+}, Cr^{3+} and Mn^{2+}, respectively, in one Norton crystal. This is the result of 10 measurements taken in one single day.

The reproducibility was verified to within the experimental error in two other tests carried out in different days, thus eliminating the possiblity of a variation in the sensitivity of the apparatus. The DPPH standard had a variation of only 5%, as measured continually during the period of these experiments.

The average g-values of Fe^{3+}, Cr^{3+}, Mn^{2+} and V^{2+} were determined as 2.0025, 1,9794, 2.0024 and 1.9821, respectively. The reported values (23) are 2.0039, 1,9797, 2,0009 and 1.9800, respectively. The observed difference is probably due to errors in crystal orientation relative to the magnetic field axis.

3.3.5 UV-Irradiation

The Hg source was fairly stable while the Xe source was not, and this was the reason for choosing the first one for all

experiments except one or two. A decrease in intensity occurred as the Hg lamp was getting older, this being easily compensated for by longer exposures. A slight difference was observed in the uniformity of the illuminated area, A_R, projected on the detector head each time the lamp-housing was moved from arrangement ii) and back to the same place. Since all distances involved were kept strictly constant, the ratio A_R/A_S was considered as being always the same.

The relative calibration curve of the EG & G detector head was verified by checking one radiometer against the other for a few wavelengths. This revealed a discrepancy varying from a factor of 1.4 at 365 nm to 0.9 at 250 nm. This means that the TL emission spectrum, where the TL was recorded as a function of the wavelength λ, is not an experiment to be greatly relied on. However, other experiments, where λ was kept constant, are fairly reliable. Also, quantitative comparisons of TL output for the same I_t but different optical arrangements are meaningless, since either different optics (types i) and ii)), or different spectral content (monochromatic vs. non-monochromatic UV) were involved. Only qualitative correlations can be made.

There existed a limitation at 250 nm set both by the light source and the monochromator. Shorter wavelengths were not possible due to the very low intensity of the source and stray light from the monochromator.

Chapter 4

RESULTS AND DISCUSSION FOR MgO-NORTON CRYSTALS

In this chapter, the results are divided into separate sections for "as received" samples, air heat treated and CO/CO_2 heat treated samples. Some TL characteristics are examined for the "as received" crystals, and the influence of the changes in impurity concentration caused by the heat treatments on the TL sensitivity are presented for all samples.

4.1 TL Characteristics in "As Received" MgO-Norton Crystals

The TL response is mostly due to absorption by Fe^{3+} as shown in the TL excitation spectrum in fig. 11. Here, the average TL response of NP2 crystals as a function of incident radiation wavelength is plotted for peaks 1 and 2, for I_t = 0.01 Ws/cm^2. The curve resembles very much that of the OA in fig. 8, curve (b), although there is a shift in the TL excitation spectrum towards longer wavelengths. The TL excitation spectrum maximum occurs here at around 300 nm as compared to the OA maximum at 285 nm, but the half-width at half amplitude is about the same, 22 nm. The TL increases towards lower wavelengths, presumably due to an emission related to the 210 nm OA band.

One of the undesirable characteristics of MgO is the fading of the TL signal. To characterize this, one set of NP2 samples was given an exposure of 0.2 Ws/cm^2, 289 nm, and kept in the dark at room temperature. The TL response was measured at different intervals of time. The fading of TL peaks 1 and 2 is shown in fig. 12. After

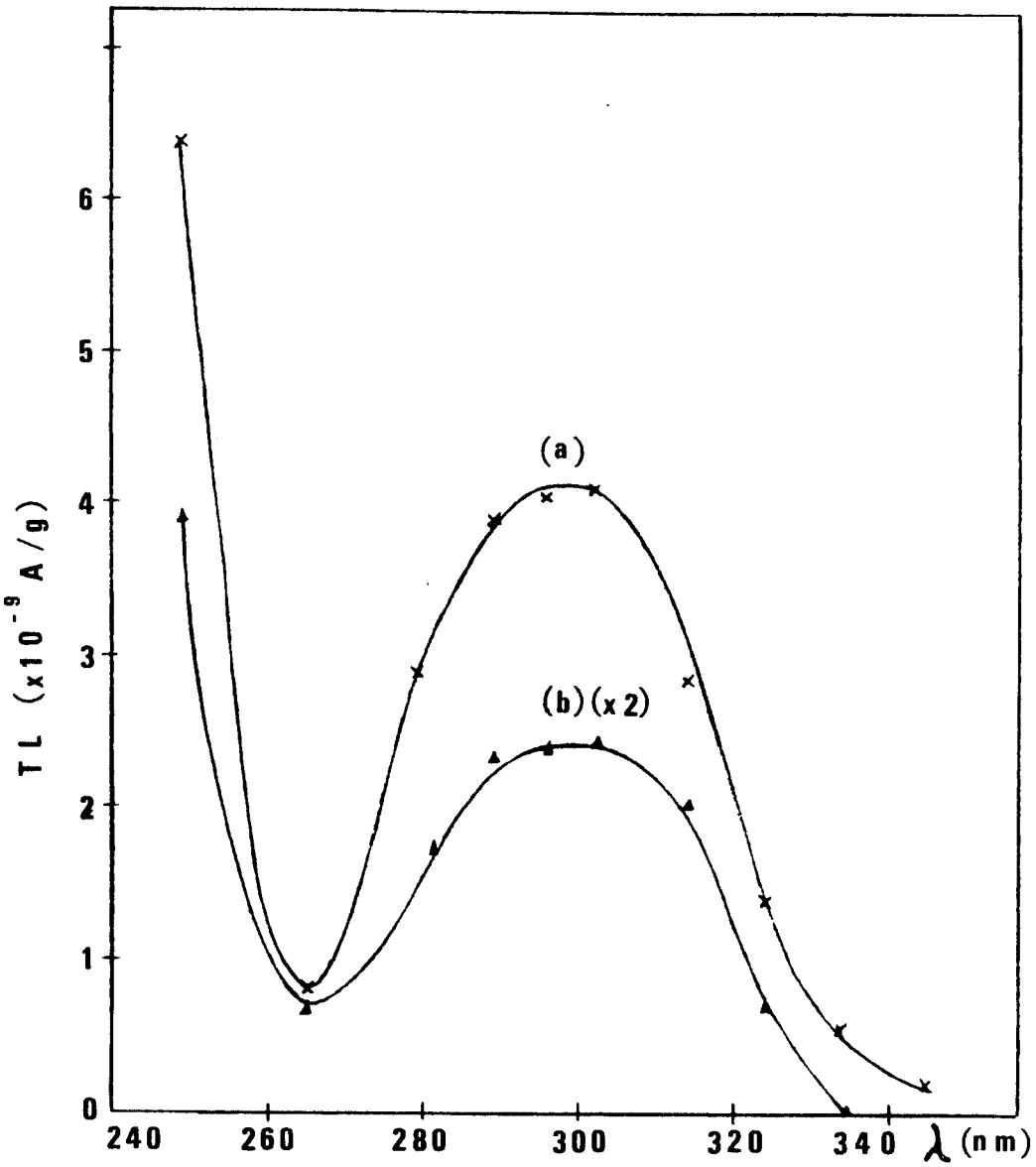

Fig. 11. TL excitation spectrum for peaks 1 and 2 in NP2 crystals, I_t = 0.01 Ws/cm^2. (a) peak 1, (b) peak 2.

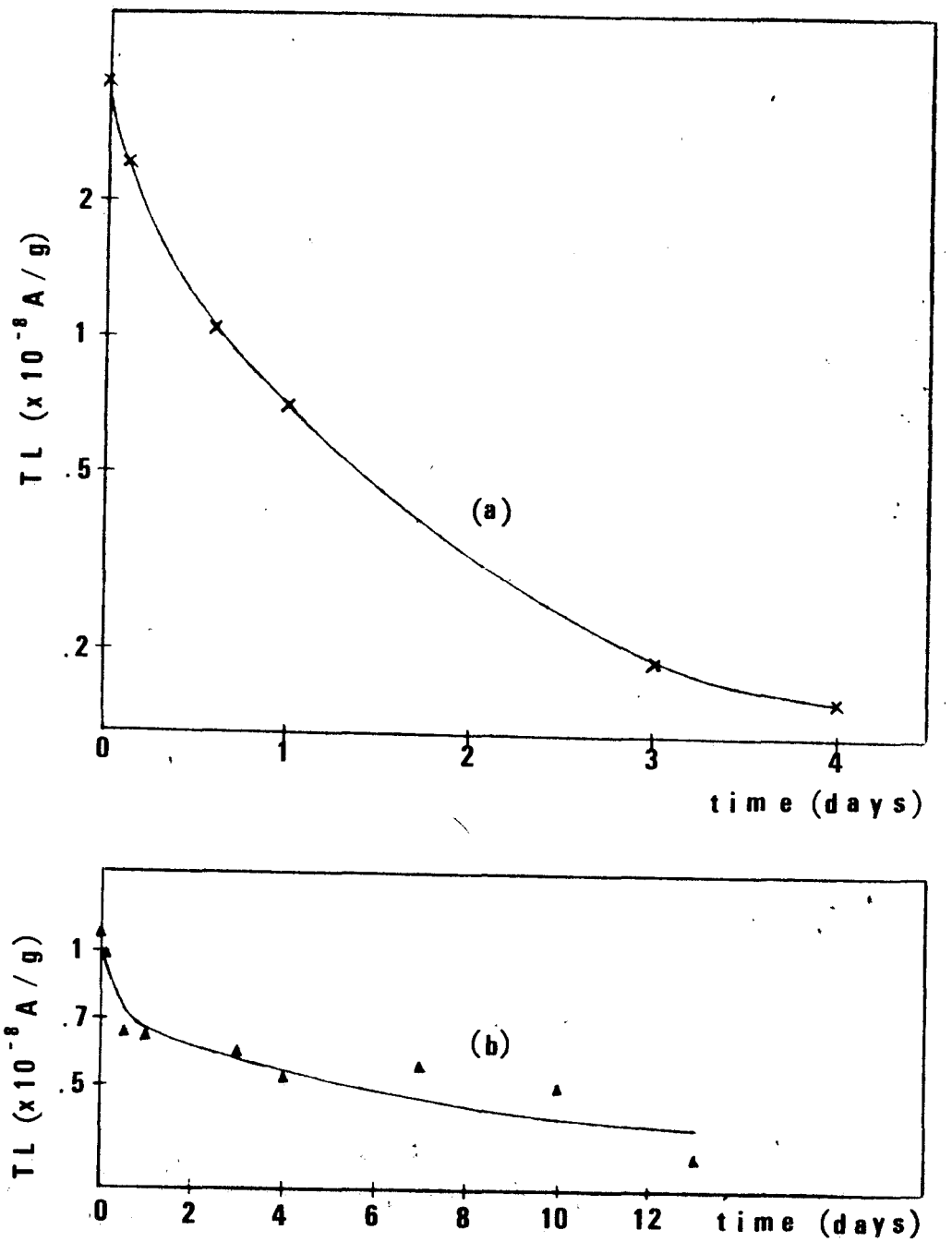

Fig. 12. Fading of TL peaks 1 and 2 for NP2 crystals exposed to 289 nm, I_t = 0.2 Ws/cm^2. (a) peak 1, (b) peak 2.

43 h. there is only about 10% of peak 1 and 54% of peak 2 left. The decay curves, not being simple exponentials, indicate that there is more than one trapping center associated with each TL peak, each center having a different stability. It is known that centers such as V_{Al} and V_{OH} have a half-life of about 10 h. They could be responsible for part of the fading behavior in MgO. Other impurity related V centers with lower and higher stabilities must also be involved in the process. The involvement of more stable centers would account for the slower fading of TL peak 2; this could possibly relate even to the V^- center which has a reported stability of over one year.

In the application of MgO as a UV dosimeter, it would be desirable to have a linear relationship between TL and I_t for a given wavelength or range of wavelengths. The TL response of peaks 1 and 2 as a function of I_t was verified for NP3 crystals in three different cases, namely: a) non-monochromatic exposure type ii), b) exposure to 249 nm and c) exposure to 289 nm. These are shown in figs. 13 to 15, respectively. In fig. 13, the TL response is linear for exposures up to 1 Ws/cm^2, becoming sublinear and saturating around 10 Ws/cm^2. In fig. 14, there is an initial linear increase followed by a supralinear behavior. In fig. 15, the deviation from linearity starts at about 0.1 Ws/cm^2. In all three cases, peak 3 was absent and peak 4 appeared only for high I_t values. For 249 nm and low exposures, another peak, called 1', appeared as a

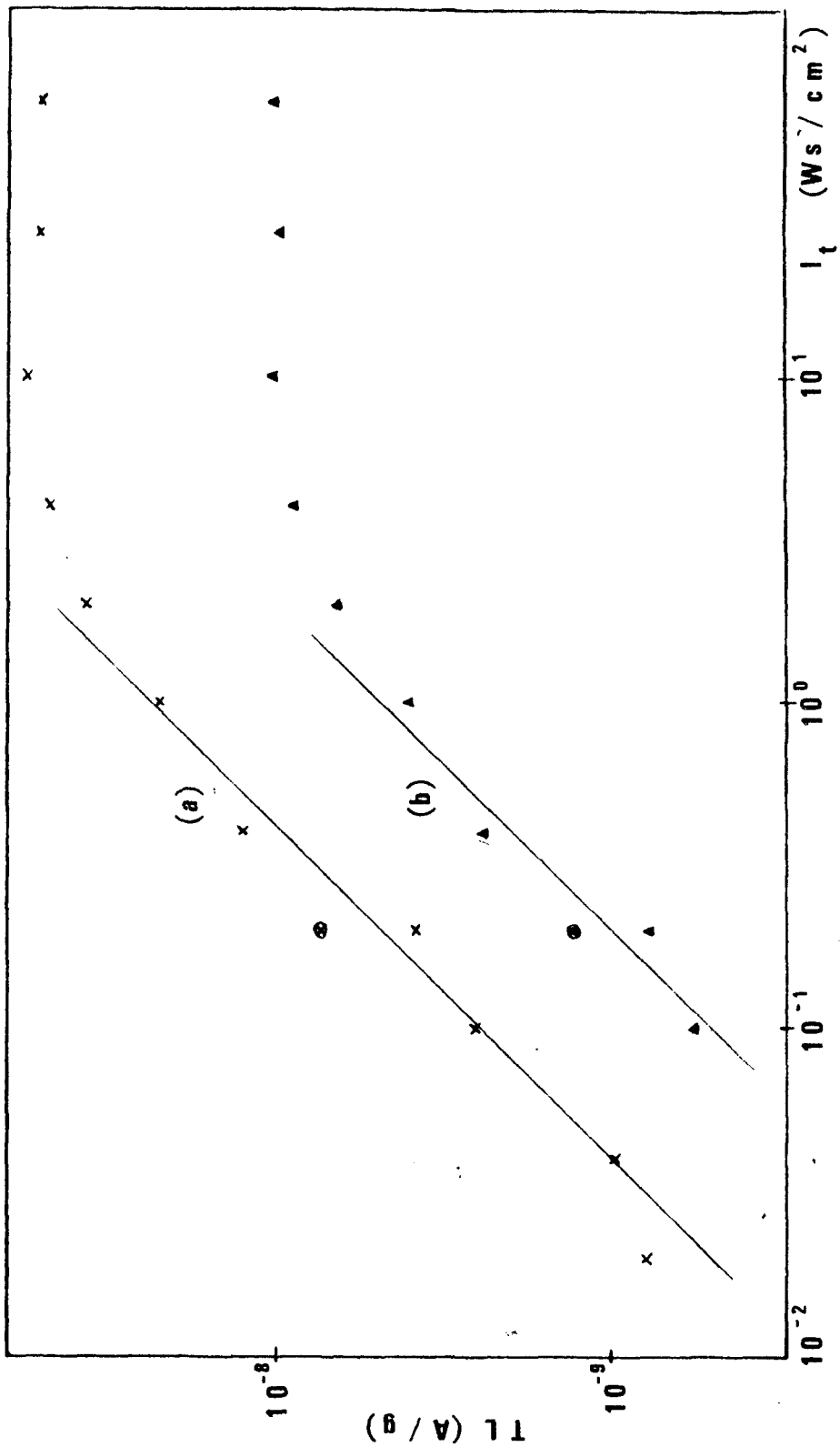

Fig. 13. TL response as a function of I_t, treatment a) non-monochromatic light type ii), for peaks 1 and 2 in NP3 crystals. (a) peak 1, (b) peak 2; encircled symbols were obtained after exposing to 70 Ws/cm^2; solid lines represent linearity.

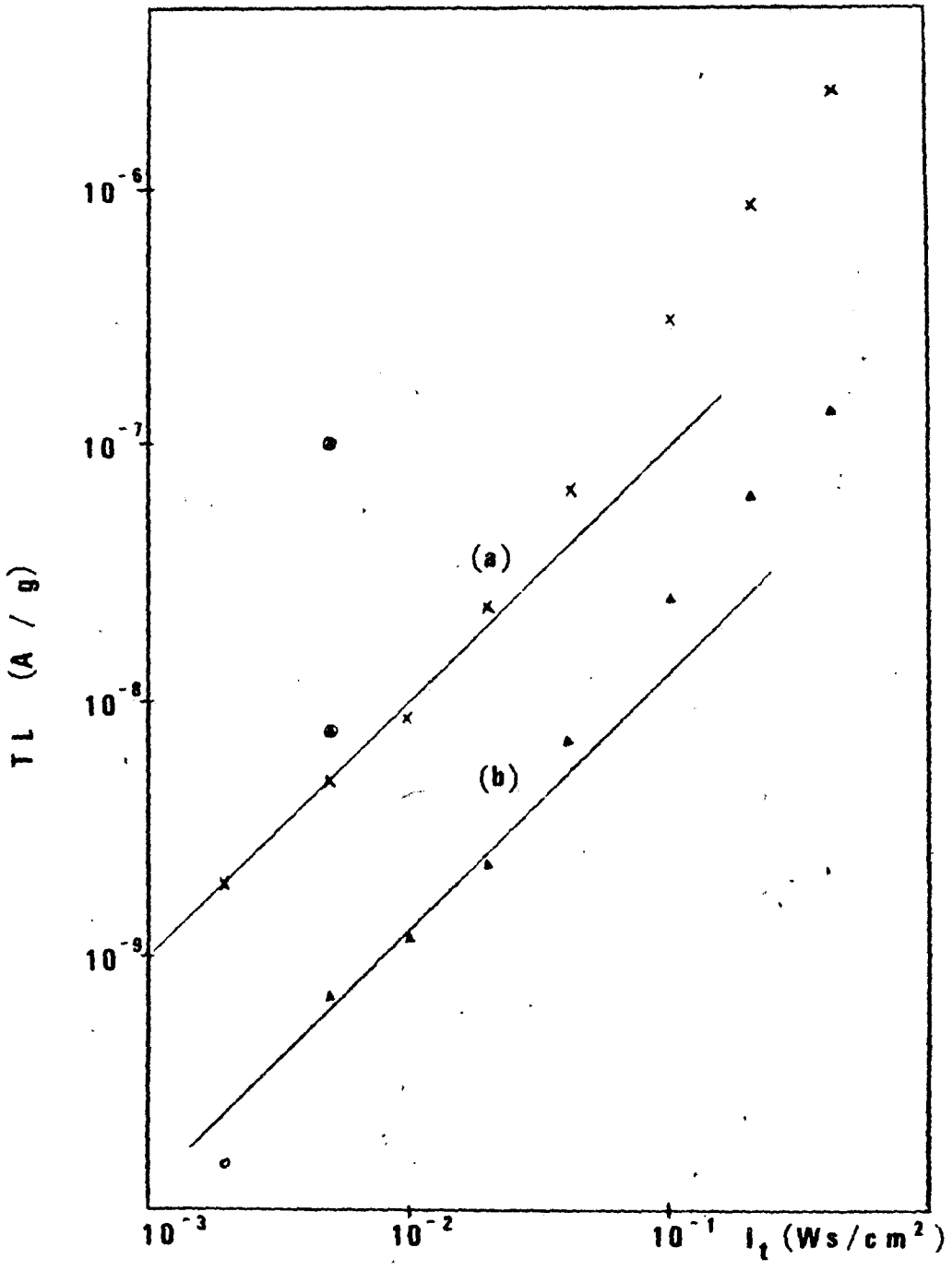

Fig. 14. TL response as a function of I_t, treatment b) 249 nm, for peaks 1 and 2 in NP3 crystals. (a) peak 1, (b) peak 2; the open circle (o) represents peak 1'; encircled symbols were obtained after exposing to 0.4 Ws/cm^2; solid lines represent linearity.

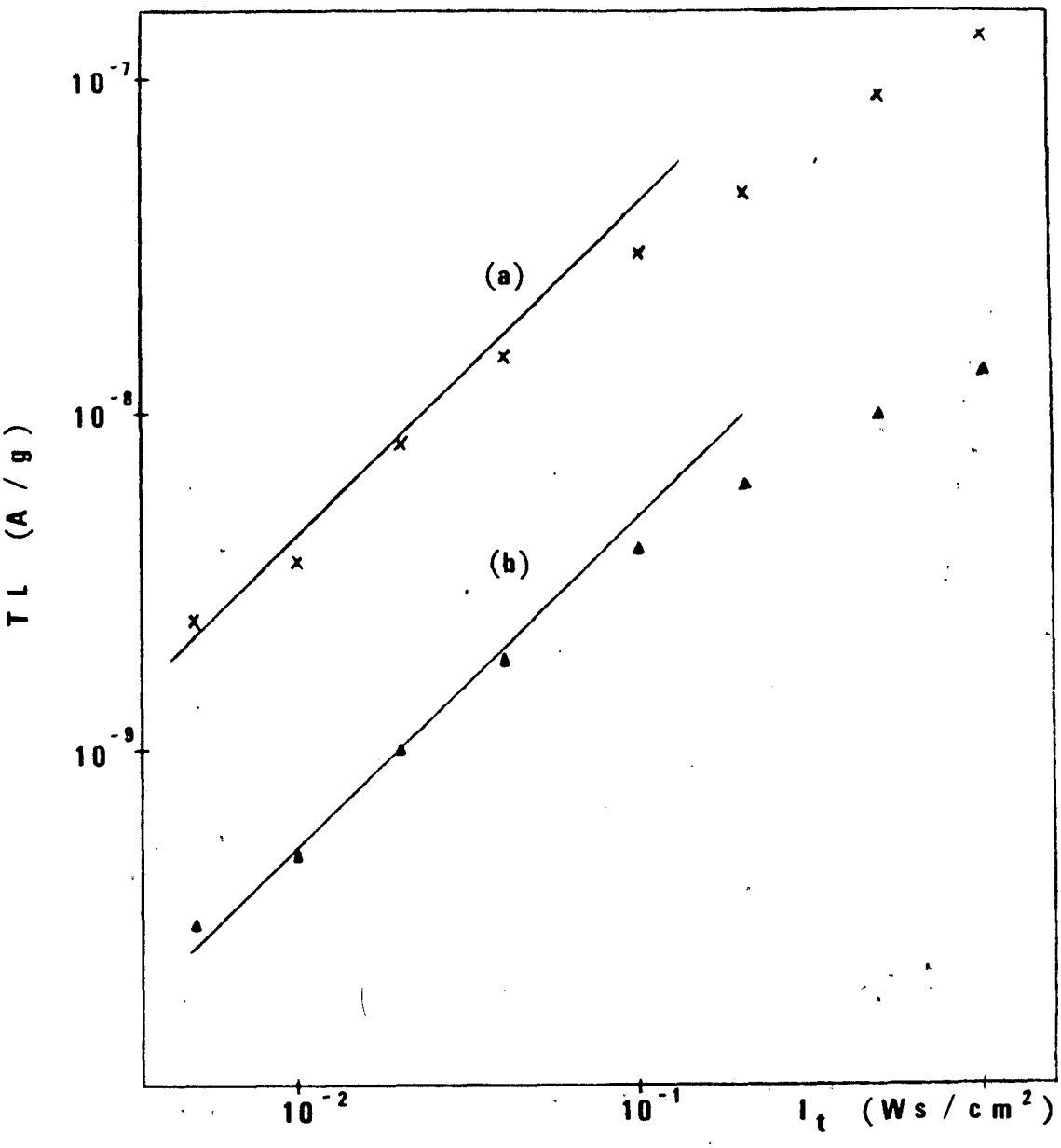

Fig. 15. TL response as a function of I_t, treatment c) 289 nm, for peaks 1 and 2 in NP3 crystals. (a) peak 1, (b) peak 2; solid lines represent linearity.

shoulder at about 90° C, giving way to peak 2 at a higher temperature and higher exposures. Peak 1' is shown as an open circle in fig. 14.

It is worth remembering here that non-monochromatic light, used in fig. 13, is a spectral composition of all wavelengths in the UV, as determined by the UV filter, so that most of the light transmitted comes from the region around 320 nm. This is expected to give results qualitatively similar to those for 289 nm, but not for 249 nm.

In each of these experiments, three crystals were used and exposed successively to increasing intensities I_t, with intermediate TL readings, in order to avoid non-reproducibility when using many crystals. One consequence of this successive method is that the sample becomes sensitized to low exposures after it has been exposed to high values of I_t. For example, in fig. 13, after irradiating with 70 Ws/cm^2, the crystals were exposed again to 0.2 Ws/cm^2 and the TL response, shown by the encircled symbols, increased by a factor of 1.9 and 1.7 for peaks 1 and 2, respectively, as compared to the first exposure to 0.2 Ws/cm^2. For 249 nm, fig. 14, the sensitization factor is about 20 for peak 1 and 10 for peak 2.

In order to determine whether the sensitization effect is due to the exposure to UV light or to the heating cycles from room temperature to T_m, experiment c) (fig. 15) was done twice, using two different values of T_m: 250° C and 350° C. The TL response curve was essentially the same in both cases, although the relative TL sensitivity was slightly different, being higher for the 350° C case.

In a related experiment, crystals were annealed in a low temperature range (200°C-400°C) for the period of one hour, instead of being only read out to T_m. A sensitization exposure or pre-exposure, defined as the irradiation to 27.6 Ws/cm^2 with non-monochromatic light type i), and an exposure test, as the irradiation to 0.2 Ws/cm^2, 289 nm, were used with three sets of samples. The first one, used as a reference, was not annealed and had the pre-exposure followed by the exposure test. The same was done for the second set, except that three sub-sets of crystals were annealed at 205° C, 302° C and 402° C. The third set was annealed at these same temperatures, but only submitted to the exposure test. Increasing the annealing temperature causes the TL response to non-monochromatic light to increase. The pre-exposure apparently does not sensitize the sample except for pre-annealing at 402° C; the sensitization factor, defined as TL [pre-exposure + 289 nm]/ TL [289 nm] was 0.7, 0.8 and 1.16 for annealing at 205° C, 302° C and 402° C, respectively. The results for the samples not annealed agree with those for the samples annealed at 302° C, probably because they had been previously read out to 315° C.

The sensitization effect, therefore, is not due to the pre-exposure treatment, as observed by Dhar (11), but probably due to the annealing itself. For our purposes it is sufficient to perform the TL reading up to 250° C, since the intermediate annealing treatment used by many authors did not prove to be helpful in

improving reproducibility. This is rather dependent on the state of impurities, as it will be discussed in detail later.

4.1.1 Impurity Concentration Changes with UV Treatment

It is known that the transition metal ions in their different valence states play an important role in the TL behavior. The impurity concentration of eight Norton samples was examined using ESR, showing ESR signals due mainly to Fe^{3+}, Cr^{3+}, Mn^{2+} and in two cases, V^{2+}. These impurities will be treated in this order in the discussion below.

The samples employed in these experiments were: NPO, NP3, ND-2, ND-5, ND-6, ND-7, ND-9 and ND-11. Two sets of three NP3 crystals were used, a) pre-exposed to non-monochromatic light type ii), I_t = 27.6 Ws/cm^2, followed by a test of 0.2 Ws/cm^2 at b) 249 nm for the first set and c) 289 nm for the second one. The interval between each exposure and TL reading, Δt_{UV-TL}, was about 2 h. Three NPO crystals were exposed to c), Δ_{UV-TL} = 42 h. and d) non-monochromatic light type i), I_t = 27.6 Ws/cm^2, Δt_{UV-TL} = 5 h. All ND crystals, four in each set, had the same exposure as in d). Changes in concentration as measured using ESR are reported as ratios: R_1 is the concentration before UV exposure divided by that after UV exposure and R_2 is the concentration after UV exposure divided by that after TL reading.

Table 2 shows a summary of the results obtained for Fe^{3+}, including the relative amount of this impurity in the "as received"

Sample	UV treat.	R_1‡	R_2‡‡	Conc. (a.u./g)	ΔH_{PP} (G)	$\alpha(285)$ (cm^{-1})	$\frac{[Fe^{3+}]}{\alpha(285)}$
NP3	a***	1.05	0.92	185.9	4.77	24.7	7.5
	b†	1.15	0.80				
	c††	1.09	0.93				
NP2				432.6	4.77	63.0	6.9
NP0	c	1.01	1.08	363.4	4.73	48.6	7.5
	d†††	1.12	0.82				
ND-2	d	1.10	1.08	15.6	6.24		
ND-5*	d	1.34/0.78	0.88/1.11	27.0/14.4	5.72		
ND-6	d	1.31	1.04	140.2	5.19		
ND-7	d	1.75	0.85	168.6	5.09		
ND-9	d	1.30	1.02	122.3	5.40		
ND-11**	d	∿1.67	——	∿5.6	∿4.10		

sample, in arbitrary units per weight in grams (a.u./g), and the linewidth, ΔH_{pp}, in G. NP2 is included for later reference. The results of OA measurements and the ratio $[Fe^{3+}]/\alpha(285\ nm)$ are listed for NPO, NP2 and NP3 for the purpose of checking the consistency of the ESR results. Ratios between 0.90 and 1.10 are considered to be included in the ESR inaccuracy and not to be real changes. The results in table 2 indicate that the concentration of Fe^{3+} decreases after a UV exposure, especially for 249 nm and non-monochromatic light, and increases or remains approximately constant after TL. In two of the ND-5 samples, the reverse occurs, that is, Fe^{3+} decreases with UV and increases after TL, probably because the ratio Fe^{3+}/Fe total is too small or for other reasons discussed later. Sample ND-11 is the most impure of all and the ESR results are only approximate.

The value of ΔH_{pp}, an average of the three measurements, before UV, after UV and after TL, is smaller for the purer crystals NPO, NP2 and NP3, than for the ND samples. It is possible that in the case of a large total amount of impurities such as in ND samples, the impurities interact with each other contributing to this increase of the linewidth.

Table 3 relates the same quantities as in table 2, but now for Cr^{3+}. In this case, the Cr^{3+} content decreases with UV light and increases with TL for two ND-5 samples and in case b), 249 nm. The reverse occurs for ND-2 and the two other ND-5 samples. Again, ratios between 0.90 and 1.10 are considered as no real change. ΔH_{pp} differs among different samples possibly because of the impurity environment, being the largest for ND-11 which contains a large amount of Cr^{3+}.

Table 3. ESR Results for Cr^{3+} in "As Received" MgO-Norton Samples

Sample	UV treat.	R_1	R_2	Conc. (a.u./g)	ΔH_{PP} (G)
NP3	a b c	0.91 1.21 0.95	0.95 0.81 0.99	29.48	1.04
NP2				12.71	1.15
NP0	c d	0.93 1.03	1.06 0.95	22.21	1.13
ND-2	d	0.15	2.18	1.40	0.97
ND-5*	d	0.72/1.43	1.14/1.09	2.76/6.33	0.98
ND-6	d	1.06	0.96	8.86	1.05
ND-7	d	1.02	0.91	9.47	1.05
ND-9	d	0.98	1.04	10.46	1.05
ND-11	d	∿1.0	∿1.0	∿313.1	∿2.06

*See note in table 2.

Next, the results for Mn^{2+} are presented, in table 4. On the average, Mn^{2+} does not change with UV or TL, except in two cases; the ratio R_1 is seen to increase when Mn^{2+} content decreases with 289 nm exposure for NPO and with non-monochromatic light for ND-7. ΔH_{pp} varies from sample to sample and appears to be increasing with Mn^{2+} content, except for the ND samples.

Finally, table 5 gives the results for V^{2+}, which was detected only in ND-2 and ND-11. In this case, it seems that there is a tendency for V^{2+} to increase its concentration with the TL reading. ND-2 crystals have a large concentration of V^{2+} as compared to ND-11. ΔH_{pp} is larger than usual in sample ND-11, again because of interactions among impurities.

Other paramagnetic impurities may be present in MgO, but probably in such small concentrations that it becomes very difficult to detect them at room temperature by ESR. The Cr^{3+} in [100] symmetry, discussed in chapter 3, was detected in all ND samples. NP2 and NP3 were not investigated for the impurity in this configuration. Cr^{3+} in [100] symmetry means that a defect is present along the [100] direction relative to Cr^{3+}, possibly a vacancy for charge compensation purposes.

4.1.2 TL Sensitivity

The TL sensitivity of all Norton samples was studied under different UV exposure conditions and the results are presented in table 6. Besides the TL amplitude for the four TL peaks and their temperatures, the ratios between peak 1 and peaks 2, 3 and 4,

Table 4. ESR Results for Mn^{2+} in "As Received" MgO-Norton Samples

Sample	UV treat.	R_1	R_2	Conc. (a.u./g)	ΔH_{pp} (G)
NP3	a b c	1.07 1.02 0.96	0.98 0.94 0.99	24.70	1.16
NP2				39.54	1.36
NP0	c d	1.14 0.93	1.02 1.05	25.07	1.32
ND-2	d	1.00	0.94	30.31	1.03
ND-5*	d	1.01/0.98	0.98/0.99	30.28/31.07	1.07
ND-6	d	1.12	1.00	31.50	1.18
ND-7	d	1.23	0.96	35.06	1.19
ND-9	d	1.05	0.99	38.20	1.17
ND-11	d	∿0.95	∿0.96	∿28.56	∿2.22

*See note in table 2.

Table 5. ESR Results for V^{2+} in "As Received" MgO-Norton Samples

Sample	UV treat.	R_1	R_2	Conc. (a.u./g)	ΔH_{pp} (G)
ND-2	d	1.05	0.88	20.65	0.60
ND-11	d	∿1.02	∿1.11	∿8.88	∿1.59

Table 6. TL Sensitivity to UV Light of "As Received" MgO-Norton Samples

Notes:

$r_{12} \equiv TL_1/TL_2$, $r_{13} \equiv TL_1/TL_3$, $r_{14} \equiv TL_1/TL_4$.

*a non-monochromatic type ii).

**b 249 nm.

***c 289 nm.

†d non-monochromatic type i).

††sh. shoulder.

†††suc. successive exposures.

Sample	UV treat.	TL_1 ($X10^{-8}$A/g)	TL_2 ($X10^{-8}$A/g)	TL_3 ($X10^{-8}$A/g)	TL_4 ($X10^{-9}$A/g)	T_1 (°C)	T_2 (°C)	T_3 (°C)	T_4 (°C)	r_{12}	r_{13}	r_{14}	Δt_{UV-TL} (h.)
NP3	a*	4.16	0.78	sh.††	1.82	77	123	166	221	5.3	—	22.8	2
	b**	31.0	3.58	sh.	5.99					8.6	—	51.7	2
	b suc.	88.9	6.24	—	—					14.3	—		suc.†††
	c***	3.60	0.66	sh.	1.66					5.4	—	21.7	2
	c suc.	5.02	0.84	sh.	1.35					6.0	—	37.2	suc.
	d†	29.8	3.79	1.35 sh.	5.34					8.3	22.1	55.8	0
NP2	b	8.02	2.49	—	—	72	129	162	230	3.2	—	—	0
	c	4.59	1.32	—	—					3.5	—	—	0
	d	9.60	2.40	sh.	3.70					4.0	—	25.9	0
NP0	c	10.5	4.24	—	8.02	76	126	171	223	2.5	—	13.1	0
	d	13.5	5.70	sh.	11.4					2.4		11.8	5
ND-2	d	1.50	—	0.43	—	114	—	207	—	—	3.5	—	5
ND-5	d	5.90	0.69	0.24	1.97	111	154	203	243	8.5	24.2	29.9	5
ND-6	d	0.33	sh.	0.18	2.36	81	—	178	223	—	1.8	1.4	5
ND-7	d	1.52	sh.	1.09	13.1	83	—	184	219	—	1.4	1.2	5
ND-9	d	0.38	—	0.21	2.70	83	—	184	231	—	1.8	1.4	5
ND-11	d	—	—	—	—	—	—	—	—	—	—	—	5

respectively, r_{12}, r_{13} and r_{14} are also listed. The values of Δt_{UV-TL} are also shown, to remind us that fading must be taken into account when making comparisons.

The relative height of the TL peaks is different for each group of samples, and depends on the UV treatment employed. NP2 and NP3 in case c), 289 nm, have approximately the same TL sensitivity for peak 1, but peak 2 is lower in NP3, as is evidenced by the different ratios r_{12}. For treatment b), 249 nm, NP2 is less sensitive than NP3. If crystal NP3 is exposed successively to 249 nm (fig. 14) or 289 nm (fig. 15), the TL amplitude is even higher. From the ratio r_{12}, in cases b) and c), it can be seen that peak 1 is sensitized by successive exposures more than peak 2. If crystal NP3 is exposed to non-monochromatic light d) after 249 nm, the TL response of peak 1 is about 3 times higher than for NP2 without the 249 nm exposure. NPO is more sensitive to UV light than NP2 and NP3. Peak 3 is usually only a shoulder and peak 4 is more well defined; peak 4 is more prominent in NPO than in the other two samples, shown by the ratio r_{14}.

In summary, the ratio r_{12} for NPO is smaller or about the same as for NP2 if fading is considered, and larger for NP3. The ratio r_{12} does not depend on the type of exposure, except for NP3, which has a larger r_{12} for 249 nm. This indicates that NP2 does not show a supralinearity effect as NP3 does for 249 nm in fig. 14.

Within the experimental error, the peak temperatures are approximately the same for the three samples discussed.

The set of ND crystals also shows different TL sensitivities. They can be divided in two groups: ND-2 and ND-5 in the first one, with peak 1 at about 114° C, and in the second, ND-6, ND-7 and ND-9 with peak 1 at about 83° C. The other peaks also appear at different temperatures for these two groups. Actually, the difference in temperature between peaks 1, 2 and 3 is roughly the same in all Norton samples. Sample ND-11 has no TL sensitivity to UV; this must be the quenching effect of Cr^{3+} which is present in a very large quantity. The crystals in the second group have approximately the same concentrations of Fe^{3+}, Cr^{3+}, and Mn^{2+}, even though the total Fe, Cr and Mn can be different. Their TL sensitivities, however, are not all the same. The TL peak 1 for ND-7 is about 4 to 5 times more sensitive than ND-6 and ND-9. The ratios r_{13} and r_{14} are approximately the same.

In the first group, ND-2 and ND-5 also have different TL sensitivities and even different ratios r_{12}, r_{13} and r_{14}. These ratios, for ND-5, resemble those of NP3 in some cases. Reverse trends for Fe and Cr were observed in crystals of the same group, ND-5. The fact that two of these crystals had been exposed to non-monochromatic light before carrying out the experiment, while the other two had not, could be the reason for the observed behavior.

4.1.3 V Center Correlations

V centers were also investigated in a qualitative manner, via ESR for NPO, which shows the V^- and V_{Al} centers together, and

via IR for NP2 and NP3, which shows the V_{OH} center and other OH related complexes. Since the V center ESR signal decayed about 75% in 70 h., it seems reasonable to assume that at least 75% of this signal is composed of V_{Al} centers, which have a half-life of about 10 h., and the remaining 25% of the signal, of V^- centers and possibly other V-type centers with different stabilities, as discussed earlier. The V° and the V_{OH} centers are eliminated because they have a distinctive ESR spectrum which was not observed. The IR spectrum showed lines at 3323 cm^{-1} and 3550 cm^{-1}, the former interpreted as the V_{OH} line, and the latter as due to $Fe(OH)_2$ precipitates. The V_{OH} concentration is larger in NP3 than in NP2, and the 3550 cm^{-1} line, smaller than the V_{OH} line, absorbs more in NP2 than in NP3.

It is important to note here that the V centers observed by ESR appear only after a UV exposure, being eliminated after a TL reading, while the IR absorption lines are present before UV, as well as after UV and TL reading.

In none of the ND samples, exposed to UV light, was the ESR signal characteristic of the V centers detected.

4.2 TL Characteristics of MgO-Norton Heat Treated in Air

Since the mechanism for TL involves the transition metal ions in their different valence states, it would be interesting to change the valence state of one or more of these impurities in a given sample, and observe the effect on the TL response. One way of accomplishing this is to heat treat the samples in oxidizing or

reducing atmospheres. This section will deal with the former, and the following section with the latter.

Three sets of seven NP0, three NP2 and three NP3 samples, were annealed in air at 1400° C for a period of 3 h. Two more sets of three NP2 samples and three NP3 were annealed at 1000° C, for the same period. Three more NP3 samples were also heat treated at 1400° C for 24 h.

Table 7 shows the increase in Fe^{3+} concentration, as measured by ESR, in terms of $\Delta[Fe^{3+}]/[Fe^{3+}]$, where $\Delta[Fe^{3+}]$ is the concentration of Fe^{3+} before the heat treatment subtracted from that after the heat treatment. This is divided by the Fe^{3+} concentration present before the annealing. The ratio represents, therefore, the amount of converted Fe^{3+} relative to the initial Fe^{3+} concentration. The oxidation of Fe is more effective at 1400° C than at 1000° C and also is more effective for longer periods of time. It has been reported (24) that in an oxidation process at least 20% of the iron remains as Fe^{2+}, so that it is believed that saturation has not occurred in the present case. Comparing the oxidation ratios, $\Delta[Fe^{3+}]/[Fe^{3+}]$, for NP2 and NP3, which have respectively 432.6 a.u./g and 185.9 a.u./g of Fe^{3+} in the "as received" condition, it can be seen that the air heat treatment tends to bring both samples to approximately the same equilibrium conditions, because $\Delta[Fe^{3+}]/[Fe^{3+}]$ is larger in NP3 than in NP2.

These two samples were irradiated with non-monochromatic light, treatment d), and had the ESR recorded before UV, after UV

Table 7. ESR Results for Fe^{3+} in Air Heat Treated MgO-Norton Samples

Sample	Heat treat.	UV treat.	R_1*	R_2**	$\frac{\Delta[Fe^{3+}]}{[Fe^{3+}]}$	ΔH_{pp} (G)
NP3	1000° C 3 h.	d	1.24	0.91	0.90	4.74
	1400° C 3 h.	d	1.30	0.88	2.96	4.75
	1400° C 24 h.	d	1.45	0.90	3.27	4.78
NP2	1000° C 3 h.	d	1.25	0.91	0.60	4.90
	1400° C 3 h.	d	1.17	0.96	1.08	4.99
NP0	1400° C 3 h.	c	1.06	0.95	0.62	4.79

*R_1 ratio of concentrations before and after UV treatment.

**R_2 ratio of concentrations after UV treatment and after TL reading.

and after TL. Sample NP0 was exposed to 289 nm, treatment c), and the same measurements were performed. The ratios R_1 and R_2, already defined in the previous section, are shown in table 7 for Fe^{3+}, together with ΔH_{pp}. Fe^{3+} was reduced by UV light and increased again with the TL reading, but not back to its initial value. In general, the ratio R_1, which is the impurity concentration before UV exposure divided by the concentration after UV exposure, is larger for the heat treated samples than for the "as received" ones (see table 2), indicating that the UV light is more effective in reducing Fe^{3+} when this has been oxidized. This and the fact that Fe^{3+} is not completely restored by TL reading indicate therefore, that the impurities were not in an equilibrium state after the heat treatment. This was the reason for performing heat treatments in controlled atmosphere, the subject of the following section.

Continuing the analysis of table 7, ΔH_{pp} is essentially not affected by annealing in air except for NP2, in which case ΔH_{pp} increased after the heat treatment.

As for the Cr^{3+} concentration, annealing in air has a tendency to reduce this impurity, which can be explained by the equilibrium equation referred in chapter 2:

$$Fe^{2+} + Cr^{3+} \overset{air}{\rightleftharpoons} Fe^{3+} + Cr^{2+}$$

Table 8 shows the ratios R_1 and R_2 and ΔH_{pp} for Cr^{3+}. This impurity does not change significantly with UV light and subsequent TL

Table 8. ESR Results for Cr^{3+} in Air Heat Treated MgO-Norton Samples

Sample	Heat treat.	UV treat.	R_1	R_2	ΔH_{pp} (G)
NP3	1000° C 3 h.	d	0.96	1.07	1.03
	1400° C 3 h.	d	0.92	1.00	1.11
	1400° C 24 h.	d	0.93	1.02	1.15
NP2	1000° C 3 h.	d	0.96	0.94	1.16
	1400° C 3 h.	d	1.03	0.97	1.23
NP0	1400° C 3 h.	c	0.97	1.00	1.18

reading. The linewidth ΔH_{pp} clearly increases with annealing temperature and when compared to the "as received" crystals (table 3).

The results for Mn^{2+} are shown in table 9. The concentration of Mn^{2+} had a tendency to increase after the heat treatment in air, and this behavior can be accounted for by the following equilibrium equation:

$$Fe^{2+} + Mn^{3+} \overset{air}{\rightleftharpoons} Fe^{3+} + Mn^{2+},$$

where the assumption of the existence of Mn^{3+} is made.

The Mn^{2+} content decreases with UV exposure and the original content is not recovered with the TL reading, as can be verified by the ratios R_1 and R_2. Mn^{2+} behaves much like Fe^{3+} as far as the UV light and TL, which reverse the impurity equilibrium set by the annealing treatment. In the Mn^{2+} case, this effect is more pronounced, or in other words, R_1 is larger than for Fe^{3+}. R_1 also increases with the heat treatment temperature.

The TL sensitivity results of the air heat treated samples are summarized in table 10, which may be compared with those of the "as received" samples NP2 and NP3 in table 6. Keeping in mind the fading that must occur during the longer storage times noted in table 10, the crystals become sensitized by the air annealing. This sensitization effect becomes more pronounced for TL peaks of higher temperature, that is, peaks 2 and 3, as verified by the observed

Table 9. ESR Results for Mn^{2+} in Air Heat Treated MgO-Norton Samples

Sample	Heat treat.	UV treat.	R_1	R_2	ΔH_{PP} (G)
NP3	1000° C 3 h.	d	1.16	0.99	1.15
	1400° C 3 h.	d	1.60	1.22	1.30
	1400° C 24 h.	d	2.02	1.02	1.31
NP2	1000° C 3 h.	d	1.35	0.95	1.38
	1400° C 3 h.	d	1.78	1.03	1.45
NP0	1400° C 3 h.	c	1.12	1.00	1.43

Table 10. TL Sensitivity to UV Light of Air Heat Treated MgO-Norton Samples

Sample	Heat treat.	UV treat.	TL_1 ($X10^{-8}$A/g)	TL_2 ($X10^{-8}$A/g)	TL_3 ($X10^{-8}$A/g)	T_1 (°C)	T_2 (°C)	T_3 (°C)	r_{12}	r_{13}	Δt_{UV-TL} (h.)
NP3	1000° C 3 h.	d	10.9	1.91	1.87				5.7	5.8	5
	1400° C 3 h.	d	14.4	5.64	5.76	79	119	174	2.5	2.5	5
	1400° C 24 h.	d	26.0	7.01	8.23				3.7	3.1	0
		d	12.2	4.46	6.20				2.7	2.0	9
		c	7.72	3.00	3.17				2.6	2.4	0
NP2	1000° C 3 h.	d	3.76	1.36	2.10	78	126	177	2.8	1.8	5
	1400° C 3 h.	d	4.89	2.28	3.12				2.1	1.6	5
NP0	1400° C 3 h.	c	1.60	1.18	1.69	80	125	178	1.3	0.95	42

ratios r_{12} and r_{13}. The TL of peak 1 increases but by a small factor as compared to the other two peaks. Peak 4, which appears in the "as received" samples, tends to disappear in some cases after heat treatment; in other cases, peak 4 appears as a shoulder, showing little consistency in terms of peak height and position, since, being only a shoulder, exact determinations are difficult.

The most important result of this section is the sensitization of peaks 2 and 3, especially of peak 3, which was only a shoulder before the heat treatment and is higher than peak 2 after the annealing. In consequence, peak 3's position shifts to higher temperatures while the other peaks remain approximately at the same temperatures as before the heat treatment. The sensitization effect is possibly connected to the oxidation of Fe, and to changes in Mn content, to be discussed in more detail later.

Fading was studied for sample NP2 by measuring the TL immediately after a standard exposure to 289 nm, and after 42 h. There is no difference in fading between the air heat treated and the "as received" samples (fig. 12). Samples annealed in air and irradiated with non-monochromatic light have approximately the same fading characteristics; the ratio between the TL immediately after the UV exposure and after 42 h. is about 9.0, 2.0 and 1.8 for TL peaks 1, 2 and 3, respectively. The presence of V centers in these samples was observed using OA, ESR and IR. At 1400° C, the V_{OH} and almost all of the 3550 cm^{-1} lines in NP2 and NP3 were eliminated. The ESR spectrum indicated the presence of the V^{-}-V_{Al} signal in one

NP3 sample exposed to non-monochromatic light. The OA in the visible, on the other hand, showed an increased background, which is visually observed as a dark coloration after the exposure to UV light. This corresponds to the absorption of V centers, which are known to absorb at about 540 nm, but since no resolved band was observed, it was not possible to identify which V centers were formed. The visual darkening of the samples disappears after the TL reading.

4.3 TL Characteristics of MgO-Norton Heat Treated in CO/CO_2 Atmospheres

In this section, the effects of a reducing treatment on the TL response are investigated. NPO crystals were heat treated at 1400° C in a controlled atmosphere containing a CO/CO_2 mixture. The reduction of Fe^{3+} to Fe^{2+} is shown in fig. 16 as a function of P_{CO}/P_{CO_2}, on a semi-logarithmic scale. Each experimental point is the average of 3 to 7 crystals. The change in Fe^{3+} concentration is represented by $\Delta[Fe^{3+}]/[Fe^{3+}]$, where $\Delta[Fe^{3+}]$ now is the concentration of Fe^{3+} after the heat treatment subtracted from that before the heat treatment. The ratio represents then, the fraction of converted Fe^{2+} relative to the initial Fe^{3+} concentration.

The data in fig. 16 may be represented by straight lines of at least two different slopes, indicating that the reduction occurs according to two or more different processes. Some of the points were checked by OA, giving results reproducible to within the

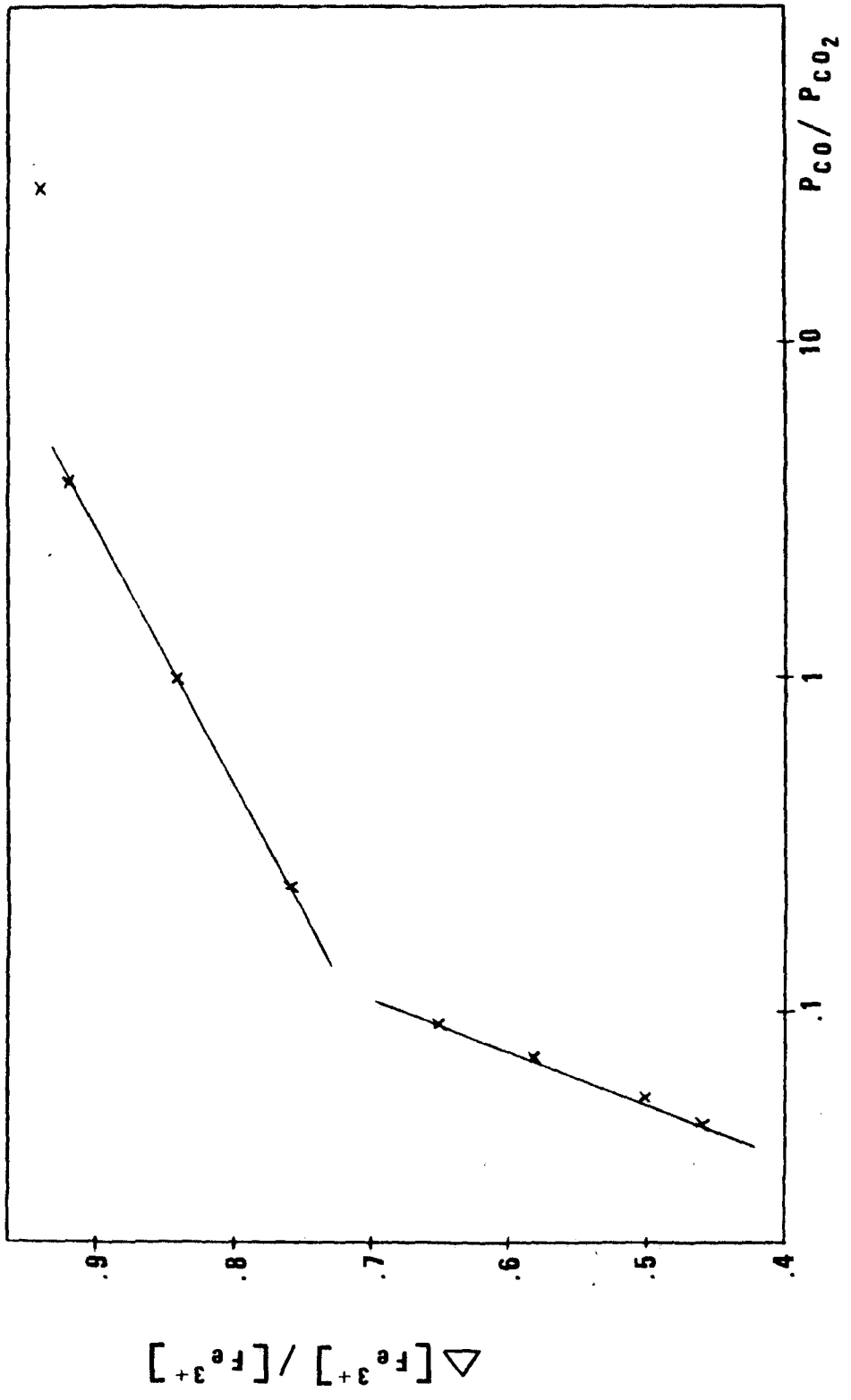

Fig. 16. Reduction of Fe^{3+} to Fe^{2+} as a function of the CO/CO_2 partial pressure, for NPO crystals heat treated at 1400° C for 3 to 10 h.

experimental error. The experimental point at P_{CO}/P_{CO_2} = 27.6 has an uncertainty associated with it due to an interference at the same position where the Fe^{3+} ESR absorption appears. The interfering signal could be the lines of $V_{\parallel}^{-}$ and $V_{Al_{\parallel}}$, which have the same g-value as Fe^{3+} although no evidence for $V_{\perp}$ or $V_{Al_{\perp}}$ was found. The reason for the different observed slopes is not clearly understood.

The reduced crystals, as well as air heat treated and "as received" samples, were exposed to treatment c) for Δt_{UV-TL} = 42 h. The TL output as a function of Fe^{3+} concentration, measured before the UV irradiation, is shown in fig. 17 for the four TL peaks. The TL response is linear for peaks 1 and 4, but is a power function of $[Fe^{3+}]$ for peaks 2 and 3. This is another piece of evidence showing that air annealed samples, included in the plot, are sensitized as far as the TL peaks 2 and 3 are concerned. The experimental values are distributed in two curves, (a_i) and (b_i), where i refers to the peak number. One possible explanation for the difference in TL sensitivity between (a_i) and (b_i), except for peak 4, is that the concentration of V centers is lower in case (b_i) for which most of the crystals have been re-treated in CO/CO_2. This re-treatment was done for longer periods (10 h.), since the first heat treatment for 3 h. was not sufficient for thermal equilibrium to occur. As it will be seen below, the V centers play an important part in the TL mechanism. In fig. 17, the TL response increases with increasing Fe^{3+} concentration, in spite of the experimental scatter. Subsequent monochromatic and non-monochromatic irradiations however,

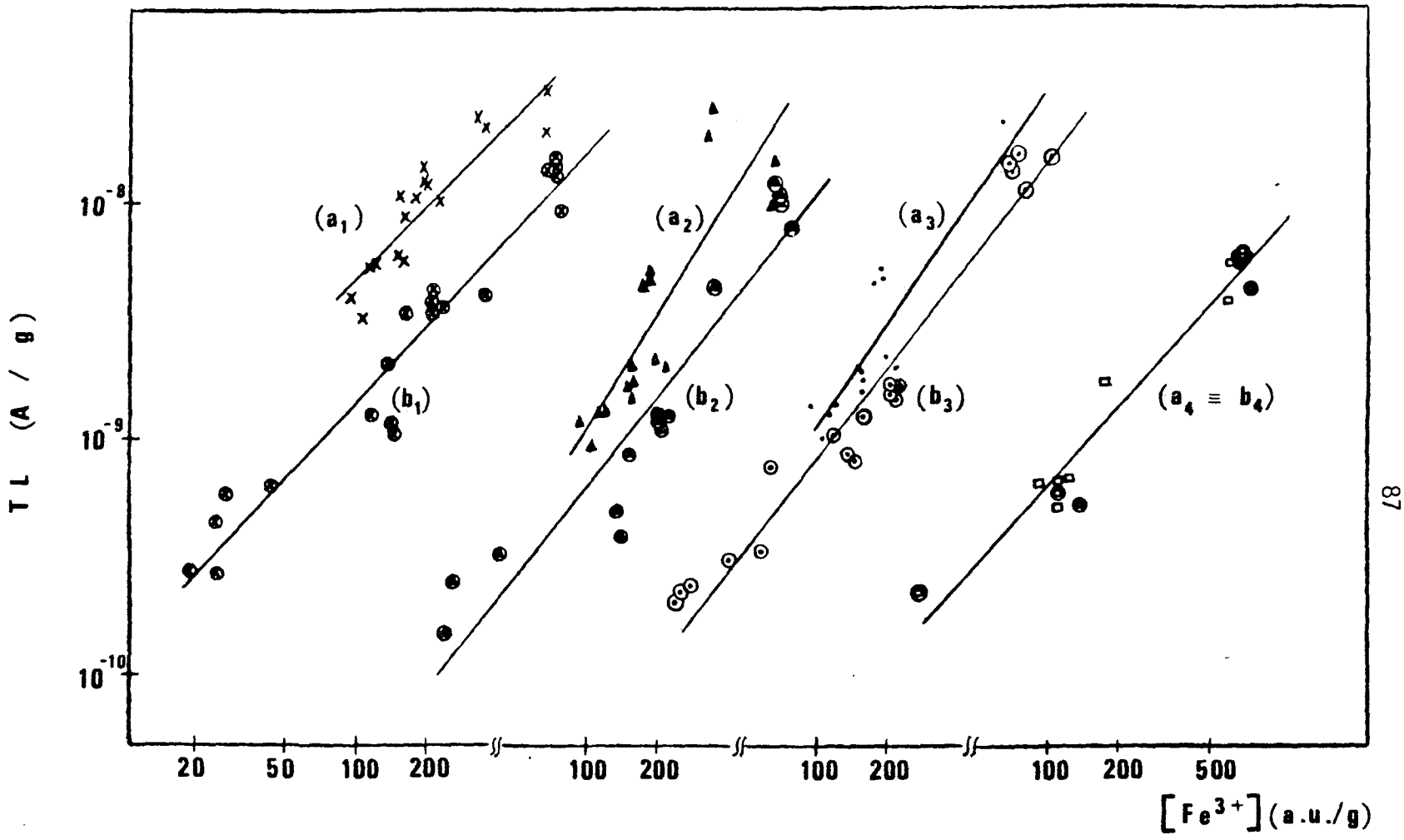

Fig. 17. TL response of reduced NPO crystals as a function of Fe^{3+} concentration. Heat treated once: (a_1) peak 1, (a_2) peak 2, (a_3) peak 3 and (a_4) peak 4; heat treated twice: (b_1) peak 1, (b_2) peak 2, (b_3) peak 3 and (b_4) peak 4. Log-log scale.

did not give reproducible results, and the experimental points had a tendency to be spread off the plotted curve indicating possibly a non-equilibrium impurity situation caused by the UV light and/or TL reading.

The changes in Fe^{3+} concentration were followed after an exposure to 289 nm and also after treatment d), Δt_{UV-TL} = 5 h. Table 11 relates the Fe^{3+}, Cr^{3+} and Mn^{2+} concentrations in CO/CO_2 heat treated samples. The average ratios R_1 and R_2 of all reduced samples, and ΔH_{pp}, which increases with increasing P_{CO}/P_{CO_2}, are shown. Within the experimental errors, there is no change in the Fe^{3+} concentration with UV and TL, although the tendency is to decrease the Fe^{3+} concentration with UV and increase with TL. However, those crystals that were strongly reduced showed the opposite effect, probably because the concentration of Fe^{3+} in equilibrium in MgO is higher than was achieved by the heat treatment.

While Fe^{3+} is being reduced, there is a tendency for the Cr^{3+} concentration to increase, according to the equilibrium equation:

$$Fe^{3+} + Cr^{2+} \overset{CO/CO_2}{\rightleftharpoons} Fe^{2+} + Cr^{3+}.$$

The concentration of Mn^{2+} also increases during the reducing treatment, showing that Mn^{3+} is probably present in MgO. V^{2+} was observed, but only under strongly reducting conditions and UV treatment d). This latter observation leads to the conclusion that V^{3+} must be the normal state of vanadium in MgO.

Table 11. ESR Results for Fe^{3+}, Cr^{3+} and Mn^{2+} in CO/CO_2 Heat Treated MgO-Norton Samples

Sample	Heat treat.	Ion	UV treat.	R_1	R_2	ΔH_{pp} (G)
NPO	1400° C 3-10 h.	Fe^{3+}	c	1.04	0.95	4.72-5.32**
			d	1.03	0.94	
			d	0.83*	1.05	
		Cr^{3+}	c	0.96	0.98	1.02***
			d	0.98	1.02	
		Mn^{2+}	c	1.03	0.96	1.13***
			d	0.99	1.00	

*Strongly reduced crystals.

**The linewidth increases within the interval shown for increasing P_{CO}/P_{CO_2}.

***Average for all P_{CO}/P_{CO_2}.

The ratios R_1 and R_2 and ΔH_{pp} for Cr^{3+} and Mn^{2+}, presented in table 11, show no change for these ions with UV and TL treatment. The value of ΔH_{pp} is smaller than for the "as received" samples (see tables 3 and 4).

If the TL response results in fig. 17 are normalized for $[Fe^{3+}]$ and plotted as a function of $[Cr^{3+}] + [Mn^{2+}]$, a small exponential decay is obtained. In other words, the TL response shows a small exponential decrease with increasing Cr^{3+} and Mn^{2+} content. In this case, it seems that Cr^{3+} and Mn^{2+} act as quenchers of TL.

From IR and ESR results, it was observed that the V_{OH} centers were annealed out for the CO/CO_2 treated samples, and that the V^--V_{Al} signal decreased gradually with increasing P_{CO}/P_{CO_2}.

4.4 TL Mechanisms and Discussion

Based on the results presented in the last three sections, TL mechanisms are proposed in this section to explain the TL characteristics of Norton MgO samples.

4.4.1 Charge Transfer Interactions

The measurements after heat treatments showed that Fe was oxidized in the presence of air. This can be expressed by the following equilibrium reaction, originally proposed by Wertz et al. (23):

$$2Fe^{2+} + \frac{1}{2} O_2 \rightleftharpoons 2Fe^{3+} + O^{2-} + V^{=}$$

The oxygen ion enters the MgO lattice by acquiring electrons from the Fe^{2+}, which becomes Fe^{3+}, and creating cation vacancies, denoted as $V^{=}$, in the process, for charge compensation. Vacancies are also generated when, at 1400° C, V_{OH} centers dissociate according to the equation:

$$V_{OH} \rightleftharpoons V^{=} + \text{hole} + H^{+} ,$$

where H^{+} is a proton. These vacancies can capture holes, under UV irradiation, and become V^{-} centers. They can also associate with trivalent metal impurities M and form V_M centers, such as V_{Al}. At this temperature, only a sufficient number of vacancies are produced so that the stoichiometry and thermal equilibrium principles are obeyed. At 1000° C, the V_{OH} centers are still present and probably at the saturation level (39), disappearing only at 1400° C.

The dissociation of V_{OH} centers and the oxidation of Fe produce a large number of vacancies in addition to those already existent and, due to thermal equilibrium conditions, part of them must be annealed out or become associated with other impurities. This should lead to the formation of V_M centers, other than the V_{Al}, although these have not yet been reported. One such possibility is the V_{Fe} center, already proposed by Krishnan (47). This seems to be reasonable, since Fe is the impurity most involved in the observed changes.

During the annealing process in air as well as in CO/CO_2, the $Fe(OH)_2$ precipitates, attributed to the 3550 cm^{-1} IR line, can possibly dissociate into Fe^{2+} and OH^-. In air heat treated samples, the former contributes to the increase in the Fe^{3+} concentration, and the latter has the probability of forming V_{OH} centers.

According to Wertz et al. (23), there is an equilibrium among the impurities during the initial oxidation process, such that, while Fe is being oxidized, other impurities can be reduced. In the present study, the following equilibrium reaction was verified:

$$Fe^{2+} + Cr^{3+} + Mn^{3+} \rightleftharpoons Fe^{3+} + Cr^{2+} + Mn^{2+},$$

where the major change is $Fe^{2+} \longrightarrow Fe^{3+}$.

The same equilibrium equation proposed for the oxidation process is valid for reduction in the CO/CO_2 atmosphere. In this case,

$$2Fe^{3+} + O^{2-} + V^{=} \rightleftharpoons 2Fe^{2+} + \frac{1}{2} O_2,$$

where Fe^{3+} captures electrons from the oxygen, becoming reduced to Fe^{2+}, while vacancies migrate to the surface, no longer being necessary for charge compensation. For the same reason, the vacancies created by the dissociation of V_{OH} centers are not stable and the related centers V^- and V_{Al} disappear gradually as the P_{CO}/P_{CO_2} ratio increases. It could be speculated that the two different slopes seen in fig. 16 are related to the annealing of different V centers.

The IR line attributed to $Fe(OH)_2$ also disappears with heat treatment, leading to the formation of Fe^{2+} and OH^-, which probably dissociate since there are not enough vacancies to form V_{OH} centers, as seen in the IR spectrum of a reduced NPO sample.

The overall impurity behavior suggests that the following process occurs:

$$Fe^{3+} + Cr^{2+} + Mn^{3+} + V^{3+} \rightleftharpoons Fe^{2+} + Cr^{3+} + Mn^{2+} + V^{2+},$$

again, the most important change being that related to Fe.

The changes occurring during the UV exposure and TL reading can be summarized with similar equilibrium equations which will be presented in three parts: "as received," air heat-treated and CO/CO_2-treated samples.

For the "as received" ND samples, the representative equations are:

$$Fe^{3+} + Cr^{2+} \underset{TL}{\overset{d)}{\rightleftharpoons}} Fe^{2+} + Cr^{3+} \quad \begin{pmatrix} ND\text{-}2 \\ ND\text{-}5 \end{pmatrix} \quad \text{and}$$

$$Fe^{3+} + Mn^{2+} \underset{TL}{\overset{d)}{\rightleftharpoons}} Fe^{2+} + Mn^{3+} \quad \begin{pmatrix} ND\text{-}6 \\ ND\text{-}7 \\ ND\text{-}9 \end{pmatrix},$$

where the samples for which the reaction occurs is indicated, as well as the UV treatment utilized, d) in this case. A small arrow for the reverse reaction during TL reading means that none or only part of the ions were reconverted to the initial concentration.

The reverse reaction of that shown for ND-5 samples was also observed to be operative for two of the ND-5 samples, and this behavior seems to be related to previous treatments the samples were subjected to. For ND-2, V^{2+} increases slightly during TL, but this is not shown in the equations above.

The equations correspond to the two groups of crystals, in table 6, which have different TL peak temperatures. The first one involves Fe and Cr and the second, Fe and Mn.

These TL mechanisms do not include the V-type centers which were not detected in the ND samples. The Cr^{3+}[100] centers, however, are a constant in these samples and the constituent vacancies could act as traps for the holes released by UV light from the cubic Fe^{3+} and Cr^{3+}. This is an improbable situation, however, since the Cr^{3+}[100] are neutral centers. A simpler model would be a direct charge transfer between Fe^{3+} and Cr^{2+}, Fe^{2+} and Cr^{3+} and Fe^{3+} and Mn^{2+}, as has been proposed by Takeuchi et al. (14), for Fe^{2+} and Cr^{3+}.

For the "as received" NP3 samples, the following equation is proposed:

$$Fe^{3+} + Cr^{3+} + V^{=} \underset{TL}{\overset{b)}{\rightleftharpoons}} Fe^{2+} + Cr^{2+} + V_{Al} + V^{-},$$

where the UV light reduces Fe^{3+} and Cr^{3+} by releasing holes which are trapped at vacancies, forming the V_{Al} and V^{-} centers.

For the "as received" NPO samples, the equation can be written as:

$$Fe^{3+} + V^{=} \underset{TL}{\overset{d)}{\rightleftharpoons}} Fe^{2+} + V_{Al} + V^{-} \ ,$$

where only Fe^{3+} seems to contribute to V^{-} centers formation and consequent TL.

The V_{OH} centers do not take part in the process since they do not seem to change during UV and TL, the same applying to Mn^{2+}, except in the case of NPO, under 289 nm radiation.

For all air heat treated samples, the following equation is proposed:

$$Fe^{3+} + Mn^{2+} + V^{=} \underset{TL}{\overset{c)d)}{\rightleftharpoons}} Fe^{2+} + Mn^{3+} + V_{Al} + V^{-}.$$

In this case, holes released by Fe^{3+} are trapped at vacancies and Mn^{2+} sites, producing V_{Al} and V^{-} centers, and Mn^{3+} ions. The process is reversed by TL, but not completely. Cr^{3+} ions do not participate in the reaction since they are fairly stable under UV and TL, and V_{OH} centers are absent.

The CO/CO_2 treated NPO samples present the least changes of all cases studied. There is a tendency for the following reaction to occur:

$$Fe^{3+} + V^{=} \underset{TL}{\overset{c)d)}{\rightleftharpoons}} Fe^{2+} + V_{Al} + V^{-} \ .$$

Here, the concentration of the V centers is very small and gradually disappears with increasing P_{CO}/P_{CO_2}. The strongly reduced crystals have no detectable V centers and

$$Fe^{2+} \underset{TL}{\overset{d)}{\rightleftharpoons}} Fe^{3+} + e^{-}.$$

Cr^{3+} and Mn^{2+} do not take part in the TL mechanism, but V^{2+} is a possibility for the strongly reduced samples. V_{OH} centers are absent.

The main characteristics for Norton crystals can be summarized as follows. During UV irradiation, there is charge transfer between impurities and vacancies, when these are available in sufficient amount, the process being partially reversible upon TL reading. When the number of vacancies is very small, a direct charge transfer occurs between the impurity ions. For "as received" samples, charge transfer usually occurs between Fe and Cr or between Fe and Mn. For air heat treated samples, there is interaction between Fe and Mn, and for reduced samples, only Fe changes or possibly Fe and V interactions occur. V_{OH} centers do not take part in the TL mechanism.

4.4.2 TL Sensitivity

The TL sensitivity of a given crystal depends on the total impurity content, tending to be higher for the purer crystals and lower for the less pure ones. Attempts to classify the Norton samples

according to their total impurity concentration, however, have failed because other factors are involved. One of these is the concentration of V-type centers, which take part in the TL mechanism as hole traps. The V center concentration should determine then the TL sensitivity, but again, some samples which showed no detectable V centers, have a rather high TL response.

A TL material is actually characterized only when the activator, trapping and emission centers are all identified. The UV light releases charges from the activator centers which are captured in the trapping centers. During the TL reading, the charges go from the trapping to the emission centers. The peak temperature depends on the energy level of the trap, while the TL sensitivity depends on the number of charges released, the efficiency of luminescence and the spectral emission content of each TL peak.

From OA, ESR and the TL excitation spectrum, it is clear that Fe is the impurity most involved in the TL mechanism in all Norton samples studied, and therefore, Fe^{3+} can be identified as the main activator center. Fe^{2+}, Cr^{2+}, Cr^{3+} and Mn^{2+}, to a smaller extent, also act as activators, either releasing holes or electrons, depending on the sample and the treatment.

The trapping centers are believed to be mainly V-type centers. In the NP crystal series, these are the V_{Al} and V^{-} centers, but in the ND series, no V centers were observed. Comparing the analysis and the ESR results (tables 1 and 2) and using the conversion factors from section 3.2.3, it is evident that in the ND samples, almost all

the iron is present as Fe^{2+}, indicating a low concentration of vacancies. This is not so in the NP samples where $[Fe^{3+}]$ is 2 to 30 times higher than in ND samples, resulting in a large vacancy concentration, as was observed. The ND crystals showed, in addition, the Cr^{3+}[100] line, which by definition is the V_{Cr} center, in higher concentration than in NP. If this center is more stable than V_{Al}, which is thought to be responsible for the 76° C peak in NP samples, it could account for the higher temperature of peak 1 in the ND samples. However, this is an assumption that needs further verification. If the V_{Cr} centers are not involved in the process, the impurities themselves act as trapping centers and the mechanism is that of charge transfer between impurities. The observed temperatures of TL peak 1 in the two groups of ND samples indicates that two different trap levels are involved, probably related to different impurities.

From the fading experiments, it seems that each TL peak is associated with a discrete distribution of V centers, the most stable ones evidently being responsible for the higher temperature peaks. Since the V^- centers are much more stable than the V_{Al} centers, it is reasonable to assume that an intermediate center exists, such that its half-life is between those of V_{Al} and V^-. This center could be, in principle, any V_M center, but since many vacancies are charge compensating for Fe^{3+} ions, it is reasonable to identify this as V_{Fe}. The vacancy does not need to be immediately next to the Fe^{3+} ion but may be a few lattice sites away, so that the

Fe^{3+} ESR line can still be considered as cubic, or only slightly perturbed by a distant removed neighbor. One point of evidence for this is the fact that ΔH_{pp} is different in each sample and changes with heat treatment, indicating interactions between Fe^{3+} and the environment.

The observation that the difference in temperature between the TL peaks is approximately the same for all samples, including the Spicer crystals presented in Chapter 5, is not well understood. The way the experiments were done, measuring the impurity concentration after all the TL emission has been released, makes it impossible to relate a specific trapping center to each TL peak.

The emission centers can be identified via ESR measurements by observing those impurities that change after a TL reading. Most of the emission comes from the recombination of holes, released from V-type centers, with Fe^{2+} ions, forming Fe^{3+} in the excited state, Fe^{3+*}. This exited state atom then emits light when returning to the ground state. From the R_2 ratios in tables 2, 3, 5, and 9, it can be seen that other ions, such as Cr^{2+}, Cr^{3+} and probably Mn^{3+}, V^{2+} and Fe^{2+} are also emission centers, although some of these ratios are very close to unity. It was also verified that the TL reading is not a completely reversible process, meaning that not all charges released by the UV light recombine with the impurity ions during TL. This makes it even more difficult to assign the emission centers responsible for TL. Another difficulty arises from the fact that

each TL peak may be the result of several emission centers, with different relative intensities. This problem would be solved by measuring the TL emission spectrum. Without an emission spectrum measurement, the wavelength of the emitted light can be only speculated about, taking into account particular experiments in the literature and other indirect evidence.

It is likely that the blue TL emission of MgO can be efficiently detected only when the crystal is exposed to a high energy radiation such as γ-rays (19), X-rays (6,7,17) or to an electron beam (59,60,62). On the other hand, a much lower excitation energy, such as UV, seems to be more efficient in causing TL emissions of correspondingly lower energies, such as the observed orange emission (21). Red lines are reported for both X-rays (6) and UV radiation (47). Qualitatively, only orange and red were seen in our samples; no quantitative study was undertaken. Some blue emission could possibly be caused by UV excitation energies higher than 5.0eV (248 nm), but it is likely that this would be an inefficient process; CL results (59,60) show that the corrected blue to red intensity ratio is about 1/300. These references (59,60) also indicate that the blue and red emissions are enhanced, respectively after heat treatments in air and in a reducing atmosphere.

Our results show that the TL sensitivity decreases with reducing treatments. In fig. 17, for example, it was seen that the TL response of peak 1 decreases linearly with decreasing $[Fe^{3+}]$. The air heat treatments, on the other hand, were seen to sensitize the TL

response of MgO crystals. Since the spectral sensitivity of the PMT in the TL reader decreases from the blue to the red region, the above results can be explained by a shift in the TL emission towards the orange for the sensitized peaks, and a shift towards the red for the reduced samples. A second explanation is that the number of vacancies, which act as trapping centers for TL, decreases with increasing P_{CO}/P_{CO_2} ratios, contributing to a lower TL sensitivity; this number increases with air heat treatments, resulting in the increased sensitivity.

Comparing the sensitivity of TL peak 2 between NP2 and NP3 in table 6, it was observed by the ratio r_{12} that this peak was more sensitized in sample NP2 which contains more $[Fe^{3+}]$ than in sample NP3. Samples from the same block as NP3 showed the same effect, where those with slightly higher $[Fe^{3+}]$ showed a higher peak 2. V_{Fe} is probably the trapping center for peak 2, with possible emission in the orange region due to Fe^{3+*}. When these samples are annealed in air, peak 3 develops and becomes more sensitized than peak 2. The TL mechanism indicates that holes are released from Fe^{3+} and captured at vacancies and also at Mn^{2+} ions. Mn^{2+} does not release holes during TL. It seems then that the sensitization of peak 3 is related to Mn^{2+} ions acting as trapping centers. The emission is possibly orange, and due to Fe^{3+*}.

The ND samples, which have $[Fe^{3+}] << [Fe^{2+}]$, showed peak 3, but not peak 2, as opposed to "as received" NP samples. This is in aggreement with the above propositions, since ND samples do not seem

to contain V_{Fe} centers, responsible for TL peak 2. In addition, the ESR results revealed that Mn^{2+} takes part in the TL mechanism in ND samples probably as a hole trap. This is evident, especially for the second group of ND crystals, where peak 3 is more sensitive, suggesting again that Mn^{2+} is the trapping center for TL peak 3.

All of these results were obtained with non-monochromatic light which excites mostly the Fe^{3+} ions. If the more energetic wavelength, 249 nm, is employed, peaks 1 and 2 show a supralinearity effect with increasing irradiation intensity. Changes in Cr^{3+} were observed under 249 nm irradiation suggesting that this ion is somehow preferentially related to the lower temperature peaks. In this case, the ratio R_2 indicates that emission from Cr^{3+*} occurs. It seems, therefore, that the R-lines of Cr^{3+} are more efficiently excited if UV light of 249 nm is used to irradiate the samples. Others have reported that this wavelength releases electrons, and this agrees with the proposed TL mechanism, where Cr^{3+} ions would capture electrons, becoming reduced to Cr^{2+}. The source of electrons in this process is not known. A simpler way for Cr^{3+} to reduce to Cr^{2+} by UV light, however, is by releasing holes.

While Cr^{3+} is involved in the TL behavior only at higher UV energies, the ion which accounts actually for most of the TL mechanism in the region from 250 nm to 340 nm is Fe^{3+}.

4.4.3 Discussion of Results

The results for Norton crystals can be summarized as follows. From the TL excitation spectrum, and the OA and ESR results, Fe^{3+}

is the major activator impurity for UV in MgO. This behavior agrees with the results reported by Krishnan (47), Wertz et al. (16) and Hansler and Segelken (22), who state that Fe^{3+} is reduced by UV light. Conversely, Fe^{2+} is the major recombination center for holes. The emission associated with the $Fe^{3+*} \longrightarrow Fe^{3+}$ transition is probably in the orange region of the spectrum as proposed by Krishnan (47). Others (6,19,62) have assigned the blue emission to the $Fe^{3+*} \longrightarrow Fe^{3+}$ transition, but for the low energy of the UV radiation, our assumption seems to be reasonable, as already discussed in section 4.4.2. The orange emission must be related to the most probable conversion in our system, that is, the $Fe^{2+} \longrightarrow Fe^{3+}$ conversion.

The evidence for the existence of the V_{Fe} center is based only on the TL measurements and the ESR observations for Fe^{3+}; the center itself has not been seen in the MgO ESR spectrum. Based on similar measurements, Krishnan (47) came to the same conclusion, that is, that vacancies, charge compensating for Fe^{3+} at sites close but not next to the Fe^{3+} ions, are responsible for the V_{Fe} center. Another indication of its existence is the variation observed in the linewidth ΔH_{pp}, caused by interactions among vacancies, Fe^{3+} ions and other impurities. Krishnan (47) attributed the emission lines at 645 nm and 659 nm to Fe^{3+} in distorted octahedral sites and to Fe^{3+} with a nnn vacancy (V_{Fe} center), respectively. Our assumption here is that the vacancy in the V_{Fe} center acts as a trapping center, whereas the Fe^{3+} ion, disturbed by vacancies, acts as an emission

center for TL. Our conclusion is based on the observed relationship between TL peak 2 and the Fe^{3+} concentration, and on the fading characteristics of the V-type centers. It is assumed that the following hierarchy in stabilities is valid: $V_{Al} < V_{Fe} < \ldots < V_M \ldots < V^-$, where V_{Al} is the least stable center. In principle, these centers could be associated with the TL peaks seen progressively with increasing temperature: V_{Al} would be the trapping center for peak 1, V_{Fe} for peak 2 and so on. Actually, since the fading curve of TL peak 1 is not simply exponential, it seems that more than one trapping center, or a gaussian energy distribution of trapping centers, is associated with each TL peak, as once suggested by Soshea et al. (15).

It has already been mentioned that Cr^{3+} takes part in the TL mechanism only in a few samples and when the exciting radiation is of high energy. The well-known Cr^{3+} R-emission line is better seen in samples which have been X-irradiated (7), since X-rays are much more energetic than UV radiation. It is suggested here, then, that the efficiency of the Cr^{3+} emission depends on the incident radiation energy. According to the TL mechanism proposed by Wertz et al. (7), Cr^{3+} captures electrons during the first stage of irradiation. This means that the radiation must be effective in releasing electrons from the valence band or from activator impurities. This does not seem to be the case with UV wavelengths longer than 250 nm, although for shorter wavelengths this would be possible, since excitons, which

are hole-electron pairs, are created, as reported by Kirsh et al. (9) and Takeuchi et al. (14).

As was noted in chapter 2, Mn^{2+} is reported by most investigators to be a very stable impurity ion. Our results disagree fundamentally with the literature, for it was observed in this work that Mn^{2+} acts as a hole trap for TL peak 3. This behavior becomes effective when the sample has been oxidized in air. If Mn^{2+} is not a hole trap, the only explanation for the observed decrease in Mn^{2+} concentration with UV exposure would be the association of some of these ions with other defects or vacancies, so that the ESR spectrum would account only for the remaining non-associated Mn^{2+} ions. This seems highly improbable, because such a behavior would require diffusion of Mn^{2+} ions, which cannot be achieved by the UV radiation alone. There is actually an involvement of Mn^{2+} with other defects, as evidenced by the changes in ΔH_{pp}, but this is accomplished instead by heat treatments which then allow diffusion to occur, or by high concentrations of defects, vacancies or impurities already present in the "as received" material. Although Mn^{3+} has been seen only in MgO samples doped with about 600 ppm Mn (53), and only as a very small fraction of the total Mn content (1-2%), it seems reasonable to assume that the UV light converts Mn^{2+} to Mn^{3+} by capturing holes. There seems to be an ideal equilibrium state between Mn^{2+} and Mn^{3+} in the lattice, with the UV light contributing to it. When this equilibrium is achieved, the TL reading does not cause any more changes, as has been observed.

Nambi (68) has published a report summarizing the TL properties and correlations with ESR, OA and other measurements in a series of materials, including LiF, $CaSO_4$ and CaF_2, the last two doped with rare-earth ions (RE). His TL mechanisms in $CaSO_4$ (RE) and CaF_2 (RE) are proposed on the basis of charge transfer between the RE^{3+} impurity ions and the SO_4^- and F^- ions, in a similar fashion as it is proposed for MgO. The difference is that the charge transfer in MgO involves vacancies, which are not mentioned in the TL mechanisms for the two samples above, although the holes released from M^{3+} impurity ions in MgO are trapped at the oxygen ions, in analogy to holes being trapped at sulfate and fluorine sites. Nambi also mentions that the TL emission maxima observed in the TL spectral emission curves correspond to different excited electronic levels of the RE^{3+} ions. This means that at a given temperature, a particular excited impurity ion can emit lines corresponding to the transitions between the different excited levels and the ground state. Thus it is possible to have a blue emission from Fe^{3+*} and also the 654 nm and 659 nm lines from the same ion, as observed by Krishnan (47).

The process of charge transfer, either involving vacancies as an intermediate step, or being a direct charge transfer between impurity ions (14), is basically related to the equiibrium of these ions in the lattice with respect to the UV radiation. Therefore, the UV radiation is capable of producing reversible reactions between

the impurity ions, according to the equilibrium rules dictated by the concentrations of impurities in the lattice.

To complement the discussion about the charge transfer mechanism, it is worth commenting on the concentration quenching effect. Nambi (68) points out that there exists an optimum concentration level for maximum TL sensitivity, where an atom, to be an effective emission center, needs a minimum "free lattice space" around it without another atom of the same kind being present. Therefore, an effective charge transfer mechanism, as far as the TL sensitivity is concerned, depends on a certain critical impurity concentration. Cr^{3+}, for example, was seen to cause a quenching effect in MgO. In general, it can be said that a large total concentration of impurities causes the quenching of TL. This will be further discussed in the conclusions for Spicer samples, but it can be advanced here that the Norton samples are less sensitive than the Spicer samples, because the former have higher impurity concentrations than the latter.

Chapter 5

RESULTS AND DISCUSSION FOR MgO-SPICER CRYSTALS

In this chapter, the results for "as received" and air heat treated Spicer crystals are shown. Spicer samples are much purer than Norton samples as seen in table 1, especially for Fe content. Finally the TL sensitivity and TL mechanisms are also discussed.

5.1 TL Characteristics in "As Received" MgO-Spicer Crystals

The TL excitation spectrum of a Spicer sample is basically the same as that for a Norton sample. This is shown in fig.18, for peaks 1, 2 and 3, I_t = 0.01 Ws/cm^2, which can be compared directly with fig. 11 for Norton samples. The TL excitation spectrum maximum occurs here at around 292 nm, indicating that Fe^{3+} is the principal ion responsible for TL in Spicer as well. The half-width at half amplitude is about 20 nm in fig. 18. The wavelength where the maximum occurs, about 300 nm for Norton samples and 292 nm for Spicer samples, is slightly different, possibly due to the way Fe^{3+} interacts with the lattice defects.

The TL response as a function of I_t was studied in three cases: a) non-monochromatic exposure type ii), b) exposure to 249 nm and c) exposure to 289 nm, shown in figs. 19 to 21, respectively. In case a), the TL response is sublinear up to 1.0 Ws/cm^2, saturating around 10 Ws/cm^2. In case b), there is an initial increase followed by a supralinear behavior. Peak 3 is not shown; it

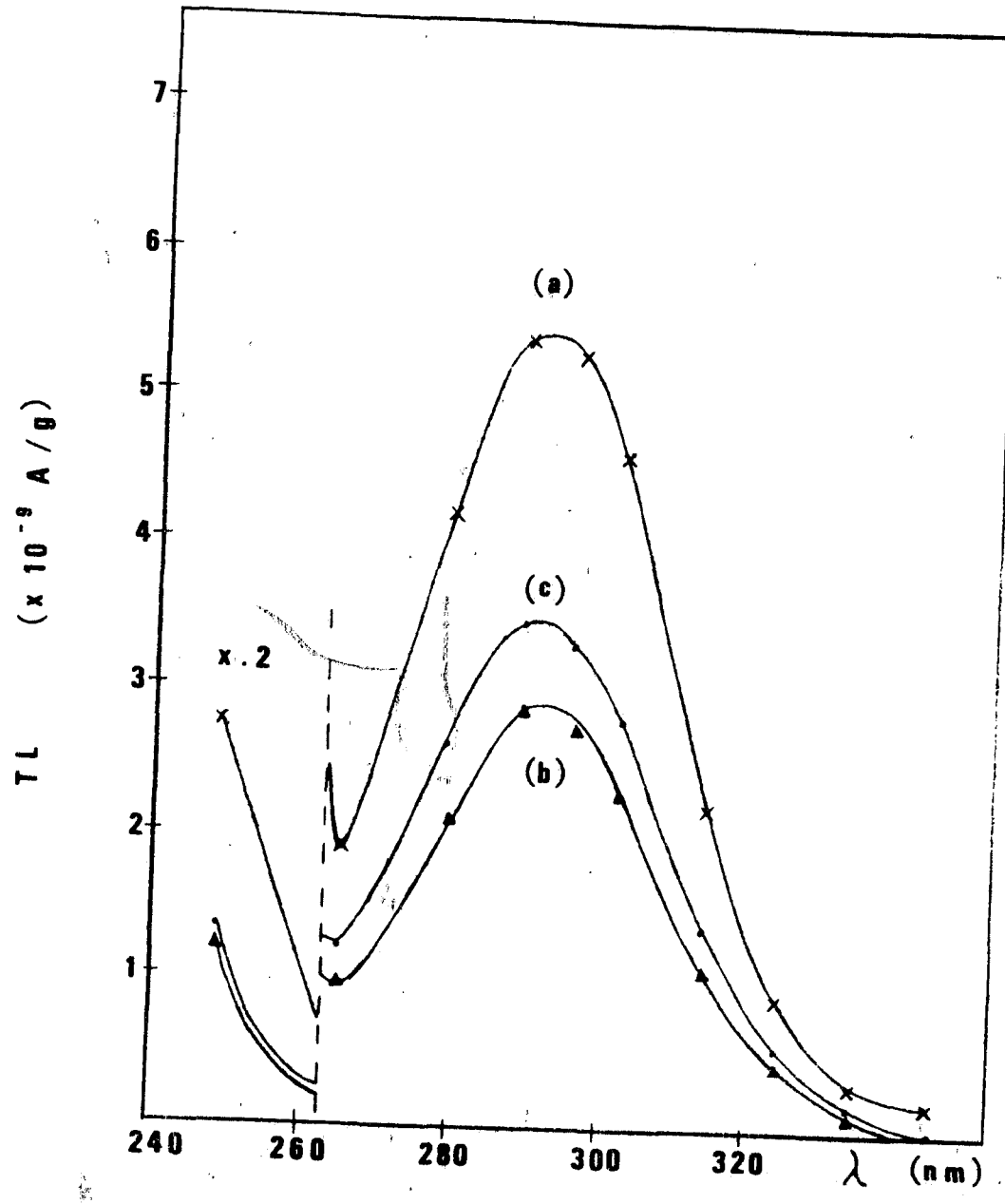

Fig. 18. TL excitation spectrum for peaks 1, 2 and 3 in Spicer crystals S-B and S-C, I_t = 0.01 Ws/cm2. (a) peak 1, (b) peak 2, (c) peak 3.

Fig. 19. TL response as a function of I_t, treatment a) non-monochromatic light type ii), for peaks 1 and 3 in Spicer crystals S-B and S-C. (a) peak 1, (b) peak 3; encircled symbols were obtained after exposing to 70 Ws/cm^2; solid lines represent linearity.

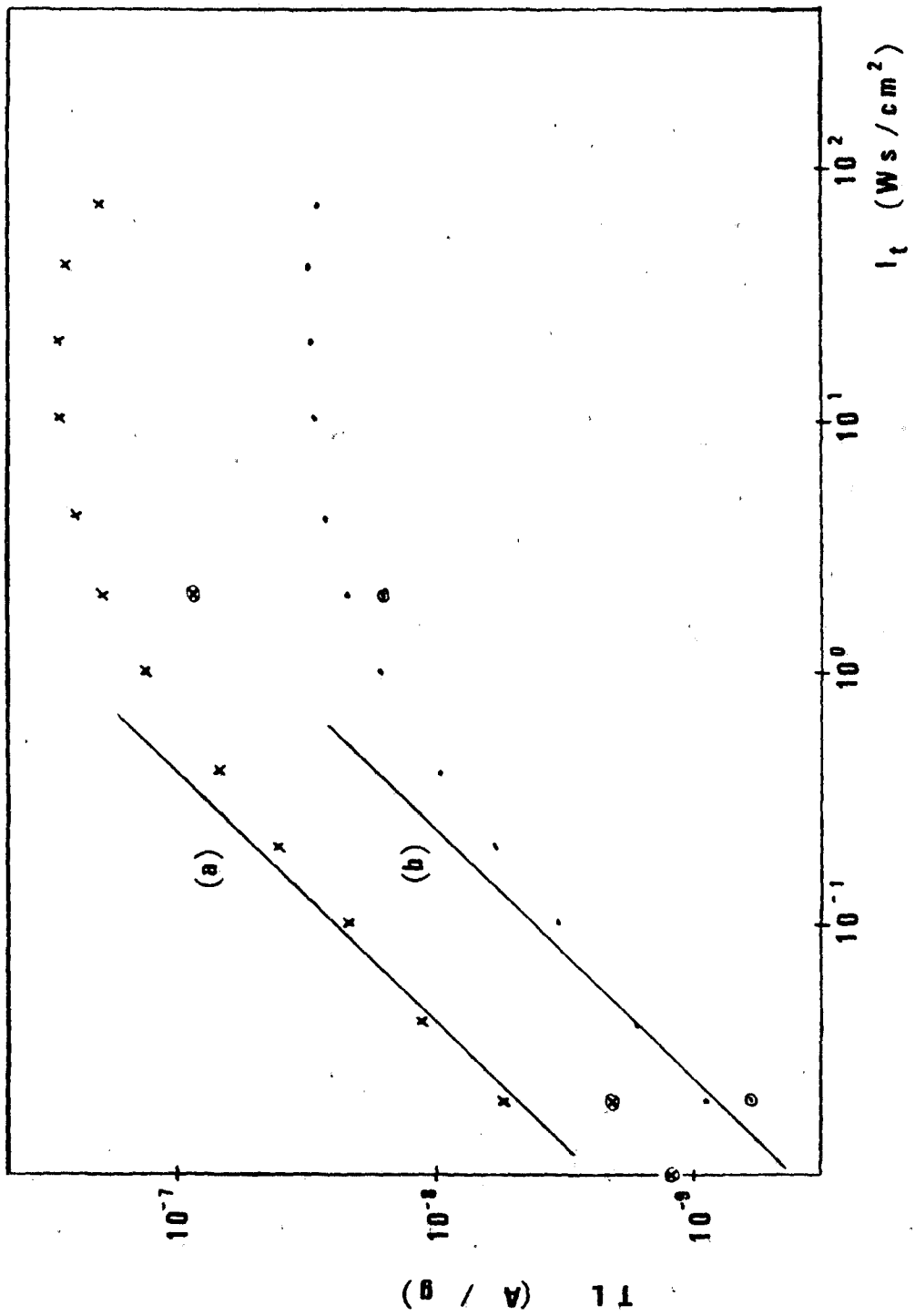
10^{-7}
10^{-8}
10^{-9}
TL (A / g)
(a)
(b)
10^{-1}
10^{0}
10^{1}
10^{2}
I_t (Ws / cm^2)

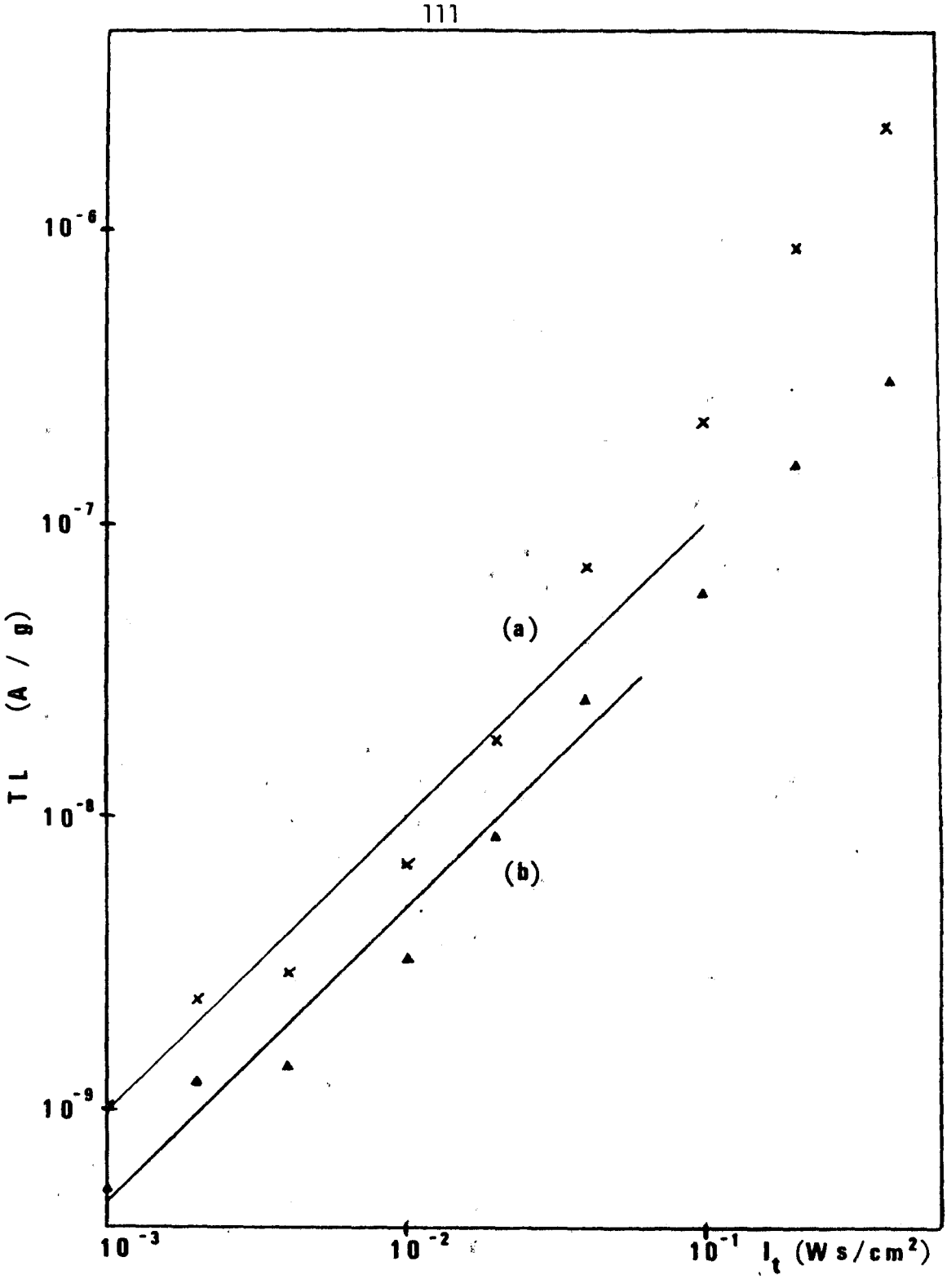

Fig. 20. TL response as a function of I_t, treatment b) 249 nm, for peaks 1 and 2 in Spicer crystals S-B and S-C. (a) peak 1, (b) peak 2; solid lines represent linearity.

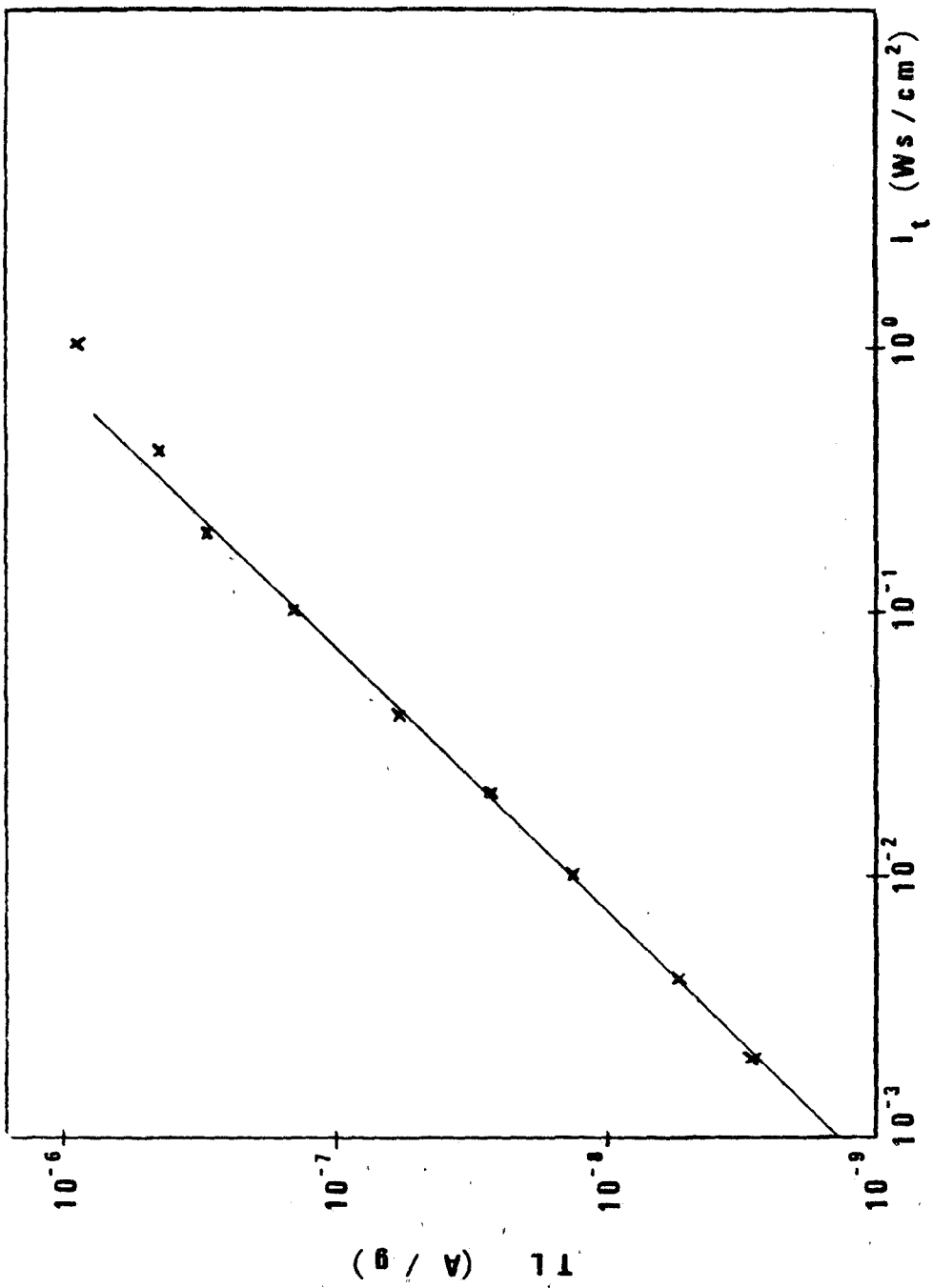

Fig. 21. TL response as a function of I_t, treatment c) 289 nm, for peak 1 in S-B crystals. Solid line represents linearity.

increases with I_t, but not as fast as the other peaks; it becomes a shoulder towards larger I_t's as a result of the faster increase of peaks 1 and 2. In case c), shown only for peak 1, the TL is linear in the range studied. The other two peaks also increase with I_t but become shoulders as I_t increases. There is another TL peak that appears at about 78° C, but only for the successive exposures to 249 nm. Peak 1 occurs at 97° C. It was seen that in Norton samples for this same wavelength, peak 1 was at 76° C and peak 1' at 90° C. It seems then, that there are two trapping levels responsible for these two peaks, the one at lower temperature being dominant in Norton and the one at higher temperature being dominant in Spicer.

In fig. 19, after the exposure to 70 Ws/cm^2, the crystals were exposed to 10^{-2}, 10^{-1} and 0.2 Ws/cm^2, and the TL response was systematically lower than before. This is a desensitization effect, caused by the UV light in this particular experiment. Spicer crystals, in other experiments, show sometimes the reverse effect, that is, they become sensitized after successive exposures to UV light. The reason for this is not well understood, but it could be related to the impurity equilibrium being disturbed by UV light.

The concentrations of Fe^{3+}, Cr^{3+}, Mn^{2+} and V^{2+} ions were measured by ESR in different sets of S-B and S-C crystals. Three UV treatments were employed, following the same nomenclature as for Norton, namely: b) exposure to 249 nm, I_t = 0.2 Ws/cm^2, c) exposure to 289 nm, I_t = 0.2 Ws/cm^2 and d) exposure to non-monochromatic light type i), I_t = 27.6 Ws/cm^2.

The changes in Fe^{3+} concentration are reported in table 12 as the ratios R_1 and R_2; the "as received" Fe^{3+} concentration as determined using ESR, the linewidth ΔH_{pp} in G, the absorption coefficient of the 210 nm band and the ratio $[Fe^{3+}]/\alpha(210)$ are also shown. As can be seen by the ratios R_1 and R_2, the Fe^{3+} content decreases with UV exposure and increases with TL reading, but does not return to the initial value. Compared to the Norton samples in table 2, the changes for Spicer samples are much larger, that is, a relative larger fraction of charges are released by UV light and recombine during TL. The linewidth for Spicer is smaller than for Norton, probably because the former has a smaller total impurity concentration than the latter; similar effects were also observed among different Norton samples. The "as received" Fe^{3+} concentration varies considerably from sample to sample in the same set. The reported values represent an average, which differs from set to set, showing that the original block of crystal from which all the samples were cleaved did not have a homogeneous impurity distribution. The OA band at 210 nm is difficult to measure and only a few results are shown to enable comparison with ESR results.

ESR measurements were also carried out for Cr^{3+} and table 13 is a summary of the observations. Cr^{3+} does not change with UV and TL, except perhaps in case b), where it decreases slightly with 249 nm irradiation. The Cr^{3+} concentration is more uniform among the Spicer crystals and is about 10 times lower than in the NP crystals. The linewidth is also smaller than for the Norton samples.

Table 12. ESR Results for Fe^{3+} in "As Received" MgO-Spicer Samples

Sample	UV treat.	R_1	R_2	Conc (a.u./g)	ΔH_{pp} (G)	$\alpha(210)$ (cm^{-1})	$\frac{[Fe^{3+}]}{\alpha(210)}$
S-B	b	2.68	0.51	29.0			
S-B	c	1.95	0.64	26.7	4.30		
S-B & S-C	d	3.36	0.37	28.5		29.7	0.96
S-C	d	4.42	0.24	22.1	4.34	29.6	0.75
S-B	—	——	——	17.4	4.43	25.2	0.69

Table 13. ESR Results for Cr^{3+} in "As Received" MgO-Spicer Samples

Sample	UV treat.	R_1	R_2	Conc. (a.u./g)	ΔH_{pp} (G)
S-B	b	1.15	1.01	2.39	
S-B	c	1.11	0.98	2.40	0.94
S-B & S-C	d	1.03	1.04	2.60	
S-C	d	1.00	0.91	2.11	0.91
S-B	—	——	——	2.52	0.93

The results for Mn^{2+} are shown in table 14. The Mn^{2+} concentration increases with UV light and decreases with TL, in this case back to the initial value. The concentration changes from one set of samples to the other and is more than 10 times smaller than in Norton samples. The linewidth is also smaller in Spicer, as compared to Norton samples.

Finally, table 15 contains the results for V^{2+}, the concentration of which varies a great deal among the several sets. This impurity increases in concentration upon UV irradiation, in cases b) and d) and does not change significantly with TL reading. In case c) the reverse occurs, that is, the concentration decreases with UV light and increases with TL.

The TL sensitivity was studied for those UV treatments described above and a summary is presented in table 16. The TL amplitude of peak 1 depends on the treatment, but particularly on the sample, varying by a factor of about 30 from one crystal to the other, as seen for samples S-B & S-C in table 16. Peaks 2 and 3 are very small and appear only as shoulders. The peak temperatures, as well as the interval between UV irradiation and TL reading are also reported. The ranges of TL response for peak 1, case d), (tables 6 and 16), vary from 0.3×10^{-8} to 0.3×10^{-6} A/g and from 0.3×10^{-6} to 1.0×10^{-5} A/g, respectively for Norton and Spicer samples.

It seems then, that a high TL sensitivity is achieved in pure crystals and for those in which the ratios R_1 and R_2 reveal significant changes in impurity concentration, mainly of Fe^{3+}. The

Table 14. ESR Results for Mn^{2+} in "As Received" MgO-Spicer Samples

Sample	UV treat.	R_1	R_2	Conc. (a.u./g)	ΔH_{pp} (G)
S-B	b	0.86	1.14	2.08	
S-B	c	0.92	1.15	2.15	1.02
S-B & S-C	d	0.74	1.40	1.83	
S-C	d	0.77	1.29	1.47	1.02
S-B	—	——	——	2.71	1.04

Table 15. ESR Results for V^{2+} in "As Received" MgO-Spicer Samples

Sample	UV treat.	R_1	R_2	Conc. (a.u./g)	ΔH_{pp} (G)
S-B	b	0.79	1.16	2.37	
S-B	c	1.24	0.88	2.91	0.56
S-B & S-C	d	0.58	1.08	1.46	
S-C	d	0.59	1.00	0.61	0.55
S-B	—	——	——	3.21	0.54

Table 16. TL Sensitivity to UV Light of "As Received" MgO-Spicer Samples

Sample	UV treat.	TL_1 ($X10^{-6}$A/g)	TL_2 ($X10^{-6}$A/g)	TL_3 ($X10^{-6}$A/g)	T_1 (°C)	T_2 (°C)	T_3 (°C)	Δt_{UV-TL} (h.)
S-B	b	0.67-5.57	sh.	sh.				2
S-B	c	0.12-2.59	sh.	sh.	94	143	178	3
S-B & S-C	d	0.34-10.3	sh.	sh.				24
S-C	d	0.44-5.11	sh. 0.13	sh. 0.09	92	140	171	4.5
S-B	c	0.08-2.16	sh.	sh.	90			0

peak temperatures for the Spicer samples are higher than those for NP crystals and between the temperatures of the two groups of ND samples, especially for peak 1.

Assuming that the TL response of the TL peaks is linearly proportional to $[Fe^{3+}]$ as was found for Norton samples in fig. 17, the TL results from table 16, except for S-C, were normalized for $[Fe^{3+}]$ and for thickness, and plotted as a function of V^{2+} concentration, as shown in fig. 22. It is interesting to observe that the TL response is a power function of $[V^{2+}]$. This indicates that the wide non-reproducibility in the results among the crystals may be explained by their V^{2+} content. The reason for this behavior, though, is not understood, especially because this ion is not involved in the emission process, but is related to the activator center, V^{3+}.

In an attempt to identify the different trapping and emission centers responsible for each TL peak, a series of partial TL readings was performed, consisting of the following steps:

i) UV irradiation, treatment d);

ii) TL reading up to T_a, $T_1 < T_a < T_2$, to erase only peak 1;

iii) TL reading up to T_b, $T_2 < T_b < T_3$, to erase only peak 2;

iv) TL reading up to T_c, $T_c > T_3$, to erase peak 3.

The experiment was first carried out using T_a = 140° C and, joining steps iii) and iv), using T_c = 250° C. Then the complete cycle was repeated, using T_a = 100° C, T_b = 180° C and T_c = 250° C.

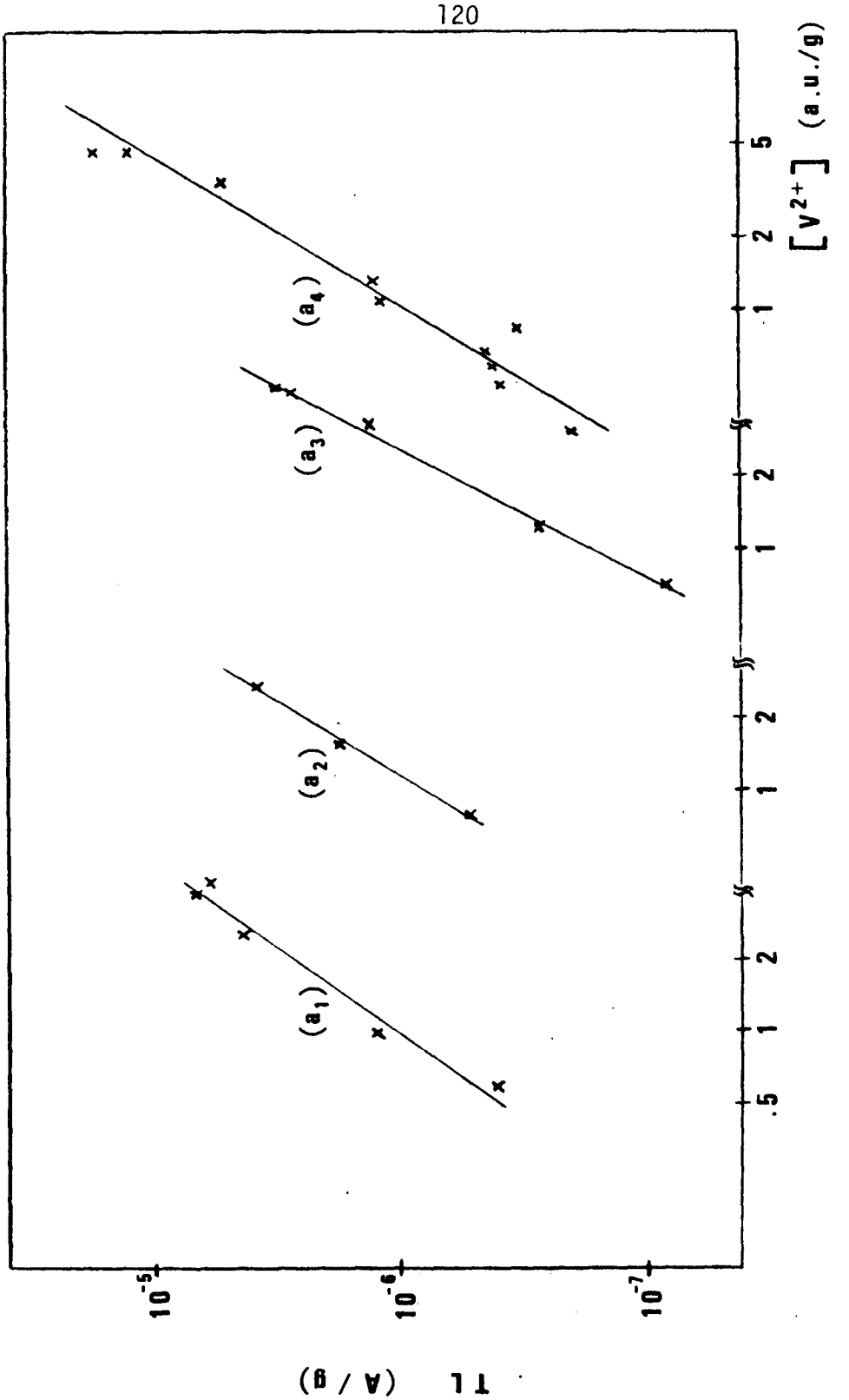
TL (A / g)
10^{-5}
10^{-6}
10^{-7}
(a_1)
(a_2)
(a_3)
(a_4)
.5 1 2 5 1 2 5 1 2 5 1 2 5
$[V^{2+}]$ (a.u./g)

Fig. 22. TL response of peak 1 normalized for Fe^{3+} concentration (30 a.u./g) and thickness (1.5 mm) as a function of V^{2+} concentration. (a_1) S-B, treatment b) 249 nm, Δ_{UV-TL} = 2 h.; (a_2) S-B, treatment c) 289 nm, Δ_{UV-TL} = 0 h.; (a_3) S-B, treatment c) 289 nm, Δ_{UV-TL} = 3 h.; (a_4) S-B and S-C, treatment d) non-monochromatic light type i), Δt_{UV-TL} = 24 h. Log-log scale.

The ESR was recorded between each of the three last steps, and the results, together with the TL output, are presented in table 17. One set of three S-B crystals was employed. The concentration ratios between each step are indicated for each ion, where the number after R_2 indicates the maximum temperature for the TL reading. R_3 is the ratio between two consecutive TL readings. The ratio R_1 was taken from tables 12 to 14, for Fe^{3+}, Cr^{3+} and Mn^{2+}, and it was assumed for V^{2+} that the TL reading does not change its concentration. Therefore, the ratio R_2-140 is assumed to be equal to one for V^{2+}, and from this value the ratio R_1 was extrapolated.

In this experiment, the Fe^{3+} concentration decreased during UV irradiation, Mn^{2+} and V^{2+} increased and Cr^{3+} remained constant, as already seen. Most of the recombination for Fe^{3+} occurs when TL peak 1 is recorded, and less recombination when peaks 2 and 3 are read out. When the experiment was repeated, in three partial TL readings, the same behavior was observed, more recombination occurring at lower temperatures and less recombination occurring at higher temperatures. When reading up to 100° C, TL peak 1 was not completely erased, since about 25% of it was still present in the next TL reading. The results agree with the TL sensitivity in "as received" Spicer, since peaks 2 and 3 are only shoulders and, accordingly, the fraction of charges recombining with Fe^{2+} during readout of these peaks is small, in comparison with peak 1. Most of the recombination occurs during readout of peak 1, which is the most sensitive of the three peaks.

Table 17. Partial TL Readings in "As Received" MgO-Spicer Samples

Peak	Ratios	Fe^{3+}	Cr^{3+}	Mn^{2+}	V^{2+}	TL/g ($X10^{-6}$A/g)
	Sample S-B--UV treat. d)					
	R_1	2.32	1.00	0.85	0.48	
1	R_2-140	0.48	1.01	1.17	1.00	3.98
2	R_3-140-250	0.80	0.97	1.12	1.01	0.16
3						0.18
	R_1	2.32	1.00	0.74	0.83	
1	R_2-100	0.62	0.98	1.13	1.00	4.37
1	R_3-100-180	0.74	1.01	1.14	1.18	1.09
3	R_3-180-250	0.81	1.07	0.96	0.98	0.06

The concentration of Mn^{2+} decreases during the TL reading; the recombination is not as effective as for Fe^{3+}, but it seems that most of it occurs at lower temperatures.

V centers were investigated in a few "as received" samples using ESR. The results showed that the V_{Al}-V^- center was present in a concentration somewhat lower than in the "as received" NPO crystal.

The IR spectrum for Spicer samples showed lines at 3296 cm^{-1}, due to the V_{OH}^- center, at about 3690 cm^{-1}, due possibly to $Mg(OH)_2$ or $Co(OH)_2$ precipitates, and very small absorptions at about 3550 cm^{-1}, attributed to $Fe(OH)_2$ precipitates. After a UV exposure, there is a tendency for all these lines to decrease, but this behavior could not be investigated in detail because of the difficulties in measuring the IR absorption in very thin crystals. The IR spectrum of the Spicer samples is different from that of Norton samples; the former has V_{OH}^- centers, while the latter shows neutral V_{OH} centers, that is, V_{OH}^- which have captured a hole. It could also be possible that the absorptions at 3296 cm^{-1} and at 3323 cm^{-1} in these two samples are due to the same V_{OH} or V_{OH}^- centers, perturbed by trivalent impurities. The lower energy absorption in Spicer could then be the result of a smaller perturbation, since there are fewer impurities, as compared to Norton. This interpretation, though, is not supported by the literature. For example, Vance and Mallard (69) report the line at 3296 cm^{-1} as due to V_{OH}^- centers which, upon γ-radiation, shifts to 3323 cm^{-1}. They

associate the V_{OH}^{-}-M^{3+} complexes rather to higher energy satellites of the 3296 cm^{-1} line, such as the 3310 cm^{-1} line. Another difference is the second most prominent line, which in Spicer is at 3690 cm^{-1}, and for Norton, at 3550 cm^{-1}. The presence of V centers in Spicer samples can also be inferred from OA measurements, which showed an increased background in the visible region of the spectrum. This is also seen as a darkening coloration every time the crystal is exposed to UV light.

Spicer crystals also show the Cr^{3+}[100] line in a much lower concentration than in the ND samples, but about the same as the NPO crystals.

5.2 TL Characteristics in Air Heat Treated MgO-Spicer Crystals

Two sets of S-C samples were heat treated in air at 1000° C and 1400° C for 3 h., and one set of S-B, at 1400° C for 24 h. The usual series of measurements were performed and the results for Fe^{3+} are shown in table 18. The oxidation of Fe, represented by the ratio $\Delta[Fe^{3+}]/[Fe^{3+}]$, is seen to be more efficient at 1400° C and for longer annealing times. This ratio is comparable to those for NP3 in table 7. The UV light reduces the Fe^{3+} concentration, which is recovered with the TL reading. For S-B, however, the recovery is not complete. This could be a true effect or a discrepancy in the ESR results, since Mn^{2+} behaves differently than expected, as mentioned below. The first two rows of figures for each heat treatment with S-C correspond to Δt_{UV-TL} = 4.5 h., while the third

row corresponds to Δt_{UV-TL} = 51 h. For S-B, Δt_{UV-TL} = 9 h. The linewidth does not change much with the air heat treatment, but it increases with UV exposure, decreasing after TL.

Table 18. ESR Results for Fe^{3+} in Air Heat Treated MgO-Spicer Samples

Sample	Heat treat.	UV treat.	R_1	R_2	$\frac{\Delta[Fe^{3+}]}{[Fe^{3+}]}$	ΔH_{pp} (G)
S-C	1000° C 3 h.	d	3.78	0.28		
		d	3.01	0.37	1.24	4.40
		d	2.22	0.49		
S-C	1400° C 3 h.	d	2.74	0.41		
		c	1.80	0.57	1.72	4.59
		c	1.65	0.62		
S-B	1400° C 24 h.	d	2.32	0.56	3.60	4.41

Similar to the results from Norton samples, the annealing in air has a tendency to reduce Cr^{3+}, but only at 1000° C. At 1400° C, Cr^{3+} is already stabilized. Table 19 shows the results for this ion, indicating that no significant changes occur with UV exposure and TL reading. The linewidth is somewhat smaller than in the "as received" case, but the difference is not significant, as opposed to the case of Norton, for which the heat treatment caused the linewidth to increase.

Table 19. ESR Results for Cr^{3+} in Air Heat Treated MgO-Spicer Samples

Sample	Heat treat.	UV treat.	R_1	R_2	ΔH_{PP} (G)
S-C	1000° C 3 h.	d	1.01	0.92	
		d	0.95	1.01	0.89
		d	0.97	1.00	
S-C	1400° C 3 h.	d	1.02	1.02	
		c	1.00	1.06	0.89
		c	0.97	1.09	
S-B	1400° C 24 h.	d	1.11	0.90	0.93

As for Mn^{2+}, there is a tendency for this ion to be oxidized at 1000° C, but at 1400° C, the reverse effect was observed, that is, its concentration increased, similar to the results for Norton. In this case, different equilibrium reactions are probably involved at different temperatures, depending on the concentration of other impurities. Table 20 summarizes the results for Mn^{2+}, showing that its concentration increases with UV light and decreases with TL. The conversion is complete, except when it is the first exposure after the heat treatment, as shown in the first row of figures for each set of samples. Only in the case of S-B, R_1 is larger than 1.0, which does not agree with the results for S-C. It is likely that the equilibrium concentration was affected in a different way here,

during the annealing treatment or the UV treatment. The linewidth is somewhat larger in the heat treated samples, but not significantly so.

Table 20. ESR Results for Mn^{2+} in Air Heat Treated MgO-Spicer Samples

Sample	Heat treat.	UV treat.	R_1	R_2	ΔH_{pp} (G)
S-C	1000° C 3 h.	d	0.83	2.31	
		d	0.48	2.05	1.03
		d	0.51	1.92	
S-C	1400° C 3 h.	d	0.92	1.60	
		c	0.74	1.22	1.04
		c	0.75	1.20	
S-B	1400° C 24 h.	d	1.23	1.34	1.08

V^{2+} is completely oxidized in air, at least within the detection range of the ESR measurement. Therefore, the ratio R_1 reported as zero in table 21 is for those samples exposed the first time to UV light, after the heat treatment. The UV light regenerates V^{2+} which stays approximately constant in the subsequent exposures and TL readings, within the experimental error; the error is much larger for this ion due to noise interference. There is no significant change in the linewidth with heat treatments.

Table 21. ESR Results for V^{2+} in Air Heat Treated MgO-Spicer Samples

Sample	Heat treat.	UV treat.	R_1	R_2	ΔH_{PP} (G)
S-C	1000° C 3 h.	d	0	1.39	
		d	0.85	1.03	0.54
		d	0.91	0.97	
S-C	1400° C 3 h.	d	0	1.06	
		c	0.99	1.14	0.52
		c	0.96	1.13	
S-B	1400° C 24 h.	d	0	1.10	0.54

After annealing at 1400° C, but not at 1000° C, the TL response is more homogeneous among the crystals and so is the V^{2+} concentration. It seems, therefore, that this heat treatment tends to stabilize vanadium, so that the TL sensitivity becomes more reproducible.

The TL sensitivity of the annealed crystals is shown in table 22, where the first, third and fourth rows of each set of samples correspond to those in the previous tables 18 to 21. The peak temperatures, the ratio between TL peak amplitudes and Δt_{UV-TL} are also listed. It can be seen that TL peak 1 becomes sensitized by a factor greater than 3, when comparing the results of annealing at 1400° C with those for 1000° C. At 1000° C, however, the

Table 22. TL Sensitivity to UV Light of Air Heat Treated MgO-Spicer Samples

Sample	Heat treat.	UV treat.	TL_1 ($X10^{-6}$A/g)	TL_2 ($X10^{-6}$A/g)	TL_3 ($X10^{-6}$A/g)	T_1 (°C)	T_2 (°C)	T_3 (°C)	r_{12}	r_{13}	Δt_{UV-TL} (h.)
S-C	1000° C 3 h.	d	1.97	sh.	0.14 sh.	93	—	174	—	14.1	4.5
		d	2.20	—	sh.				—	—	0
		d	2.05	—	sh.				—	—	4.5
		d	1.52	—	sh.				—	—	51.0
S-C	1400° C 3 h.	d	7.31	3.30	sh.	94	135	177	2.2	—	4.5
		c	1.26	0.65	0.08				1.9	15.7	0
		c	0.88	0.48	0.07				1.8	12.6	4.5
		c	0.64	0.41	0.06				1.6	10.7	51.0
S-B	1400° C 24 h.	d	6.49	1.64 sh.	0.21 sh.	92	132	173	3.9	30.9	0
		d	3.71	0.97 sh.	0.16 sh.				3.8	23.2	9

sensitization factor for this peak is about 1.3 as compared to the "as received" crystals. TL peak 2 becomes sensitized only at 1400° C, probably as much as in the Norton samples, as indicated by an analysis of the r_{12} ratios. TL peak 3 is still a shoulder, and comparing the ratio r_{13} with those for Norton in table 10, the conclusion is that peak 3 is not sensitized in Spicer.

In summary, Norton samples heat treated in air show a large sensitization effect for peak 3, and a smaller one for peaks 2 and 1, as compared to "as received" samples. Spicer crystals, on the other hand, show a large sensitization effect only for peaks 1 and 2.

Fading was investigated for the Spicer samples, where the TL response was recorded at zero, 4.5 and 51.0 hs. after the UV exposure, as shown in table 22. The curves for 1000° C, treatment d) and 1400° C, treatment c) are plotted in fig. 23. Earlier results for powder samples, which had not been heat treated, and had been exposed to unfiltered non-monochromatic UV light, showed a behavior similar to that for the crystals annealed at 1000° C. One particular S-B crystal, without heat treatment, was left in the dark for four months, showing a decrease in TL peak 1 amplitude only by a factor of 12.6.

Comparing fading results between Spicer and Norton, it is evident that Spicer is much more stable, indicating that most of the trapping centers for peak 1 are probably V^- centers; these centers are more stable than the V_{Al} centers responsible for peak 1 in Norton samples. V centers were investigated using ESR in one

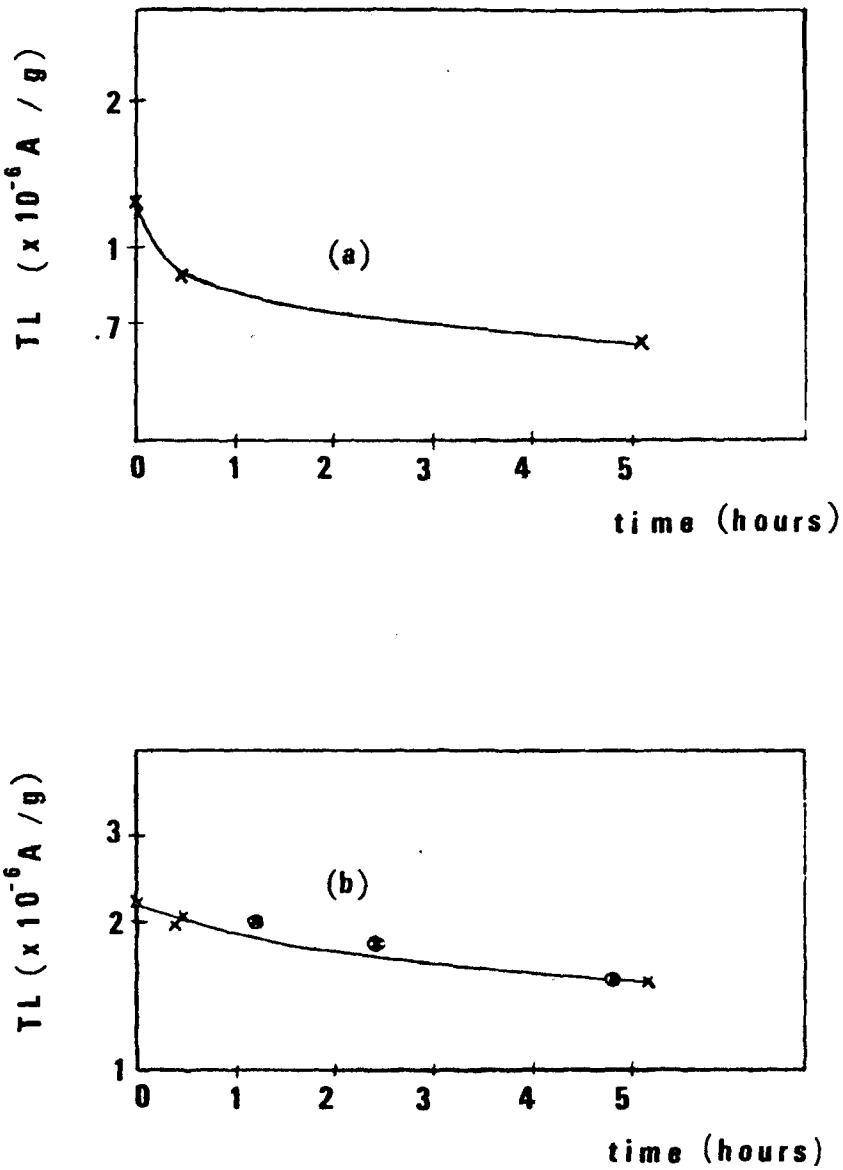

Fig. 23. Fading of TL peak 1 for S-C samples annealed in air. (a) heat treated at 1400° C for 3 h. exposed to treatment c) 289 nm, (b) heat treated at 1000° C for 3 h., exposed to treatment d) non-monochromatic light type i); encircled symbols represent "as-received" Spicer powder.

Spicer crystal, S-B, annealed at 1400° C, and exposed to non-monochromatic UV light type i). The concentration of these centers is about the same as in one NP3 annealed crystal, but higher than before the heat treatment. Observing the fading of this center by measuring the ESR signal at 45 min., and at 73 hs. after the UV exposure, the decrease was only 25% during this time interval. This means that the V centers are mostly composed by the V^- center, at least 75% of the concentration, while 25% is due to other less stable V-type centers.

Examining the OA spectrum in the visible region, the Spicer crystals absorb less than Norton, where both are air heat treated. This means that the former become less colored than the latter, with UV light. Therefore, the OA measurements show that Norton samples contain more V centers than Spicer, probably including different types than those measured by ESR, since this technique gave similar concentrations in both samples. The V_{OH}^- center and the line at 3690 cm^{-1} do not disappear at 1000° C, while the whole spectrum vanishes at 1400° C.

Partial TL readings were performed with the set of Spicer samples annealed at 1400° C and exposed to 289 nm. The temperatures were T_a = 115° C, T_b = 165° C and T_c = 250° C. Table 23 summarizes the results. Cr^{3+} and V^{2+} do not change, but Fe^{3+} and Mn^{2+} concentrations, respectively decrease and increase with UV light. The partial TL readings indicate that most of the recombination for Fe^{3+} occurs at the last stage, that is, between 165° C and 250° C. This

recombination actually increases with increasing temperature. For Mn^{2+}, the recombination is more efficient at the first and third stages. This behavior will be discussed in more detail in the next section.

Table 23. Partial TL Readings in Air Heat Treated MgO-Spicer Samples

	Sample S-C--UV treat. c)					
Peak	Ratios	Fe^{3+}	Cr^{3+}	Mn^{2+}	V^{2+}	TL/g ($X10^{-6}$A/g)
	R_1	1.80	1.00	0.74	0.99	
1	R_2-115	0.91	1.06	1.19	1.10	0.58
2	R_3-115-165	0.82	1.03	1.08	1.07	0.26
3	R_3-165-250	0.75	0.96	1.24	1.02	0.04

5.3 TL Mechanisms and Discussion

Following the same procedure in this section as for Norton samples, TL mechanisms will be proposed in terms of the results obtained for Spicer and will be compared to those for Norton.

5.3.1 TL Mechanisms

The same equilibrium reaction,

$$2Fe^{2+} + \frac{1}{2} O_2 \rightleftharpoons 2Fe^{3+} + O^{2-} + V^{=},$$

seems to be operative during the heat treatment in air and the discussion developed for Norton samples also applies in this case.

Additional vacancies are created at 1400° C according to the dissociation reaction:

$$V_{OH}^{-} \rightleftharpoons V^{=} + H^{+}.$$

This is slightly different from the reaction occurring in Norton crystals, which involve V_{OH} centers instead. Since Spicer crystals have a much lower impurity content, it is expected that these vacancies will have a low probability of associating with trivalent impurities, contributing therefore only to a low concentration of V_M-type centers. Rather most of the vacancies will be available to form the V^{-} centers, as evidenced in the fading and other experiments, discussed above.

During the oxidation process at 1000° C, the equilibrium reaction that takes place is the following:

$$Fe^{2+} + Cr^{3+} + Mn^{2+} + V^{2+} \rightleftharpoons Fe^{3+} + Cr^{2+} + Mn^{3+} + V^{3+},$$

while at 1400° C, the behavior for Mn is reversed and Cr is already stabilized, as expressed by the equation:

$$Fe^{2+} + Mn^{3+} + V^{2+} \rightleftharpoons Fe^{3+} + Mn^{2+} + V^{3+}$$

The major reactions occurring at these two temperatures are the oxidation of Fe and V, while Cr and Mn show only tendencies to one valence state or the other. This is basically the same behavior verified in Norton heat treated samples.

The equilibrium equations expressing the changes observed during UV exposure and TL reading can be written as follows:

$$Fe^{3} + Mn^{3+} + V^{3+} + V^{=} \xrightarrow{b)d)} Fe^{2+} + Mn^{2+} + V^{2+} + V^{-} + V_M,$$

$$Fe^{2+} + Mn^{2+} + V^{-} + V_M \xrightarrow{TL} Fe^{3+} + Mn^{3+} + V^{=}$$

and $$Fe^{3+} + V^{2+} + Mn^{3+} + V^{=} \underset{TL}{\overset{c)}{\rightleftharpoons}} Fe^{2+} + V^{3+} + Mn^{2+} + V^{-} + V_M$$

for "as received" samples, and

$$Fe^{3+} + Mn^{3+} + V^{3+} + V^{=} \underset{TL}{\overset{c)d)}{\rightleftharpoons}} Fe^{2+} + Mn^{2+} + V^{2+} + V^{-} + V_M$$

for air heat treated samples. For UV treatments b) and d), in "as received" crystals, V^{3+} is reduced to V^{2+} and remains constant with TL, but for treatment c), V^{2+} oxidizes to V^{3+}, reducing after TL. Mn^{3+} always reduces to Mn^{2+} with UV, which reverts to Mn^{3+} with TL reading. For air heat treated samples, vanadium is reduced to V^{2+} by UV light and its concentration does not change with TL reading. Cr^{3+} does not take part in either reaction. It is supposed that the trapping centers are mostly V^{-} centers and to a smaller extent, V_M-type centers. Both centers are formed when holes, released by UV light from Fe^{3+}, Mn^{3+} and V^{3+}, are captured by vacancies in the lattice. These ions are the activator centers.

The emission centers are probably only Fe^{2+} and Mn^{2+} ions, which capture holes thermally released from the V centers. These

ions become, respectively, Fe^{3+*} and Mn^{3+*}, emitting light seen as TL and returning to the ground state as Fe^{3+} and Mn^{3+}. Most of the emission is due to holes recombining with Fe^{2+}, that is, due to the transition Fe^{3+*} (excited state) $\longrightarrow$ Fe^{3+} (ground state), which agrees with the TL response versus wavelength curve, in the sense that the TL being recorded is both proportional to the Fe^{3+} absorption and emission. For this reason, the TL excitation spectrum peaks at lower energies, a fact known as the Stoke's shift, where the energy of emission is always lower than the energy of absorption. In this case, therefore, the emission of Fe^{3+} would be more important in the TL response than its absorption. This is also the probable explanation for having α_{eff} of the order of 8 cm^{-1} in the dependence of TL on thickness in fig. 7, and smaller than the absorption coefficient $\alpha(285)$, about 45 cm^{-1} in Norton samples. The determination of α_{eff} probably includes other TL emission lines besides that of Fe^{3+}.

The V_{OH}^{-} and the $Cr^{3+}[100]$ (or V_{Cr}) centers observed in the "as received" Spicer crystals may be involved in the TL mechanisms, but they were not investigated in any detail in this research.

The evidence indicates, therefore, that the TL mechanisms in Spicer samples are much simpler than those in Norton samples, where all sorts of additional reactions appear to occur. Comparing the TL sensitivity for both crystals, it was observed that Spicer samples are more sensitive than Norton samples by a factor of approximately 30 times, attributable mainly to the lower content of

total impurities in the Spicer samples. Another significant difference between these crystals is the stability of TL peak 1, which fades rapidly in Norton but more slowly in Spicer samples, due to the nature of the trapping centers. These are identified as V_{Al} and V^-, respectively, and are associated with the TL peak in question. In agreement with this relationship is the TL peak 1 temperature, which is about 76° C in Norton and about 96° C in Spicer, showing that the V_{Al} trapping centers are really shallower than the V^- centers.

The air heat treatment was seen to sensitize TL peak 3 in Norton samples, for which Mn^{2+} is possibly one of the trapping centers. On the other hand, this annealing does not sensitize peak 3 in Spicer, but rather TL peak 1. Accordingly, Mn^{2+} is not identified as a trapping center in Spicer. If it were, this crystal would be expected to show a sensitization effect for peak 3. Therefore, Mn^{2+} acts as a trapping center in Norton and an emission center in Spicer samples.

From the partial TL readings it was observed that in the "as received" Spicer samples the TL emission was mostly due to holes recombining with Fe^{2+} and Mn^{2+}. The recombination was more efficient at lower temperatures, giving a higher TL peak 1. In air heat treated samples the same ions were involved, but the behavior is reversed, that is, the recombination increases its efficiency with temperature. However, the sensitization effect is felt more for peak 1, but not for peak 3. This could be either a kind of thermal

quenching of the luminescence efficiency or a case where fewer trapping centers are being populated to account for the TL peak 3 emission. In the second hypothesis, the fact that Mn^{2+} is not involved as a trapping center would contribute to the low sensitivity of that peak. This ion acts rather as an emission center, where the transition Mn^{3+*} (excited state) $\longrightarrow$ Mn^{3+} (ground state) occurs probably in the orange region of the spectrum.

As for V, it was seen that V^{3+} is the activator center and from the TL response as a function of $[V^{2+}]$, which showed a power function behavior, one can say that the higher the V^{3+} concentration the more V^{2+} ions will result during UV irradiation, and thus, the higher the TL sensitivity will be. The TL sensitivity and reproducibility depend largely on the V^{2+} concentration, for when this is stabilized, the TL becomes reproducible.

Finally, to summarize, the activator centers in Norton and Spicer were identified respectively as Fe^{3+} and Fe^{3+}, Mn^{3+} and V^{3+}. The trapping centers are V_{Al}, V_{Fe} and Mn^{2+} for peaks 1, 2 and 3 in Norton, and V^{-} for peak 1 in Spicer. For the other two peaks in Spicer samples, it was not possible to assign trapping centers. The emission centers are mainly Fe^{2+} in Norton and Fe^{2+} and Mn^{2+} in Spicer, which capture holes and subsequently release light, the energy of which could possibly be assigned as being in the orange-red region for the $Fe^{3+*} \longrightarrow Fe^{3+}$ and $Mn^{3+*} \longrightarrow Mn^{3+}$ transitions. The well-established R-emission lines assigned to Cr^{3+}

transitions by Wertz et al. (7) are likely to be involved in the proposed TL mechanisms only for high energy UV radiation.

5.3.2 Discussion of results

The data for Spicer crystals confirm the result, already demonstrated for Norton samples, that Fe is the major impurity ion involved in the TL mechanism. In addition, vanadium ions seem to play an important role in Spicer samples. It has been reported (51) that V^{3+} absorbs at 240 nm, 414 nm and 620 nm, while V^{2+} absorbs at 310 nm (16), 502 nm and 714 nm (50), as already noted in chapter 2. Our results show that the 249 nm and the non-monochromatic exposures favor the $V^{3+} \longrightarrow V^{2+}$ conversion, while the $V^{2+} \longrightarrow V^{3+}$ conversion is seen to occur under 289 nm radiation, both processes being in agreement with the reported absorption bands.

The observed TL sensitivity, behaving as a power function of V^{2+} concentration, indicates that the kinetics responsible for the TL mechanism are not of first order. The functional relationship is such that the order of the kinetics involved is between 1.6 and 1.8. An appropriate model to explain this behavior can only be developed on the basis of more experimental work, such as to determine the role of vacancies directly related to these ions, and the interactions between V ions and other impurities. These interactions are very important when it comes to the TL reproducibility in MgO, since the equilibrium of V^{2+} impurities achieved after air heat treatment seems to contribute to a better TL reproducibility.

The V^{2+} power function behavior can be interpreted in terms of equilibrium reactions such as those proposed in section 5.3.1. The UV exposure and the TL reading, respectively, set the forward and reverse reactions, so that the reversible reaction

$$\alpha Fe^{3+} + \beta Mn^{3+} + \gamma V^{3+} + \delta V^{=} \underset{TL}{\overset{UV}{\rightleftharpoons}} \alpha' Fe^{2+} + \beta' Mn^{2+} + \gamma' V^{2} + \delta' V^{-}$$

would be characterized by an equilibrium constant

$$k_e = \frac{[Fe^{2+}]_e^{\alpha'} \; [Mn^{2+}]_e^{\beta'} \; [V^{2+}]_e^{\gamma'} \; [V^{=}]_e^{\delta'}}{[Fe^{3+}]_e^{\alpha} \; [Mn^{3+}]_e^{\beta} \; [V^{3+}]_e^{\gamma} \; [V^{-}]_e^{\delta}}$$

where $\gamma' \simeq 1.6$ and $\alpha \simeq 1.0$; the other parameters are not known. The observed fact that in several cases k_e appears to be greater than one, that is, that the reverse reaction (TL reading) does not restore the initial conditions, would indicate that the divalent impurities are present in higher equilibrium concentrations than their trivalent counterparts or that the primed exponents are larger than the non-primed ones.

The greatest experimental difficulty encountered in a study of this type is to be able to change significantly the concentration of only one impurity of a given valence state without affecting the others, or to change the concentration of an impurity such as Mn^{2+} only by means of heat treatments. To affect changes in individual ion concentrations is the only sure way that the parameters in an

equation such as that above can be determined using UV exposure and TL readings.

The existence of V_{Fe} centers has not been postulated previously for Spicer samples, by virtue of the low Fe^{3+} concentration in this material, and therefore of the low vacancy concentration, but these centers are not to be ruled out as a possibility, even at very low concentrations. In the Norton samples, where the V_{Fe} concentration may be higher than in Spicer, it is likely that the Fe^{3+}-vacancy complex works as an entity during UV irradiation and subsequent TL reading, in the sense that the charge transfer mechanism is a local process occurring within this complex, and not between the vacancies of the V_{Fe} centers and other unrelated impurities. The charge transfer, being the result of low energy radiation such as UV, is more likely to occur between impurity ions and nearby vacancies as in the case of the V_{Fe} centers, with no need for the charge being released from the Fe^{3+} ion to be completely ionized before being trapped at the oxygen ion next to the vacancy. Similar processes would be operative involving other V_M centers as well.

The partial TL reading experiments performed simultaneously with the ESR measurements could provide one additional piece of information if the V centers were easily observed. Krishnan (47), using ESR below room temperature, was able to observe the decrease in the V centers concentration and the increase in the Fe^{3+} concentration, for increasing temperatures of TL readings. Unfortunately,

these types of experiments show only the general TL mechanism, but they do not tell anything about the specific structural situation of the impurities in the lattice, such as the existence of the V_{Fe} centers.

At first sight, it would seem natural to correlate the supralinear behavior of the TL peak 1 with the 249 nm intensity in figs. 14 and 20 with the power function relationship of the TL and V^{2+} concentration in fig. 22. This correlation probably would be incorrect, because the same V^{2+} concentration dependence is observed for all wavelengths studied, while the supralinear behavior is a characteristic only of the 249 nm radiation.

From the present results, the supralinearity is interpreted as the sum of the 76° C and 97° C TL peak responses, which increase with UV intensity at different rates. The 76° C peak is most intense in Norton samples, while the 97° C peak is most intense in Spicer samples. The final result is the same for both, since the TL response for peak 1 in both figs. 14 and 20 is about the same. Higher temperature peaks have a tendency to be less supralinear, an effect also seen in $CaSO_4$:Dy (70,71); this is explained by a model of competition between deep traps and high energy traps which correspond to the TL peaks observed at the high temperature side of the normal TL peak. The supralinear effect in MgO is believed to be the result of Cr^{3+} emission in addition to the Fe^{3+} emission, the former being effective at higher energies, as already seen.

The reason for the TL mechanisms involving Mn being different in Spicer and Norton crystals could be due to the critical equilibrium concentration. Thus, in Spicer crystals, which have a low Mn^{2+} concentration, the UV light tends to increase the Mn^{2+} concentration, while in Norton crystals, where the Mn^{2+} content is higher than in Spicer, the UV light tends to decrease its concentration. Ideally then, the same critical concentration would be reached in both cases, provided that other parameters were the same, such as the concentration of other impurities. This is not the case between Spicer and Norton samples, since the former is purer than the latter relative to all impurities. The transition $Mn^{3+*} \longrightarrow Mn^{3+}$ seen in Spicer crystals probably gives an orange emission, as assumed by Ziniker et al. (21) who reported an emission band at 610 nm as probably due to Mn^{2+}. On the other hand, the conversion $Mn^{3+} \longrightarrow Mn^{2+}$ indicates that Mn^{3+} ions absorb UV light, except that the reported absorption band for this ion lies at 520 nm (54).

The most important aspect of all the results discussed for Norton and Spicer MgO crystals is that the TL mechanisms can be better understood when the effect of the equilibrium impurity concentrations on the TL behavior is understood. In other words, the maximum TL sensitivity can be achieved once one can control the concentration and equilibrium of the impurities responsible for the UV absorption and TL emission.

Chapter 6

CONCLUSIONS

The objectives of this research, as stated in chapter 1, were to investigate the charge transfer mechanisms as a result of the UV irradiation, to study the sensitization phenomenon and the TL sensitivity to UV radiation and the dependence of these parameters on impurity content and, finally, to correlate the observations on TL sensitivity with the charge transfer mechanisms. These objectives have been met by measuring the changes in impurities concentration, before and after the UV exposure and after the TL reading in "as received" and heat treated samples and establishing the charge transfer mechanisms. Correlations between the observed reactions among impurities and V-type centers and the TL sensitivity were then made in an attempt to identify the activator, trapping and emission centers in MgO crystals.

The conclusions of this work can be summarized as follows. The MgO Norton samples are generally less sensitive than the Spicer crystals, because the former are less pure than the latter, leading to what is known as the concentration quenching effect. This indicates that a better control of impurities is necessary in commercially available MgO crystals in order to achieve the highest TL sensitivity possible. A low total impurity content, however, does not necessarily imply a high TL response, since the TL emission is also important in determining the TL sensitivity. Depending on

the energy of the emitted light, a varying TL response is detected, depending on the spectral response of the photomultiplier detection system.

The sensitization phenomenon was observed in air heat treated samples as compared to "as received" crystals. TL peaks 2 and 3 were sensitized in Norton samples, and TL peaks 1 and 2 in Spicer samples. This behavior is related to the oxidation of Fe^{2+} to Fe^{3+}, where Fe^{3+} ions may have a tendency to associate with vacancies, although not necessarily as next neighbors, for charge compensation, forming V_{Fe} centers. The sensitization is also related to the decrease and increase of $[Mn^{2+}]$, respectively, in Norton and Spicer samples, caused by the UV radiation. This behavior suggests, as opposed to the reported stability of Mn^{2+}, that, in Norton, this ion is possibly a hole trap, forming Mn^{3+}. In Spicer samples, the reverse was observed, and Mn^{3+} was identified as an activator center. The reducing treatment, on the other hand, was seen to decrease the TL sensitivity, explained by the reduction of Fe^{3+} to Fe^{2+}, and/or by the decrease in the number of trapping centers, as governed by the vacancy concentration.

The fading of TL was seen to characterize the type of trapping centers that are present in the crystal, resulting in the identification of V_{Al} and V^- centers as the primary centers in Norton and Spicer samples, respectively. The TL response was determined as a linear function of $[Fe^{3+}]$, and as a power function of $[V^{2+}]$, this ion not being a recombination center for TL emission. The TL

supralinearity resulting from the 249 nm exposure was correlated with the Cr^{3+} R-emission lines.

The major activator centers were identified as Fe^{3+} and Fe^{3+}, Mn^{3+} and V^{3+} in Norton and Spicer crystals, respectively, and the common recombination center to both materials, as Fe^{2+}. The TL emission was identified, therefore, as due to the $Fe^{3+*} \longrightarrow Fe^{3+}$ transition, probably in the orange region of the spectrum. These results do not necessarily relate to other types of irradiation, such as γ- or X-rays, since samples exposed to other radiations may have different TL emission spectra due to transitions other than those observed to occur in the UV irradiated material.

Finally, the conclusions presented here apply generally to other sources of MgO crystals and, therefore, characterize the material as far as the "direct TL" behavior caused by the UV radiation is concerned.

The following suggestions for future investigations are logical extensions of the present work which would enable a better understanding of the TL mechanisms in MgO crystals exposed to UV radiation:

—ESR at low temperatures and/or ENDOR measurements, in order to study the V-type centers and their relationship to the TL mechanisms. A complete in situ system, including an optical system, TL reader and ESR/ENDOR would be desirable.

—Analysis of the TL emission spectrum, utilizing a multichannel analyser, supported by theoretical studies of the possible

transitions of transition metal ions in a ligand field, at different temperatures, so that the TL emission lines can be identified.

—Heat treatments in air at intermediate temperatures (400°C-1000°C), in order to verify the effect on the sensitization phenomenon and its correlation to the concentration of V-type centers. These investigations along with correlations between UV and X- or γ-irradiated TL studies would enable a more complete understanding of lattice defect interactions in MgO as they influence the thermoluminescent properties of this material.

LIST OF REFERENCES

1. G. H. Reiling and E. B. Hensley. Ph. Rev. 112 (6), 1106 (1958).

2. J. H. Schulman and W. D. Compton. "Color Centers in Solids." Pergamon Press, Inc., New York (1963).

3. H. W. Leverenz. "An Introduction to Luminescence of Solids." Dover Publ., Inc., New York (1968).

4. W. C. Las and S. Watanabe. "Mechanism of UV induced TL in natural calcium fluoride." Proc. IV Int. Conf. on Lumin. Dosim. Krakow, Poland, 1187 (1974).

5. D. L. Staebler and S. E. Schnatterly. Phys. Rev. B 3 (2), 516 (1971).

6. N. Takeuchi, K. Inabe and H. Nanto. Phys. Stat. Sol. (a) 33, K125 (1976).

7. J. E. Wertz, L. C. Hall, J. Hegelson, C. C. Chao and W. S. Dykoski. "Interaction of Radiation with Solids." Ed. A. Bishay, Plenum Press, New York, pg. 617 (1967).

8. J. M. Luthra, A. Sathyamoorthy and N. M. Gupta. J. Lumin 15, 395 (1977).

9. Y. Kirsh, N. Kristianpoller and R. Chen. Phil. Mag. 35 (3), 653 (1977).

10. N. Takeuchi, K. Inabe, J. Yamashita and S. Nakamura. Health Phys. 31, 519 (1976).

11. A. K. Dhar, L. A. DeWerd and T. G. Stoebe. Med. Phys. 3 (6), 415 (1976).

12. E. R. Wilson, F. M. Lin and J. R. Cameron. (TID-24640) 47383 Annual Progress Report on TL Dosimetry-COO-1105-136 (1967).

13. E. Okuno and S. Watanabe. Health Phys. 23, 377 (1972).

14. N. Takeuchi, K. Inabe and J. Yamasita. Zeitschriff für Physikalische Chemie 259 (2), 321 (1978).

15. R. W. Soshea, A. J. Dekker and J. P. Sturtz. J. Phys. Chem. Solids 5, 23 (1958).

16. J. E. Wertz, P. Auzins, J. H. E. Griffiths and J. W. Orton. Disc. Far. Soc. 26, 66 (1958).

17. K. H. Lee, J. H. Crawford, Jr. J. Lumin. 20 (1), 9 (1979).

18. Y. Chen and W. A. Sibley. Phys. Rev. 154 (3), 842 (1967).

19. W. A. Sibley, J. L. Kolopus and W. C. Mallard. Phys. Stat. Sol. 31, 223 (1969).

20. A. Sathyamoorthy, J. M. Luthra. J. Mater. Sci. 13 (12), 2637 (1978).

21. W. M. Ziniker, J. K. Merrow and J. J. Mueller. J. Phys. Chem. Sol. 33, 1619 (1972).

22. R. L. Hansler and W. G. Segelken. J. Phys. Chem. Sol. 13, 124 (1960).

23. J. E. Wertz, J. W. Orton and P. Auzins. J. Appl. Phys. Suppl. 33 (1) 322 (1962).

24. F. A. Modine, E. Sonder and R. A. Weeks. J. Appl. Phys. 48 (8), 3514 (1977).

25. K. W. Blazey. J. Phys. Chem. Sol. 38 (6), 671 (1977).

26. J. B. Lacy, M. M. Abraham, J. L. Boldu O., Y. Chen, J. Narayan and H. T. Tohver. Phys. Rev. B 18 (8), 4136 (1978).

27. J. C. Cheng and J. C. Kemp. Phys. Rev. B-Solid State III 4 (9), 2841 (1971).

28. R. W. Davidge. J. Mater. Sci. 2, 339 (1967).

29. Y. Chen, M. M. Abraham, L. C. Templeton and W. P. Unruh. Phys. Rev. B 11 (2), 881 (1975).

30. M. M. Abraham, Y. Chen and W. P. Unruh. Phys. Rev. B, 9 (4), 1842 (1974).

31. L. A. Kappers, F. Dravnieks and J. E. Wertz. Sol. State Comm. 10, 1265 (1972).

32. W. P. Unruh, Y. Chen and M. M. Abraham. Phys. Rev. Lett. 30 (10), 446 (1973).

33. E. Sonder and W. A. Sibley in "Point Defects in Solids." Vol. I, J. H. Crawford and L. M. Slifkin. General and Ionic Crystals, Plenum Press, New York (1972).

34. J. E. Wertz, P. Auzins, J. H. E. Griffiths and J. W. Orton Disc. Far. Soc. 28, 136 (1959).

35. O. F. Schirmer, P. Koidl and H. G. Reik. Phys. Stat. Sol. (b) 62, 385 (1974).

36. L. A. Kappers, F. Dravnieks, and J. E. Wertz. J. Phys. C. Sol. St. Phys., 7, 1387 (1974).

37. J. E. Wertz, G. Saville, P. Auzins and J. W. Orton. J. Phys. Soc. Japan, 18. Supp. II, 305 (1963).

38. A. M. Glass and T. M. Searle. J. Chem. Phys. 46 (6), 2092 (1967).

39. B. Henderson and W. A. Sibley. J. Chem. Phys. 55 (3), 1276 (1971).

40. L. A. Kappers, R. L. Kroes and E. B. Hensley. Phys. Rev. B. 1 (10), 4151 (1970).

41. Y. Chen, J. L. Kolopus and W. A. Sibley. J. Lumin. 1 (2), 633 (1970).

42. R. A. Weeks, E. Sonder, J. C. Pigg and K. F. Kelton. J. Physique, 37 (12), C7-411 (1976).

43. M. Sparks, H. Vora and M. Flannery. "Tabulation of impurity absorption spectra-ultraviolet and visible," vol. II. Ninth Technical Report. Contract No. DAHC, 15-73-C-0127 (1977).

44. B. Henderson, J. E. Wertz, J. P. Hall and R. D. Dowsing. J. Phys. C. 4 (1), 107 (1971).

45. J. P. Larkin, G. F. Imbush, F. Dravnieks. Phys. Rev. B. 7, (1) 495 (1973).

46. J. S. Thorp, R. A. Vasquez, C. Adcock and W. Hutton. J. Mat. Sci. 11, 89 (1976).

47. C. S. Krishnan. "An electron spin resonance study of thermoluminescence in MgO." Ph.D. thesis, Dept. Min. Met. and Cer. Eng., University of Washington (1973).

48. B. V. Haxby. "A study of color centers in magnesium oxide." Ph.D. Thesis. Univ. of Minnesota (1957).

49. W. Low. Ph. Rev. 105 (3), 801 (1957).

50. M. D. Sturge. Ph. Rev. 130 (2), 639 (1963).

51. F. A. Modine. Phys. Rev. B 8 (2), 854 (1973).

52. J. L. Boldu, M. M. Abraham and Y. Chen. Ph. Rev. B. 19 (9), 4421 (1979).

53. L. J. Challis, A. A. Ghazi and K. J. Maxwell. J. Phys. C. Sol. St. Ph. 12, 303 (1979).

54. P. Koidl and K. W. Blazey. J. Phys. C: Solid St. Phys. 9, L167 (1976).

55. S. Geschwind, P. Kisliuk, N. P. Klein, J. P. Remeika and D. L. Wood. Paramagnetic Resonance. Proc. First Int. Conf. Jerusalem, Vol. I. Ed. W. Low, pg. 113. Academic Press, New York (1963).

56. J. R. Cameron, N. Suntharalingam and G. N. Kenney. "Thermoluminescence Dosimetry." The University of Wisconsin Press, Madison (1968).

57. R. D. Newton and W. A. Sibley. Ph. Stat. Solidi a) 41, 569 (1977).

58. Y. Chen, M. M. Abraham, L. C. Templeton and E. Sonder. Solid State Comm. 18, 61 (1976).

59. S. Datta, I. M. Boswarva and D. B. Holt. J. Phys. Chem. Solids, 40, 567 (1978).

60. S. Datta, I. M. Boswarva and D. B. Holt. Third Europhysical Conf. on Lattice Defects in Ionic Solids (1979) to be published in J. Physique.

61. W. T. Peria. Phys. Rev. 112, 423 (1958).

62. R. T. Williams, J. W. Williams, T. T. Turner and K. H. Lee. Phys. Rev. B 20 (4), 1687 (1979).

63. A. G. Fitzgerald, and R. Engin. J. Mater. Sci. 9 (2) 339 (1974).

64. F. Freund, G. Debras and G. Demortier. J. Am. Cer. Soc. 61 (9-10), 429 (1978).

65. J. E. Wertz and J. R. Bolton. "ESR--Elementary Theory and Practical Applications." McGraw-Hill, New York (1972).

66. C. P. Poole, Jr. "Electron Spin Resonance--A comprehensive treatise on experimental techniques." Interscience Publishers, New York (1967).

67. R. S. Alger. "Electron Paramagnetic Resonance: Techniques and Applications." Interscience Publishers, New York (1968).

68. K. S. V. Nambi. Thermoluminescence: Its Understanding and Applications. Informaçaõ IEA54-CPDAMD1 (1977) Instituto de Energia Atomica, Saõ Paulo, Brasil.

69. E. R. Vance and W. C. Mallard. Phys. Status Solidi B, 91 (2), K155 (1979).

70. A. R. Lakshmanan, Bhuwan Chandra and R. C. Bhatt. Nuclear Instr. and Meth. 153, 581 (1978).

71. A. R. Lakshmanan and R. C. Bhatt. Nuclear Instr. and Meth. 164, 215 (1979).

VITA

Name of Author:	Wanda Cecilia Las
Place of Birth:	Saõ Paulo, Brasil
Date of Birth:	December 7, 1949
Parents:	Ceslau Las and Henryka W. K. Las
Secondary Education:	Instituto Mackenzie, High School, 1967
Degrees:	B.S. in Physics at Universidade de Saõ Paulo, 1971
	Masters in Physics at Universidade de Saõ Paulo and Instituto de Energia Atomica, 1975